SCOURING EFFECT OF RIVER BED FROM THE FLOW OVER PIPE USING CFD

ABBOD ALI MOHAMMED SAEED

FACULTY OF ENGINEERING

UNIVERSITY OF MALAYA

KUALA LUMPUR

2015

SCOURING EFFECT OF RIVER BED FROM THE FLOW OVER PIPE USING CFD

ABBOD ALI MOHAMMED SAEED

DISSERTATION SUBMITTED IN FULFILMENT OF THE REQUIREMENTS FOR THE DEGREE OF MASTER OF ENGINEERING SCIENCE

FACULTY OF ENGINEERING

UNIVERSITY OF MALAYA

KUALA LUMPUR

2015

UNIVERSITI MALAYA
ORIGINAL LITERARY WORK DECLARATION

Name of Candidate: ABBOD ALI MOHAMMED SAEED (I.C/Passport No:
Registration/Matric No: KGA120114
Name of Degree: Master of Engineering Science
Title of Project Paper/Research Report/Dissertation/Thesis ("this Work"):
Scouring effect of river bed from the flow over pipe using CFD

Field of Study: Structural Engineering & Materials
I do solemnly and sincerely declare that:

1) I am the sole author/writer of this Work;
2) This Work is original;
3) Any use of any work in which copyright exists was done by way of fair dealing and for permitted purposes and any excerpt or extract from, or reference to or reproduction of any copyright work has been disclosed expressly and sufficiently and the title of the Work and its authorship have been acknowledged in this Work;
4) I do not have any actual knowledge nor do I ought reasonably to know that the making of this work constitutes an infringement of any copyright work;
5) I hereby assign all and every rights in the copyright to this Work to the University of Malaya ("UM"), who henceforth shall be owner of the copyright in this Work and that any reproduction or use in any form or by any means whatsoever is prohibited without the written consent of UM having been first had and obtained;
6) I am fully aware that if in the course of making this Work I have infringed any copyright whether intentionally or otherwise, I may be subject to legal action or any other action as may be determined by UM.

Candidate's Signature Date . . 2014

Subscribed and solemnly declared before,

Witness's Signature Date . . 2014
Name:
Designation:

ABSTRACT

Pipes that are mounted on the river bed is mostly exposed to continuously strong flow field. This continuous flow field removes sand particles deposited around the pipe and creates a hole, which is known as local scour, and this phenomenon is known as scouring. Sometime this scouring is so intense that it leads to pipe's demage. The aim of this study was to study the effect of bluff body shapes and gap between circular body and wall of sand bed and the turbulence models sensitivity study and effect of scour depth.

A numerical investigation of incompressible and transient flow around circular pipe has been carried out at different five gap phases. Flow equations such as Navier-Stokes and continuity equations have been solved using finite volume method. Unsteady horizontal velocity and Kinetic energy square root profiles are plotted using different turbulence models and their sensitivity is checked against published experimental results. Flow parameters such as horizontal velocity under pipe, pressure coefficient, wall shear stress, drag coefficient, lift coefficient, bed roughness are studied and presented graphically to investigate the flow behavior around an immovable pipe and scoured bed.

Results reveal that among existing turbulence models, the standard k- ε turbulence model is preferred over others for more accurate prediction of local scour surrounding circular cylinder over sandy bed when compared against experimental data. In addition, It is found that in both cases with flat and scoured bed, the size of the vortex shedding increases with the increase in the gap and when the pipe closer to the bed the vortices behind the circular cylinder is unsymmetrical. It is observed that in both cases with flat and scoured bed, the drag coefficient reduces as the gap increases and lift coefficient as well. However, for the scoured bed the lift coefficient has a negative value which indicates the void under the pipe. It is found that in both cases with flat and scoured bed shear stress reduces as the gap increases. A reduction of around 82.3 % in the pressure distribution over the bed's

surface is observed with flat-bed, and a reduction of around 80 % of bed wall shear stress observes from time 10 min to 300 min at scoured bed.

ABSTRAK

Paip yang telah dipasang di dasar sungai kebanyakannya terdedah kepada medan aliran terus kuat. Bidang aliran berterusan mengeluarkan zarah-zarah pasir yang disimpan di sekeliling paip dan mewujudkan lubang, yang dikenali sebagai kerokan tempatan, dan fenomena ini dikenali sebagai penyental. Kadang-kadang penyental ini adalah begitu kuat bahawa ia membawa kepada retak paip itu. Tujuan kajian ini adalah untuk mengkaji kesan bentuk badan pembohongan dan jurang antara badan bulat dan dinding katil pasir dan kajian sensitiviti model pergolakan dan kesan kedalaman kerokan.

Penyiasatan berangka aliran tak boleh mampat dan sementara di sekeliling paip bulat telah dijalankan di lima fasa yang berbeza jurang. Persamaan aliran seperti Navier-Stokes dan persamaan kesinambungan telah diselesaikan dengan menggunakan kaedah isipadu terhingga. Halaju mendatar tak mantap dan Kinetic profil punca kuasa tenaga diplot menggunakan model pergolakan yang berbeza dan sensitiviti mereka disemak dengan keputusan eksperimen diterbitkan. Parameter aliran seperti halaju mendatar di bawah paip, pekali tekanan, tegasan ricih dinding, pekali seretan, pekali daya angkat, kekasaran katil dikaji dan dipersembahkan secara grafik untuk menyiasat kelakuan aliran sekitar sebuah paip tak alih dan katil dicari dengan rapi.

Keputusan menunjukkan bahawa antara model pergolakan yang sedia ada, k- model gelora ε standard lebih disukai berbanding lain-lain untuk ramalan yang lebih tepat kerokan tempatan di sekitar silinder bulat atas katil berpasir apabila dibandingkan dengan data eksperimen. Di samping itu, Ia mendapati bahawa dalam kedua-dua kes dengan katil rata dan dicari dengan rapi, saiz vorteks menumpahkan meningkat dengan peningkatan dalam jurang dan apabila paip yang lebih dekat dengan katil yang vorteks di belakang silinder bulat adalah simetri. Adalah diperhatikan bahawa dalam kedua-dua kes dengan

katil rata dan dicari dengan rapi, pekali seretan mengurangkan dengan peningkatan jurang dan pekali daya angkat juga. Walau bagaimanapun, bagi katil dicari dengan rapi pekali daya angkat mempunyai nilai negatif yang menunjukkan tidak sah di bawah paip. Didapati bahawa kedua-dua kes dengan tegasan ricih katil rata dan dicari dengan rapi mengurangkan jurang yang meningkat. Pengurangan sekitar 82.3% pada taburan tekanan di atas permukaan katil yang diperhatikan dengan rata-katil, dan pengurangan kira-kira 80% daripada tegasan ricih dinding katil memerhati dari masa 10 min 300 min di inap dicari dengan rapi.

ACKNOWLEDGEMENT

I would like to acknowledge and extend my heartfelt gratitude to the persons who have made the completion of this project possible. At first I thank my supervisors Dr. Poo Balan A/L Ganesan and Dr. Shatirah Binti Mohamed Akib who helped me work this project out. I would also like to thank my friend Ravi Sharma for sharing with me his Academic research experience which helped me to conduct my thesis work. And it would not be successful without **Allah SWT** who guided me in my everyday life and activities; I thank **Him** for the good health He has given me, and for the success of my study. Special thanks go to the University of Malaya (UM.C/625/1/HIR/61, account no. H-16001-00-D000061) and Exploratory Research Grant Scheme (ERGS: ER013-2013A) which are gratefully acknowledged for the financial support towards this research.

TABLE OF CONTENTS

LIST OF TABLES

LIST OF FIGURES

LIST OF ABBREVIATIONS AND SYMBOLS

Abbreviation/Symbol	Phrase
CFD	Computational fluid dynamic
$C_{1\varepsilon}$,$C_{2\varepsilon}$	Model constants
C_d	Drag coefficient
C_l	Lift coefficient
C_s	Roughness constant (m)
C_p	Pressure coefficient Cp= ($P - P0$)/ (0.5 u_{20})
D	Cylinder diameter (m)
FAVOR	Fractional Area-Volume Obstacle Representation
FVM	Finite volume method
g	Gravitational acceleration (m/s2)
G	Gap between maximum scoured bed and cylinder (m)
G_b	The generation of turbulence kinetic energy due to buoyancy
G_k	The generation of turbulence kinetic energy due to the mean velocity gradients
K	von Karman constant
k	Turbulent Kinetic Energy (TKE) (m2S2)
$\sqrt{k}$	Turbulent kinetic energy square root (m/s)
PISO	Pressure-implicit with splitting of operators
P	Dynamic pressure (Nm2)
P_0	Reference pressure (Nm2)
RANS	Reynolds-averaged Navier-Stokes equations
Re	Reynolds numbers
RNG	Renormalization group method
RSM	Reynolds stress model
SST	Shear stress transport
UDF	User-defined functions
U_0	X-direction velocity-inlet component (m/s)
U_∞	Approach velocity(m/s)
u_*	Friction (or shear) velocity, $u*$=(τ/ρ)1/2 (m/s)
$\overline{\acute{u}_i\acute{u}_j}$	Turbulent momentum flux or Reynolds stress (i, j component)
u_i	Flow velocity in i-direction (Reynolds average) (m/s)
$\acute{u}_j$	Flow velocity in i-direction (fluctuating part) (m/s)
u_j	Flow velocity in j-direction (Reynolds average) (m/s)
$\acute{u}_j$	Flow velocity in j-direction (fluctuating

	part) (m/s)
y	Water (or flow) depth (m)
y_0	Roughness height (m)
y_+	Wall distance estimation (m)
ε	Rate of dissipation of turbulent kinetic energy (k) (m^2/s^3)
ω	Specific dissipation (1/s)
τ_w	Shear stress
Δt	Time step (s)
θ	The angle indicates the position around the cylinder's surface (∘)
v	Velocity (m/s)
Γ_k and Γ_ω	Represent the effective diffusive of k and ω
Y_k and Y_ω	Represent the dissipation of k and ω to turbulence
ρ	Water density (m/s^3)
μ_t	The turbulent (or eddy) viscosity (Ns/m^2)
μ	Dynamic viscosity (Ns/m^2)
$\rho\overline{\acute{u}_\iota \acute{u}_J}$	Reynolds stresses
G_k, S_k	Source items
G_ω+D_ω+S_ω	Source items

List of Appendix

Chapter 1.0

Introduction

1.1 Background

Scouring can be defined as the erosion of sand bed sediment surrounding the obstruction i.e., cylindrical pipes when the obstruction is exposed to continuously strong flow field or flood events (Breusers et al., 1977; Chang, 1992; Kattell & Eriksson, 1998; Akib, Fayyadh, Shirazi, et al., 2011). The sand bed can be undermined due to the normal flow field subjected to the obstruction under flow conditions by which its rate increases with larger flow events. In other words, scouring is basically caused when the foundation of the bed is swept away under flood conditions in which the flow around the obstruction accelerates and induces high shear stress over the seabed surface (Adhikary et al., 2009; Akib, Fayyadh, Shirazi, et al., 2011). The resulted reduction of the sand bed around the pipe below the normal and natural river level is called the scour depth. A scour hole is a pit or void that forms as a result of the sand bed sediment removal from the river bed (Alabi, 2006).

Local and area scour threaten pipeline stability which may damage the pipe. Scour holes endanger stability when large free spans create unacceptable stress due to static deformation (Bruschi et al. 1986). During the development of the scour hole under the pipeline, the stresses inside the wall of the pipe increase due to the sagging of the pipe. The suspended part of the pipe deflects like a uniformly loaded beam with fixed or simply supported ends. The pipe will rupture if the static bending stresses exceed the ultimate strength of the pipe.

Local scouring surrounding the cylindrical pipes are considered to be one of the main causes of their damage. The local scour around river hydraulic structures are disaster mitigation of the engineering structure (Nagata et al., 2005; Fayyadh et al., 2011). Damage of hydraulic structure because of local scouring is a global concern, and it has been studied by many researchers experimentally and numerically for several decades such as (Akib, Fayyadh, & Othman, 2011; Akib, Jahangirzadeh, et al., 2014). The study

conducted by Smith (D. Smith, 1976; Sheppard et al., 2004) reported that the most of the reasons contributed for the damage and failure of pipes located or river in the period of time from 1847 to 1975 , details are shown in the Table 1.1.

Table 1.1: World-wide structure failures categories (Smith, 1976)

Classification	Reasons	Number
1	Flood scour	70
2	Inappropriate material	22
3	Overloading and Accidents	14
4	Inappropriate instalment	12
5	Earthquakes	11
6	Error in design	5
7	Wind destroy	4
8	Fatigue	4
9	Rust	1

Due to the importance of complex phenomenon of scouring around cylindrical pipe, it has been subject of research for decades and is still an open interdisciplinary research field as the mechanism of scouring are still less understood. Majority of the earlier studies focused on fields of finding applicable experimental methods to ensure structure endurance and protection rather than in-depth understanding of the phenomenon. Although these methods which mainly focused on seeking empirical equations to predict the maximum scour depth proved to be helpful to some extent, they are not always successful to extend the experimental results to the practical applications. The empirical equations are also unable to give a comprehensive prediction for the configuration of scour hole in detail. Considering the shortcomings and the high costs of laboratory tests, some researchers have instead attempted to develop numerical models since 1980s. However due to its complex nature, numerical modeling of scouring has remained relatively less developed.

1.2 Problem statement

Local scouring around pipes mounted on river are a complex phenomenon which needs more effort to be understood and clarified. Since experimental studies are not always feasible, computational study of such design shows to be an important and effective tool for understanding the effect of scouring depth. However, since scouring is very complex due to nature, simulations are quite challenging and advanced as well as proper techniques for modeling of turbulence models should be applied to ensure reliable and accurate results.

1.3 Objectives of study

This study aims to achieve the following objectives:

- To investigate the flow behavior over various shapes of a pipe (i.e,circle, rectangle, square and square with round edge) using CFD.
- To investigate the effect of the vertical distance between the flat sand bed and circular pipe surface using CFD.
- To study the sensitivity of various turbulence models (RANs types) for the investigation of the flow around a circular pipe for number of scoured (non-flat) sand bed.
- To investigate the effect of different scoured depths between sand bed and circular pipe surface.

1.1 Research project outline

This thesis consists five chapters:

Chapter 1: Introduction.

Chapter 2: Literature review. This part provides extensive and informative background on past studies that deal with the main reasons causing the formation of scouring around bridge piers and abutments.

Chapter 3: This chapter presents the research findings and their analysis for objectives 1 and 2. It discusses the effect of bluff body shapes and effect of gap between circular body and wall of sand bed. The chapter systematically describes the methods which are used in simulation of body shapes and gaps effect. This chapter consists of ten subsections namely: Introduction, Geometry of different cross sections view of pipe, Governing equations, Turbulence models, Boundary conditions, Numerical methods, Simulation cases, Mesh independence and time step test, Results and discussions, and Conclusions.

Chapter 4: This chapter presents the research findings and their analysis for objectives 3 and 4. It discusses the turbulence models sensitivity study and effect of scour gap. This chapter systematically describes the methods which are used in simulation of effect of different turbulence models and effect of scouring depth. This chapter consists ten subsections namely: Introduction, Geometry of different cross sections view of pipe, Governing equations, Turbulence models, Boundary conditions, Numerical methods, Simulation cases, Mesh independence and time step test, Results and discussions, and Conclusions.

Chapter 5: Conclusions: The conclusions and the contributions of this study and suggestions for future work are given in this chapter.

Chapter 2.0

Literature review

2.1 Introduction

Pipes that are located in the flow direction are mostly exposed to damage. Structural failure, embankment erosion and scouring are some of the main reasons which contribute to the failure of a pipe located on river bed. Scouring is the most important effects of flood on cylindrical pipes, which occurs due to the erosion of the bed foundation. The flow around the obstruction accelerates and induces high shear stress over the bed surface that sweeps away the bed foundation of river pipes. There are several types of scouring around cylindrical pipes, e.g., general scouring or erosion scouring, contractive scouring and local scouring. General scouring occurs regardless of the existence of pipes on the river bed. While a contractive scouring occurs when cylindrical pipes block the water flow and a local scouring is due to the local flow field around pipes.

Scour prediction has been a subject of interest since the beginning of civilization. Over the past years, there have been a lot of experimental and simulation based studies conducted to predict local scouring phenomenon. Obstruction,i.e., cylindrical pipes, located in the water flow direction are mostly exposed to local scour and such local scouring prediction surrounding the obstruction has been primary interest to hydraulic and ocean engineers (Kattell & Eriksson, 1998).

2.2 Mechanism of the scouring process

Figure 2.1 shows the basic mechanisms for flow around pipe and local scour formation. The flow field around an obstruction such as cylindrical pipe passes through three stages before forming a scour hole, i.e., the flow pattern at the downstream, the pressure stagnation (located at the front of the pier surface) and the vortex system. The velocity decelerates as the flow approach an obstruction and the velocity reduces to zero at the stagnation point on the obstruction surface which leads to an increase in pressure at the point. This stagnation pressure is considered as the highest pressure near to pipe surface. The flow at the downstream of the obstruction forms a strong vortex, which is called as horseshoe vortex for its similarity to a horseshoe and the down-flow (i.e., the flow from top to bottom of an obstruction) which rolls up continuously, creates a scour hole. The down-flow reaches its maximum near to the sand bed level, and it is known as the main scouring agent (B. W. Melville & Raudkivi, 1977). Furthermore, the vortex flow, which is conducive to the evolution and development of a local scour hole, is considered as the main agent for scouring as well (Dey & Barbhuiya, 2005). Beside the horseshoe vortex, there are vertical vortices downstream the pipe which is called as wake vortices (Khwairakpam & Mazumdar, 2009). Both horseshoe vortex and wake vortices remove the sand at the base region around the pier (Negm et al.; Khwairakpam & Mazumdar, 2009). Normally the flow accelerates around the pipes and make them susceptible to local scour (Zhai, 2010). Scouring is mostly harmful for the pipes located over river bed at the upstream in which it washes the erodible river bed around it and eventually creates a void that proportionally gets largely undermined with the time development (Millard et al., 1998). Briefly, local scour at the obstruction occurs due to the formation of horseshoe vortex by water accumulation on the obstruction surface at the upstream which increases shear stress and sediment transport (Pal et al., 2011).

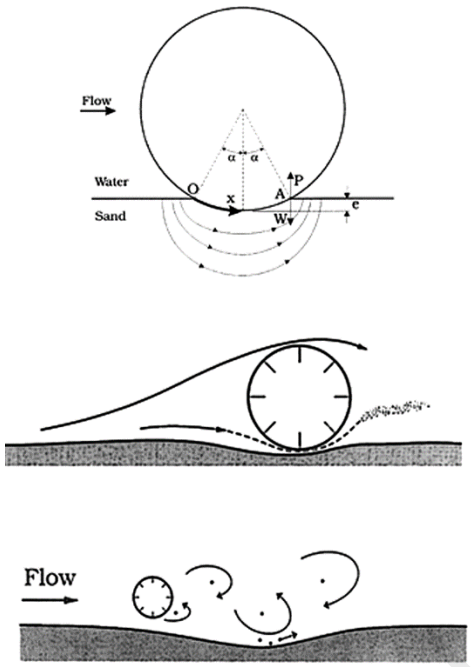

Figure 2.1: Flow pattern surrounding a pier and basic scour mechanisms.

Although numerous investigations have been conducted on scouring around cylindrical pipes, but the understanding of the complex flow field and the mechanisms of scouring combined with the complexity of geometries and various erodible beds still requires further study and this remains challenging problems.

2.3 Parameters causing local scouring

Two parameters down-flow at the upstream face of the pipe and formation of horseshoe vortex play the major role in causing the local scouring around cylindrical pipes. There have been numerous experimental investigations in the past to determine the reasons of local scouring around cylindrical pipes. Details can be found in ref (Saneie et al.; Mao, 1987; B. Jensen et al., 1990; Jones et al., 1992; B. W. Melville, 1997; Ettema et al., 1998; Millard et al., 1998; Briaud et al., 1999; Ting et al., 2001; Yanmaz & Ustun, 2001; Oliveto & Hager, 2002; Coleman et al., 2003; Bateman et al., 2005; Coleman, 2005; Dey & Barbhuiya, 2005; Ataie-Ashtiani & Beheshti, 2006; Sturm, 2006; Dey & Raikar, 2007; Haltigin et al., 2007; Mutlu Sumer, 2007; Unger & Hager, 2007; B. Melville, 2008; Beheshti & Ataie-Ashtiani, 2009; G Kirkil et al., 2009; Lee & Sturm, 2009; Mashahir et al., 2009; Bihs & Olsen, 2010; Debnath & Chaudhuri, 2010; Defanti et al., 2010; Grimaldi & Cardoso, 2010; Q. L. C. Liu & Dong, 2010; Eghbali et al., 2011; Guney et al., 2011; Khosronejad et al., 2012; Khwairakpam et al., 2012; Das et al., 2013; Nielsen et al., 2013).There have been some numerical investigations on finding the causes of scouring which focused on the scour features such as shape and size of the scour hole and time scale of void formation , while the current study focuses on the forces on cylindrical pipe ,vortex shedding and velocities for each of the bed profiles .

2.3.1 Down-flow filed

The down-flow is the accelerated flow field surrounding the obstruction e.g. pipe that leads the flow to move downward and forms a clockwise spiral around the pipe. This downward flow induces shear stress over the bed that leads to the formation of scour void. The accelerated flow around the obstruction parallel to bed surface induces shear stress over the bed which is called bed shear stress, and it experiences the maximum shear (τ_{max}) at the flow separation point which makes scouring to begin. Lu Li and Qin (2005) investigated local scour surrounding offshore pipelines by using the Re-Normalized group (RNG) turbulence model using CFD. They showed the bed shear stress is a dominated factor that involves creating a local scour profile around hydraulic structure. A CFD study to predict a flow field surrounding a circular pipeline was carried out by Zhu and Liu (2012). Authors observed the scour depth depends on three quantitative numbers which are numbers of pier, number of sediment size and the period time number (a period time number is a time that takes for a scouring hole to reach to its equilibrium stage, in that case sand stops removing.). Results were used to calculate the bed shear stress surrounding the cylinder and an expression which was taken from the results was used to get the varied scour depth with the time development. Molina et al. (1998) experimentally investigated shear stress surrounding vertical wall obstruction. Results revealed that at the upstream corner of vertical wall, the maximum shear stress occurred, and by increasing the flow velocity and the shear stress intensity, the local scour around obstruction is initiated.

The scour gap below pipelines under upward seepage affect through bed sediment was conducted by computationally and experimentally by Dey and Singh (2007). It was found that scour gap below pipelines with upward seepage influence is smaller than scour gap without upward seepage. This was because of the mechanism of scour below upward which was controlled by the decreasing of bed shear stress due to seepage reduction in

the submerged weight of the sediment particles due to seepage. Kang and Yeo (2012) and Sheppard et al. (2004) experimentally conducted to study the changes in the shear stress surrounding piers for different bed materials through the influence of time development on scour depth, the shear stress surrounding piers and the critical shear stress on particles . Results revealed that the bed shear stress gets its maximum value at the initial stage during scour formation, and it gets decreased gradually while the scour depth gets increased until it reaches the equilibrium scour depth. A numerical study on maximum scour depth below submarine pipelines was conducted by Chiew (1991). Results showed that when the shear stress and critical shear stress of sand sediment are equal, the scour depth will be at its maximum value. The results obtained by Kamil and Karim (2002) revealed that the overall bed shear stress reduced with scour accompanies time development increases and with local scour size increases. The flow field and the scour mechanism surrounding a circular pier was numerically investigated based on Large Eddy Simulation (LES). The results found that at the downstream, as the scouring depth increases, the bed shear stress decreases and approaches the undisturbed shear stress (Wei & Aode, 2006). The flow field surrounding a bridge abutment was numerically investigated. The results concluded that the maximum shear stress are condensed at a small area near the edge of the abutment upstream where the maximum scour capacity is found (Teruzzi et al., 2006).

2.3.2 Horseshoe vortex

The horseshoe vortex is simple eddies circulation model of water around cylindrical pipe that forms as a results of the strong down-flow filed which is called as horseshoe vortex for its similarity to a horseshoe. The formation and flow of vortex generates around the cylindrical pipe due to water external forces that subjected to the cylindrical pipe surface, are both cause the cylindrical pipe to be vibrated and may cause resonance phenomena besides the scouring phenomena. This section presents factors which contribute in cylindrical pipe failure that mounted on river bed.

Several experiments and numerical simulations have been done in last few decades to investigate the main reasons causing a scour to form around cylinders that are subjected to a sandy bed. Experimental investigation showed that the horseshoe vortices play the main role in the scour around the bridge piers (Dargahi, 1990; Unger & Hager, 2007; Akoz, 2009; Lee & Sturm, 2009). At the early stage scouring occurs in the wake region behind the cylinder. The primary wake vortices and accelerated side flow are the main cause of this scouring. Countermeasures surrounding bridge piers for scour reduction were applied to diminish the down-flow strength and the horseshoe vortex that consider as major reasons causing local scour around hydraulic structures (Parker et al., 1998; Y. Chiew & Lim, 2003). The horseshoe vortex were experimentally investigated and the results showed that the down-flow and the vortices are the basic mechanisms for local scour process. It has been found that the size of the vortex enlarges with the increasing of the scour void (Muzzammil et al., 2004). Dey and Raikar (2007) reported that the horseshoe vortex size becomes larger with the development of the scour pit. In other words, reducing the horseshoe vortex strength by preventing it from escaping downstream consequent in a reduction in scour depth significantly (Beg & Beg, 2013). The scale influence on turbulent flow and sand sediment scour close bridge pier was numerically investigated by Huang.et.al (2009). The computational data was obtained by Fluent, was

compared with experimental data, and the comparison showed good agreement. Results showed that some of turbulence quantities are difficult to be measured such as vortex which was the main factor lead to bed scouring. Smith and Foster (2005) investigated a numerical study to simulate and examine the steady flow surrounding a circular cylinder at five scoured phases. Both *k*-Ɛ and Smagorinsky LES turbulence models were used to simulate the flow filed modeling. The numerical results showed satisfactorily agreement against the experimental data of Jensen.et.al (1990), and it revealed that the change in grid size affects and the frequency as well as the magnitude of the shedding vortex. The experimental work reported by Unger and Hager (2007) was aimed to study local scour basic mechanisms characteristics of sediment surrounded the bridge piers. The results revealed that the horseshoe vortex within the scour pit and the vertical jet are the main scour agents. In other words, a scour pit is formed due to the horseshoe vortex that has enough strength to wash the sand sediment particles from the sand bed (Bateman et al., 2005) and as the scour depth increases the horseshoe vortex diminishes (Lagasse & Richardson, 2001). A numerical simulation was developed to study the flow surrounding obstructions. The study conducted by Das and Raikar (2007) revealed that the horseshoe vortex differs with different pier's shape. Thus, it was observed that the horseshoe vortex size of a circular pier is smaller than the square pier (Das et al., 2013). An experimental investigation was done by Melville and Raudkivi (1996) to study the effects of foundation geometry on bridge pier scour. The results revealed that the horseshoe vortex increases and deepens the scour.

2.4 CFD modeling

In following sub-sections, previous studies for predicting scour formation using CFD modeling techniques, i.e., scour modeling, multiphase-model, turbulence modeling will be discussed.

2.4.1 Scour modeling

The CFD-based methods were primarily utilized for scour modelling in the 1990s. The previous methods were run to model flow simulations coupled with a morphological description that drives the deformation of the bottom computational mesh to produce a scour hole. In the following years, a successive refinement is being applied for the calculation of the mesh deformation tensor to simplify modelling complexity. A boundary adjustment technique is a mesh deformation technique that is used to represent the factors that cause sediment redistribution as a result of scouring formation. These include the local hydrodynamics, resolved to an appropriate level, associated structures, pressure gradients and bed shear stresses (Lu et al., 2005). They have been employed which relates the magnitude of deformation to the equilibrium of the bottom shear stress (τ) and critical threshold for incipient sediment motion (τ_c), i.e. the mesh vertices are adjusted in vertical direction in response to the impinging flow until the condition $\tau = \tau_c$ is reached. More common method based on sediment transport theory in which the morphological model consists of bed-load and/or suspended sediment equations and the bed evolution is determined by solving the mass balance of sediment equation (Olsen & Melaaen, 1993; Brørs, 1999; Liang et al., 2005; X. Liu & García, 2008).

Boundary adjustment technique using deforming or moving grids have often relied upon the grid structure in order to provide a convenient mechanism for repositioning the internal grid points in response to the deforming interface. The method represents one of the techniques for tying the deformation of the internal mesh to that of the interface. In

their simplest manifestation, spines represent guiding lines to which internal mesh is constrained. The grid mesh is constructed by dividing the mesh into two regions; inner fixed mesh region and an outer moving mesh region. The moving region is constructed by defining spines that are approximately normal to the initial ablating surface and its nodes are regularly structured.

More recently, scour predictions based on two-phase (water-sand) flow considerations have been presented. Euler-Euler models treat the fluid and solids as phases as interpenetrating continua capable of exchanging properties like mass and momentum. The advantage of two-phase models is that fluid-solid and solid-solid interactions are considered and no empirical relations are required.

2.4.2 Multiphase models

The Euler-Euler (E-E) method has recently been applied to scour studies around marine pipelines (Z. Zhao & Fernando, 2007; Yeganeh-Bakhtiary et al., 2011) with promising success. The E-E method establishes conservation equations for both phases based on single-phase conservation equations with additional terms for inter phase exchanges of mass and momentum. The particle-particle interaction is governed by the kinetic theory of granular flow which describes viscosities for the kinetic, collisional and frictional regimes.

Several issues have been identified with the standard solver (fluid-sand interaction method). Using kinetic theory alone to control the maximum solid fraction, the bed is subject to strong over packing. The attenuation of flow in the near-bed area is caused by an inadequate representation of the particle-turbulence interaction which causes a strong reduction in flow velocity leading to rapid settling out of particles near the pipe. Another issue is a discrepancy in timescales. The characteristic timescale of particle-turbulence interaction is shorter than the time required for the flow to adjust to the bed morphology change, causing errors in the scour calculation which has also been reported by (Zhao & Fernando, 2007). A number of modifications are required to alleviate over packing, a particle normal force model is used that introduces a solids pressure term in the conservation equation. Initial inclusion has shown to improve the control of the maximum solid fraction. For issues with particle-turbulence interaction a number of potential remedies have been identified. Two-phase turbulence model which includes the terms for the effect of particles on turbulence was developed by (Elghobashi & Abou-Arab, 1983). Another option could be a “frozen bed switch” which entails not solving for the solid phase while the hydrodynamics are calculated; once the flow is fully developed, both phases are solved to allow for bed adjustment before returning to the previous step in figures 2.2 (a) and 2.2(b). Similarly, iterative mapping between a transient single-phase

and the E-E solver could be used to provide accurate hydrodynamics while respecting the disparity between the characteristic timescales (Melling et al., 2011).

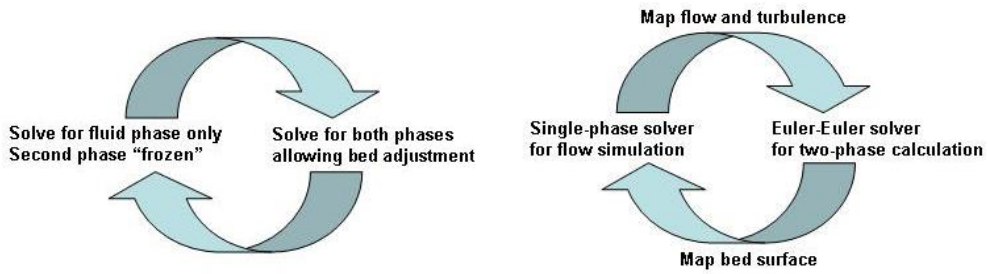

Figure 2.2: Bed adjustment of two phase models (a) Frozen bed switch, and (b) Iterative mapping between solvers (Melling et al., 2011).

The correlations of interfacial forces in multiphase flows were used to study the interaction among phases (Akib et al., 2014). The interaction between liquid (water) phase and sand is determined by solving the momentum equation which includes interfacial forces i.e., drag, lift and added mass forces. E-E model often uses the drag force as the prominent interfacial force to predict local scour surrounding circular cylinder. Many studies have used only the drag force in order to predict local scour (see table 2.1). However, some studies have used different interfacial forces simultaneously in the solving of the momentum equation. Computing a pair or all the interfacial forces in some cases will result in more accurate prediction of local scour and flow modelling around obstruction. Table 2.1 shows various multiphase methods, interfacial force and turbulence models to study the local scour and flow modelling. The table shows that, the drag and lift models can be applied in many different operation conditions while added masses forces rarely used as interfacial forces in the momentum equation for simulating local scour.

Table 2.1: Summary of numerical studies for local scour modeling

Turbulence models	Interfacial force models	Structure shape	Multiphase models	Ref.
k- ε	Symmetric drag	Circular pipe	Eulerian	(Z. Zhao & Fernando, 2008)
k- ε	Drag and lift coefficients, inter-granular stresses	Circular pipe	Euler-Euler	(M. Kazeminezhad & Yeganeh-Bakhtiary, 2011)
k- ε	Symmetric drag	Circular pipe	Eulerian	(Z. Zhao & Fernando, 2007)
k- ε	Drag, lift coefficients and added mass forces	Circular pipe	Eulerian	(Hossein Kazeminezhad et al., 2011)
k- ε	An compressive interface capturing Scheme CICSAM is used to re-sharp the interface	Circular pipe	Lagrangian Eulerian (ALE)	(X. Liu & Garciá, 2006)
k- ε	Drag and lift coefficients, inter-granular stresses	Circular pipe	Euler-Euler	(Yeganeh-Bakhtiary et al., 2011)
k- ε	Drag, lift coefficients and added mass forces	Circular pipe	Euler-Lagrange	(Fard et al.)
k- ε	Drag, lift coefficients and added mass forces	Circular pipe	Euler-Lagrange	(Hajivalie et al., 2012)
k- ε Smagorinsky LES	The interface with solid boundaries is simulated by (FAVOR) method	Circular pipe	Volume Of Fluid (VOF)	(Smith & Foster, 2005)

The drag force is the horizontal component of the hydrodynamic force relative to the flow directions. Symmetric drag model is employed to describe the interaction between fluid (water) phase and sand phase. The symmetric drag model is used for the fluid-fluid drag function, and it is recommended for flows in which the secondary (dispersed) phase in one region of the domain becomes the primary (continuous) phase in another. Note that, in numerical studies when the sand sediments have the same diameter size, a constant drag coefficient (mostly used as 0.5 for diameter size of 0.36 mm, see Table 2.2) can be used instead of the drag models in order to reduce the computational time, and some

studies have employed the drag models instead of the drag coefficient. Unlike the drag force, the lift force is the perpendicular component of the hydrodynamic force relative to the flow directions, and it has a significant effect on defining the flow pattern in the scoured bed pit. For granular flows, the effect of lift forces may be included on the secondary phase particles. Theses lift forces at on a particle due to velocity gradients in the primary phase flow filed. In most cases, the lift force is insignificant compared to the drag force. Thus, it is employed as interfacial forces. The lift coefficient for sand sediment having the same diameter size which is 0.5 for a sand diameter size of 0.36 mm can be used as an interfacial force for multiphase water-sand interaction simulation (see Table 2.2). The virtual mass force is the work performed by the sand sediment particles from the acceleration of the fluid near bed. The fluid acceleration is automatically computed through the calculation of the virtual mass force. There is no significant contribution of virtual mass model for different sand sediment particles (see Table 2.2). Table2.2 shows the two-phase system, flow velocity, sand diameter size , shields parameter and pipe diameter to study the local scour, and the flow modelling which contributes with the interfacial forces to the sand erosion and plays a major role to interfacial forces changes.

Table 2.2: Summary of the system properties of several studies reviewed

System	Flow inlet	Sand size mm	Shields parameter (θ)	Pipeline diameter (m)	Ref.
Water-sand	0.052m^3/s	0.27mm	----------	0.1m	(Thanh et al., 2014)
Water-sand	0.247m/s	0.825 mm	0.11	0.2m	(Das et al., 2013)
Water-sand	0.25m/s	0.385mm	0.0001	5.08 cm	(Zhu & Liu, 2012)
Water-sand	0.35m/s	0.36 mm	0.26	0.1m	(Yeganeh-Bakhtiary et al., 2011)
Water-sand	0.5 m/s	0.36 mm	0.08	0.1m	(M. Zhao & Cheng, 2010)
Water-sand	0.028m^3/s	0.95 mm	0.92	0.04 m	(Mashahir et al., 2009)
Water-sand	0.5 m/s	0.36 mm	0.098	0.1m	(Z. Zhao & Fernando, 2008)
Water-sand	0.31m/s	0.36 mm	0.048	0.1m	(Z. Zhao & Fernando, 2007)
Water-sand	Wave maker	0.2 mm	0.07	1 m	(X. Liu & Garciá, 2006)
Water-sand	0.35m/s	0.36 mm	0.048	0.1m	(Fard et al.)

2.4.3 Turbulence modeling

Turbulence modeling is used to predict the turbulence flow behavior and characteristics. None of the existing models can be used universally to analyze all the problems encountered in various engineering applications. However, each model has its own advantages and limitations depending upon the nature of the flow and the desired accuracy. In numerical study, turbulence models that are available to investigate the flow filed are two-equation *k*- ε models, two-equation *k*-ω models, five-equation Reynolds stress models and large eddy simulation (LES) model. Thus, the aim of this part is to discuss the advantages and limitations of each model to simulate the local scour and report the comparison among them (refer to tables 2.3, 2.4 and 2.5).

2.4.3.1 *k*- ε Models

Two-equation *k*- ε models, turbulence kinetic energy, *k* and turbulence dissipation, ε, are the simplest and the most widely used models among all turbulence models that aim to simulate the influence of turbulent in the flow. The two-equation model involves with two extra transport equations to represent the turbulence properties of the flow. There are three different models that are derived from *k*- ε model, standard *k*- ε model, Realizable *k*- ε model and Re-Normalization Group method (RNG) model. Despite of having the two common equations, these turbulence models use the different ways to calculate the principle form of the eddy viscosity equation, turbulent Prandtl number, and the generation and the dissipation term ε. is used User-specified constant value of the turbulent Prandtl numbers is used in the standard *k*- ε model (Launder et al., 1975), whereas the RNG *k*- ε model uses an analytically-derived formula (Yakhot & Orszag, 1986). The realizable *k*- ε model contains different formulation for turbulent viscosity and dissipation rate ε based on exact equation of vortices fluctuations (Yakhot & Orszag, 1986).

There are various studies carried out to investigate scouring process using *k*- ε turbulence model, see refs (Fard et al.; Celik & Rodi, 1988; Van Beek & Wind, 1990; Olsen & Melaaen, 1993; Cheong & Xue, 1997; Brørs, 1999; Jia et al., 2001; Ge et al., 2005; Ge & Sotiropoulos, 2005; Liang & Cheng, 2005; Liang et al., 2005; Nagata et al., 2005; X. Liu & Garciá, 2006; Z. Zhao & Fernando, 2007; Bihs & Olsen, 2010; M. H. Kazeminezhad et al., 2010; Kocaman et al., 2010; Hossein Kazeminezhad et al., 2011; M. Kazeminezhad & Yeganeh-Bakhtiary, 2011; Yeganeh-Bakhtiary et al., 2011; Nielsen et al., 2013) have mostly focused on the scour around piers and use of the *k*- ε turbulence model for analyzing scour process. The work reported by Liang and Cheng (2005) numerically investigated the flow filed and scouring depth underneath a pipe in currents. The performance of four turbulence models (which are standard *k*- ε, Wilcox high-Reynolds number *k*-ω, Wilcox low-Reynolds number *k*-ω and Smagorinsky subgrid scale turbulence models) are tested against flow filed surrounding a circular cylinder above a solid wall. A CFD study to predict the accurate turbulence model for simulating local scour with the time development under clear water and live bed conditions was carried out by Liang et al (2005). The standard *k*- ε model and (SGS) LES model are used to predict the flow filed, and models were compared by Tulimilli et al (2011). They found that LES turbulence model provides accurate and desired flow filed results for local scour prediction. However, its simulation takes quite long time to be completed within a day or two which can be used for practical scour simulation that required a high computer performance while the standard *k*- ε model is employed to obtain reasonable computation times. The work reported by Salaheldin et al (2004) numerically investigated the performance of several turbulence models in predicting flow field around circular pipelines. Simulations are conducted using *k*- ε turbulence models and the Reynolds stress model (RSM) turbulence models.

2.4.3.2 *k-ω* models

k-ω models, also known as two equation models, have the same definition for *k* as in *k*- *ε* model. However, it differs in the selection of second variable (ω). This model is broadly categorized into two types, the standard *k*-ω model and the Shear Stress Transport (SST) model. The standard *k*-ω model is an empirical model based on model transport equations for the turbulence energy (*k*) and the specific dissipation rate (ω), which can also be thought of as the ratio of *ε* to *k*. As the *k*-ω model has been modified over the years, production terms have been added to both the *k* and ω equations, which have improved the accuracy of the model for predicting free shear flows (Wilcox, 1998). In addition, over the last years, the *k*-ω model has been improved by adding few production terms to the *k* and ω equations. Thus, the desired free shear flows prediction gets modified. In addition, the shear stress transport (SST) *k*-ω model is also provided by FLUENT. It is improved for calculating the transport of turbulence shear stress principal. This feature makes (SST) *k*-ω model perform over other turbulence models such as standard *k*-ω and standard *k*-ε (FLUENT, 2014).

Series of numerical investigations have been done by (F. Li & Cheng, 1999; Chrisohoides et al., 2003; Akoz & Kirkgoz, 2009; Gislason et al., 2009; Zang et al., 2009; Khosronejad et al., 2012) using *k*-ω turbulence model to simulate flow pattern and scour around piers and abutments. The work reported by Esmaeili et al (2009) is concluded that *k*-ω predicts more accurate and reasonable results for simulating the scour around pier in a natural river. The work reported by Akoz and Kirkgoz (2009) numerically and experimentally investigated the flow filed around a horizontal wall mounted circular cylinder. ANSYS 10.0 FLOTRAN program was employed to solve the governing equation using Finite Element Method (FEM) and examine the performance of the standard *k*- *ε*, standard *k*-ω and SST turbulence models.

2.4.3.3 Reynolds stress model (RSM)

Unlike the previous two turbulence models, RSM abandon the calculation of eddy viscosity and solve the transport equation for Reynolds stresses. It provides four additional equations for 2-D flow and seven for 3-D flow. Having these additional equations, RSM takes comparatively more effort and time to simulate the flow. The specification of turbulent boundary condition for the RSM is the same as for the other turbulence models for all the boundaries except at boundaries where flow enters the domain (FLUENT, 2014). A CFD study is done by Salaheldin et al (2004) numerically investigated the flow field surrounding obstruction using RSM model.

2.4.3.4 Large Eddy Simulation (LES)

A large-eddy simulation (LES) model explicitly calculates the large-eddy field and parameterizes the small eddies. The large eddies in the atmospheric boundary layer are believed to be much more important and insensitive to the parameterization scheme for the small eddies. In LES, the large three-dimensional unsteady turbulent motions are directly resolved while the smaller scale motions are modelled. In terms of computational effort LES lies between RANS and DNS, and it can be expected more accurate and reliable than Reynolds-stress models for flows where large-scale unsteadiness is significant (Moeng, 1984; Ghosal & Moin, 1995; Gokhan Kirkil et al., 2005; Vass et al., 2005; Teruzzi et al., 2006).

Table 2.3: Turbulence models for predicting velocity near the bed

Turbulence Model (s)	Remarks	Ref.
k- *ε*	The k-Ɛ turbulence model is capable of modelling the velocity profile near an offshore pipeline	(Smith & Foster, 2005)
RNG *k*- *ε* realizable *k*- *ε* RSM	The standard and the RNG *k*- *ε* models slightly overestimate the velocity near the bed. The realizable *k*- *ε* model largely overestimates the velocity field near the bed and should not be used. The RSM is found to give satisfactory results for estimating the velocity variation around the pier in the case of flat bottom and for estimating the velocity field and water level variation in the case of equilibrium scour.	(Salaheldin et al., 2004)
RNG *k*- *ε*	The renormalization group (RNG) *k*- *ε* model gives a good estimation of the velocity field.	(Fluent, 2014)
k- *ε* k-ω SST	The numerical modelling using either *k*-ω or SST turbulence models provided better estimations of horizontal velocity component than the *k*- *ε* model.	(Fayyadh et al., 2011)

Table 2.4: Turbulence models for predicting bed shear stress

Turbulence Model (s)	Remarks	Ref.
k- *ε*	The standard k- *ε* model is able to accurately predict incoming seabed shear stress.	(Liang et al., 2005)
k- *ε* LES	Both models k- *ε* can predict various bed shear stresses at the upstream of the cylinder. The bed shear stress in the LES model is more intensive and extensive than the k- *ε* model. The LES model has shown better results than k- *ε* model at both up-stream and down-stream of the pier.	(Aghaee & Hakimzadeh, 2010)
k- *ε*	The model results obtained using the k- *ε* models showed some discrepancy with the measured bed stress.	(Salaheldin et al., 2004)
RNG k- *ε*	The renormalization group (RNG) k- *ε* model gives a good estimation of the bed shear stress.	(Kaniil Ali et al., 1997)

Table 2.5: Turbulence models for predicting vortex shedding

Turbulence Model (s)	Remarks	Ref.
LES (SGS) *k*-ω	SGS model over-predicts the shedding of vortices from the cylindrical. The Wilcox *k*-ω models give better predictions on the shedding of vortices than their counterparts using the wall function boundary condition.	(Liang & Cheng, 2005)
k- *ε*	The *k*- *ε* turbulence closure model is capable of simulating the vortex shedding phenomena.	(M. H. Kazeminezhad et al., 2010)
k- *ε*	The *k*- *ε* model is not capable of modelling the strong vortex shedding for a cylinder over the scoured bed	(H. D. Smith & Foster, 2005)Kattell & Eriksson, 1998
k- *ε*	*k*- *ε* model shows the inability to predict the periodic behaviour of the vortex shedding the both of horseshoe and Lee wake vortices and the model results partly be due to using wall function	(Aghaee & Hakimzadeh, 2010)
k- *ε* LES	k- *ε*was not an appropriate choice for predicting the time-varying nature of the wake namely vortex shedding. Prediction using LES was able to predict vortex shedding in the wake obstacle, with reasonable comparisons with observed Strouhal number. The length of the recirculating region in the lee of the cylinder was also well predicted with the model utilizing the LES	(H. D. Smith & Foster, 2007)

Variants *k*- *ε* models can predict velocity profile near the bed. Standard *k*- *ε* model shows an accurate result with experimental data (H. D. Smith & Foster, 2005) the RNG *k*- *ε* model slightly overestimates the velocity near the bed and the realizable *k*- *ε* model largely overestimates the velocity field near the bed (Salaheldin et al., 2004). In addition, *k*-ω models with using wall function boundary and RMS can both predict the velocity

profile near the bed. Among all turbulence methods, Standard k-ε model gives better predictions for the velocity profile near the bed and simulation using Fluent program by which k-ω models show a discrepancy with the measured data because of the non-existence of the wall function boundary option and the inability of the model to simulate the velocity in the wake region with the strong turbulence.

For simulating bed shear stress over scoured bed, the k-ε models can predict the seabed shear stress. The LES model can predict the seabed shear stress and shows better results than k-ε models (Aghaee & Hakimzadeh, 2010) . Thus, among all turbulence methods, LES model can be better predict the seabed shear stress for a circular cylinder over a scoured bed. In general, the k-ε models are not capable of modelling the vortex shedding for a cylinder over scoured bed. The k-ω models give good predictions on the shedding of vortex by using the wall function boundary condition. The RSM turbulence model may not be accurate for simulating vortex shedding, and the LES model may be capable to predict the vortex shedding, and in some cases it shows over prediction. Among all turbulence methods, LES model can be better predict the vortex shedding for a cylindrical cylinder over scoured bed.

The standard and RNG k-ε models with the use of wall function can predict the local scour surrounding circular cylinder. The k-ω and LES models can also predict the local scour around a circular cylinder over sandy bed but with some limitations. Among all turbulence methods, standard k-ε model is widely used and recommended for scour process modelling, and it shows good predictions with experimental data as it was mentioned in the literature. Table 2.6 shows turbulence models that are employed to study the local scour around circular cylinder.

Table 2.6: Comparison between the turbulence models

Turbulence Model (s)	Remarks	Ref.
k- ε , *k*-ω	Standard *k*-Ɛ outperforms than *k*-ω with the use of wall function.	(Liang & Cheng, 2005)
k- ε LES (SGS)	Both models predict the overall scour pit development reasonably well. Standard *k*- ε gives better prediction than LES (SGS) on time dependent scour profiles, especially at the later stages of the scour. Author recommended the standard *k*- ε model for the scour modelling process.	(Liang et al., 2005)
RNG *k*- ε	The RNG turbulence model is capable of predicting the equilibrium profile of local scour submarine pipeline.	(Lu et al., 2005)
RNG *k*- ε	The results obtained using the RNG *k*- ε model are virtual identical to those produced by the *k*- ε model.	(Fayyadh et al., 2011)
k-ω	The *k*-ω predicts more accurate and reasonable results among various turbulence models for simulating the scour around piers in a natural river.	(Esmaeili et al., 2009)

2.5 Summary of literature

The current literature review is summarized as follow:

- Previous studies have highlighted the two major parameters viz. the strength of the down-flow and the horseshoe vortex held responsible for local scouring formation.
- There are two numerically scour modeling methods which are Mesh deformation techniques and Multiphase models. Mesh deformation techniques are based on Boundary adjustment techniques and Sediment Transport theory models and Multiphase models are based of Eulerian-Eulerian (E-E) two phase models.
- To enhance the accuracy of prediction of local scour, interfacial forces i.e. drag, lift etc. have to be accurately selected. According to previous discussion, symmetric drag and E-E model are recommended as drag models and multiphase models, respectively. The lift model and added mass forces are often used in the investigation of local scour and they are given a value of 0.5. A proper measurement technique for sand sediment removal, shape and diameter can enhance the accuracy of simulation
- Turbulence models are not utilized to solve all problems may be faced in engineering applications thus it is better to study their advantages and limitations on simulating basic elements (such as velocity under pipe, pressure and wall shear stress around pipe etc.) which lead to scour formation. According to previous studies in the literature, simulating local scour requires proper techniques selections and factors that are affect scour depth.
- This study is aimed to study the effect on bluff body shapes and the effect of gap between circular body and wall of sand bed, and the sensitivity of

turbulence models study of the flow around the pipe by modeling unsteady horizontal velocity and square root turbulent kinetic energy and to computationally study the scour gap effect of unsteady flow around pipe

Chapter 3.0

The effect of bluff body shapes and gap between horizontal circular body and wall of sand bed

3.1 Introduction

In this chapter, a numerical investigation is carried out to study the effect of the different pipe cross section geometry on the flow. Furthermore, the effect of the gap between the sand bed and pipe surface on the flow has also been investigated. In order to study the effect of the geometry, four different shapes which are cylinder, square, square with round edges, and rectangle have been chosen to simulate their effect on the flow characteristics. These kinds of bodies are also known as bluff bodies. This section is divided into three sub-sections which are velocity profiles around bluff bodies, pressure distribution around bluff bodies, and turbulence models sensitivity in producing vortex shedding. Six turbulence models (variants k- ε models; standard k- ε model, Realizable k- ε model and Renormalization Group model (RNG), variants k-ω models; standard k-ω model and the shear stress transport (SST) model, and Reynolds Stress Model (RMS)) have been utilized to conduct the sensitivity study while Standard k- ε model has been used to simulate the velocity and pressure distribution around the bluff bodies.

To study the effect of the gap between the sand bed and pipe surface (circular shape), five gaps G/D = 0.0, 0.1, 0.2, 0.4 and 0.8 using Standard $k-\varepsilon$ turbulence model have been used to simulate the flow around the circular shape. This part is divided into three sections, which are the effect of gaps between the wall bed and cylinder on the flow, pressure over surface bed, and wall shear stress over sand wall bed surface.

3.2 Geometry of different cross section view of pipe

Figure 3.1 shows the schematic of the two dimensional (2D) geometrical domain used in the present study along with the corresponding boundary conditions and Fig 3.2 shows the different geometries chosen in this study. The domain for these simulations were chosen as suggested by Jensen et al. (1990) for flat-bed wall .The length of the domain is 20D, where D is the diameter of pipe and the height of the domain is 4D. The pipe has been placed in such a way that its center distance from the inlet is 5D and from the outlet is 15D, as shown in Fig 3.1the chosen pipe diameter D in the current investigation is 0.1m.

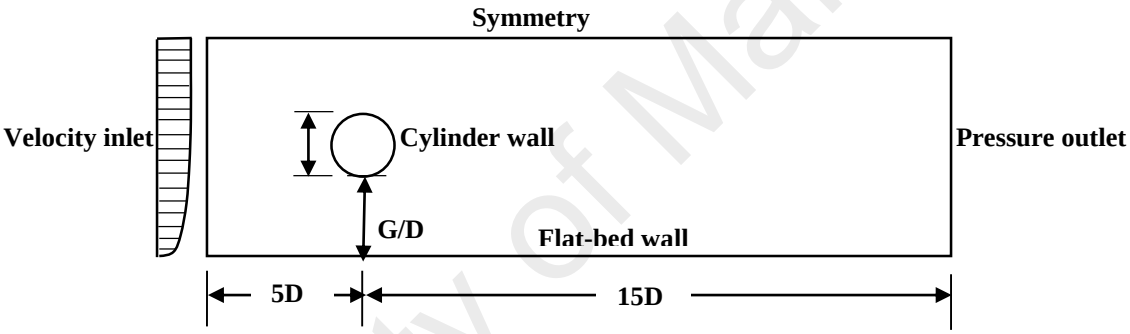

Figure 3.1: Geometrical model of computational domain and boundary conditions.

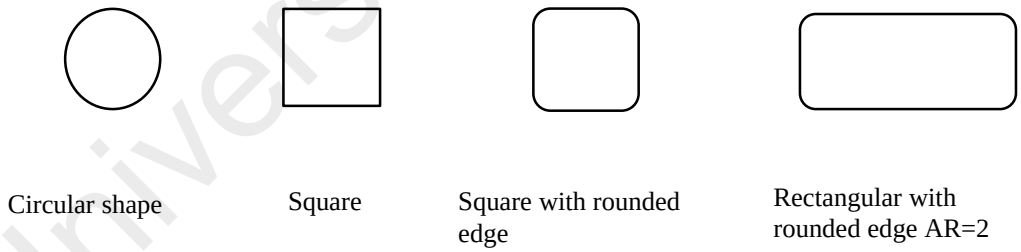

Figure 3.2: Selected geometrical shape of pipes for the present investigation

3.3 Governing equations

The continuity and the momentum equations for the present case are as given below:

Continuity equation:

$$\frac{\partial u}{\partial x}+\frac{\partial v}{\partial y}=0 \tag{1}$$

X-component of the momentum equation:

$$\rho\left(u\frac{\partial u}{\partial x}+v\frac{\partial u}{\partial y}\right)=-\frac{\partial \rho}{\partial x}+\mu\left(\frac{\partial^2 u}{\partial x^2}+\frac{\partial^2 u}{\partial y^2}\right) \tag{2}$$

Y-component of the momentum equation:

$$\rho\left(u\frac{\partial v}{\partial x}+v\frac{\partial v}{\partial y}\right)=-\frac{\partial \rho}{\partial y}+\rho g+\mu\left(\frac{\partial^2 v}{\partial x^2}+\frac{\partial^2 v}{\partial y^2}\right) \tag{3}$$

3. 4 Turbulence models

Turbulence models of two-equation *k*- ε, two-equation *k*-ω models and five-equation Reynolds stress models are used in the present research and their results are compared with experimental data from the literature (B. Jensen et al., 1990).

3.4.1 *k*- ε models

Two-equation *k*- ε models, turbulent kinetic energy *k* and turbulent dissipation ε, are the simplest and the most widely used models among all turbulence models that aim to study the effect of turbulence in the flow. The two-equation model signifies that it includes two extra transport equations (Eq.5, 6) to represent the turbulence properties of the flow. There are three different models that are derived from *k*- ε model, standard *k*- ε model, Realizable *k*- ε model and Renormalization Group model (RNG). Despite of having the two general equations, these turbulence models use the different way to calculate the principle form of the eddy viscosity equation.

The variants *k*- ε models approximate the eddy viscosity as

$$\mu_t = \frac{\rho C_u k^2}{\varepsilon} \tag{4}$$

The turbulent kinetic energy (*k*) and its dissipation rate (ε) for the standard *k*- ε model are calculated from:

$$\frac{\partial}{\partial t}(\rho k) + \frac{\partial}{\partial x_i}(\rho k u_i) = \frac{\partial}{\partial x_j}\left[\left(\mu + \frac{\mu_t}{\sigma_k}\right)\frac{\partial k}{\partial x_j}\right] + G_k + G_b - \rho\varepsilon + S_k \tag{5}$$

$$\frac{\partial}{\partial t}(\rho \varepsilon) + \frac{\partial}{\partial x_i}(\rho \varepsilon u_j) = \frac{\partial}{\partial x_j}\left[\left(\mu + \frac{\mu_t}{\sigma_\varepsilon}\right)\frac{\partial \varepsilon}{\partial x_j}\right] + C_{1\varepsilon}\frac{\varepsilon}{k}(G_k + C_{3\varepsilon}G_b) - C_{2\varepsilon}\frac{\varepsilon^2}{k} + S_\varepsilon \tag{6}$$

The model constants are $C_{1\epsilon} = 1.44, C_{2\epsilon} = 1.92, C_{3\epsilon} = -0.33, C_\mu = 0.09, \sigma_k = 1.0, \sigma_\epsilon = 1.3$

The modeled transport equations for (*k*) and (ε) in the RNG *k*- ε model are:

$$\frac{\partial}{\partial t}(\rho k) + \frac{\partial}{\partial x_i}(\rho k u_i) = \frac{\partial}{\partial x_j}\left(\alpha_k u_{eff}\frac{\partial k}{\partial x_j}\right) + G_k + G_b - \rho\varepsilon + S_k \tag{7}$$

$$\frac{\partial}{\partial t}(\rho \varepsilon) + \frac{\partial}{\partial x_j}(\rho \varepsilon u_i) = \frac{\partial}{\partial x_j}\left(\alpha_\varepsilon u_{eff}\frac{\partial \varepsilon}{\partial x_j}\right) + C_{1\varepsilon}\frac{\varepsilon}{k}(G_k + C_{3\varepsilon}G_b) - C_{2\varepsilon}\rho\frac{\varepsilon^2}{k} - R_\varepsilon + S_\varepsilon \tag{8}$$

The model constants are $C_{1\epsilon} = 1.42, C_{2\epsilon} = 1.68, C_\mu = 0.084$.

The modeled transport equations for (*k*) and (ε) in the realizable *k*- ε model are:

$$\frac{\partial}{\partial t}(\rho \kappa) + \frac{\partial}{\partial x_j}(\rho \kappa u_j) = \frac{\partial}{\partial x_j}\left[\left(u + \frac{u_t}{\sigma_\kappa}\right)\frac{\partial \kappa}{\partial x_j}\right] + G_\kappa + G_b - \rho\varepsilon + s_\kappa \tag{9}$$

$$\frac{\partial}{\partial t}(\rho \varepsilon) + \frac{\partial}{\partial x_j}(\rho \varepsilon u_j) = \frac{\partial}{\partial x_j}\left[\left(u + \frac{u_t}{\sigma_\kappa}\right)\frac{\partial \varepsilon}{\partial x_j}\right] + \rho C_{1\varepsilon}S_\varepsilon + \rho C_2\frac{\varepsilon^2}{\kappa + \sqrt{\nu\varepsilon}} + C_{1\varepsilon}\frac{\varepsilon}{\kappa}C_{3\varepsilon}G_b + S_\varepsilon \tag{10}$$

The model constants $C_2, \sigma_k,$ and σ_ε have been established to ensure that the model performs well for certain flows. The model constants are:

$C_{1\varepsilon} = 1.44, C_2 = 1.9, \sigma_k = 1.0, \sigma_\varepsilon = 1.2$

3.4.2 *k*-ω models

k-ω models, also known as two equation models, have the same definition for *k* as in *k*- ε model. However, it differs in the selection of second variable (ω). This model is broadly categorized into two types, the standard *k*-ω model and the shear stress transport (SST) model.

The turbulent viscosity μ_t for the *k*-ω model is computed by combining (*k*) and (ω) as follows:

$$\mu_t = \alpha^* \frac{\rho k}{\omega} \tag{11}$$

The modeled transport equations for (*k*) and (ω) in the standard *k*-ω model are:

$$\frac{\partial}{\partial t}(\rho k) + \frac{\partial}{\partial x_i}(\rho k u_i) = \frac{\partial}{\partial x_j}\left(\Gamma_k \frac{\partial k}{\partial x_j}\right) + G_k + S_k \tag{12}$$

$$\frac{\partial}{\partial t}(\rho \omega) + \frac{\partial}{\partial x_i}(\rho \omega u_i) = \frac{\partial}{\partial x_j}\left(\Gamma_\omega \frac{\partial \omega}{\partial x_j}\right) + G_\omega + S_\omega \tag{13}$$

The modeled transport equations for (*k*) and (ω) in the SST *k*-ω model are:

$$\frac{\partial}{\partial t}(\rho k) + \frac{\partial}{\partial x_j}(\rho k u_i) = \frac{\partial}{\partial x_j}\left(\Gamma_k \frac{\partial k}{\partial x_j}\right) + G_k + S_k \tag{14}$$

$$\frac{\partial}{\partial t}(\rho \omega) + \frac{\partial}{\partial x_j}(\rho \omega u_j) = \frac{\partial}{\partial x_j}\left(\Gamma_\omega \frac{\partial \omega}{\partial x_j}\right) + G_\omega + D_\omega + S_\omega \tag{15}$$

3.4.3 Reynolds stress model (RSM)

Reynolds stress model (RSM) abandons the calculation of eddy viscosity and solve the transport equation for Reynolds stresses. It provides four additional equations for 2-D flow and seven for 3-D flow (Fluent, 2014). Having these additional equations, RSM takes comparatively more effort and time to simulate the flow.

The exact transport equation for the Reynolds stresses $\left(\rho\overline{u_i'u_j'}\right)$ is written as follows:

$$\frac{\partial}{\partial t}\left(\rho\overline{u_i'u_j'}\right)+\frac{\partial}{\partial x_k}\left(\rho u_k\overline{u_i'u_j'}\right)=-\frac{\partial}{\partial x_k}\left[\rho\overline{u_i'u_j'u_k'}+\overline{\rho\left(\delta_{kj}u_i'+\delta_{ik}u_j'\right)}\right]+\frac{\partial}{\partial x_k}\left[\mu\frac{\partial}{\partial x_k}\left(\overline{u_i'u_j'}\right)\right]$$
$$-\rho\left(\overline{u_i'u_k'}\frac{\partial u_j}{\partial x_k}+\overline{u_j'u_k'}\frac{\partial u_i}{\partial x_k}\right)-\rho\beta\left(g_i\overline{u_j'\theta}+g_j\overline{u_i'\theta}\right)+\rho'\left(\frac{\partial u_i'}{\partial x_j}+\frac{\partial u_j'}{\partial x_i}\right)-2\mu\overline{\frac{\partial u_i'}{\partial x_k}\frac{\partial u_j'}{\partial x_k}}$$
$$-2\rho\Omega_k\left(\overline{u'_j\,u'_m}\varepsilon_{ikm}+\overline{u'_i\,u'_m}\varepsilon_{jkm}\right)-2\left(\overline{u'_j\,u'_m}\varepsilon_{jkm}+\overline{u'_i\,u'_m}\varepsilon_{jkm}\right) \qquad (16)$$

3. 5 Boundary Conditions

A logarithmic velocity profile as shown in Fig.3.3 is generated using as user-defined functions (UDF) in Fluent 14.0 (Appendix (A)) based on the formulation in equation (20). A logarithmic velocity profile with U_∞ = 0.3 m/s and the intensity and hydraulic diameter were set for the velocity inlet and pressure outlet, respectively, 10 % and 0.4 m. Equations from (17) to (20) represent the boundary conditions.

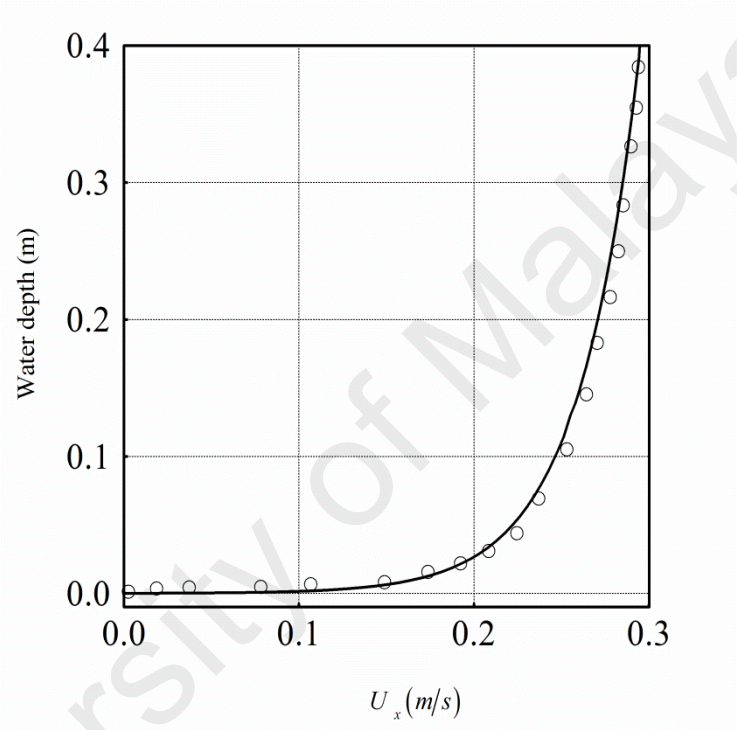

Figure 3.3: Comparison of the horizontal logarithmic velocity-inlet ($\boldsymbol{U_0}$) in the total water depth between, ○present numerical investigation and, ━ experimental work of Dudley RD (Dudley, 2007).

Pressure outlet, P = 0 (17)

Symmetry surface, $\frac{\partial u}{\partial z} = \frac{\partial v}{\partial z} = \frac{\partial k}{\partial z} = \frac{\partial \varepsilon}{\partial z} = P = 0$ (18)

Water at wall surface, (no slip condition) $u = \upsilon = 0$ (19)

Velocity inlet, $u_\infty = \frac{u_*}{K} \ln \frac{y}{y_0}$ (20)

3. 6 Numerical methods

The commercial CFD software FLUENT 14.0, which is based on finite volume method (FVM), is used to solve the Reynolds-averaged Navier-Stokes equations for an incompressible flow. The transport governing equations are discretized using the second order upwind spatial discretization method. The pressure-implicit with splitting of operators (PISO) scheme was used for the coupling of the pressure and the velocity fields. The under-relaxation factor of all the components, such as velocity components and pressure correction is kept at 0.3. The scaled residual of 1×10^{-6} is set as the convergence criteria for the continuity and momentum equations. Transient model based on implicit scheme with a time step of 0.01 were used in the current numerical study.

The typical wall treatment function y^+ (= yU_τ/ν) value of the first node in all turbulence models near the bed profile is less than 1. It is used to describe how coarse or fine a mesh for a particular flow and presents the ratio between the turbulent and laminar influences in a cell. The current study shows that the non-dimensional y^+ less than 1 is a suitable selection criterion for determining the appropriate mesh configuration and turbulence model, coupled with near wall treatment, that lead to accurate computational predictions in FLUENT.

3. 7 Simulation cases

A total of 19 cases were analyzed in the present study and have been shown in Table 3.1. Cases (1-5) which are based on circular shape, were run for the calculation of the mean drag coefficient ($\overline{C_d}$), and the mean lift coefficient ($\overline{C_l}$) and the results were compared with Jensen et al.(1990). Six simulation cases (6-11) were run to study the turbulence models sensitivity for identifying the preferred turbulence model for vortex shedding formation and the results are presented in Section 3.8.2.1. Cases (12-14) have been carried out to evaluate the effect of bluff bodies on velocity profiles and pressure distribution using Standard $k-\varepsilon$ model and their results are presented and discussed in Sections 3.8.2.2 and 3.8.2.3 respectively. For this study, circular shape, square shape, square with rounded edges, and rectangular with rounded edge were used. These shapes are commonly used in bridge piers construction. Thus, they were chosen to conduct this part of the current study.

Five simulation cases (15-19) were run to obtain the effect of gap between the sand bed and circular shape on vortex formation, pressure and wall shear stress distribution over the sand bed surface. Five different gaps at G/D=0.0,0.1,0.2,0.4,and 0.8 were chosen based on B. Jensen et al.(1990) experimental data for flat-bed using Standard $k-\varepsilon$ turbulence model and the results are presented and discussed at Section 3.8.3.1, 3.8.3.2, and 3.8.3.3 respectively. These particular gaps were chosen to validate current study with B. Jensen et al. (1990) experimental data and they are equal to the gaps for scoured bed.

Table 3.1: Simulation cases, gaps and turbulence models

Sim* Cases	**Domain**	**Gap (G/D)**	**Turbulence Models**	**Remark**
1-5	(1) (circular cylinder)	0.15	Standard $k-\varepsilon$	To validate the mean drag coefficient ($\overline{C_d}$), and the mean lift coefficient $\overline{C_l}$ (B. Jensen et al., 1990)
6-11	(1) (circular cylinder)	0.15	Standard $k-\varepsilon$ RNG $k-\varepsilon$ Realizable $k-\varepsilon$ Standard $k-\omega$ SST $k-\omega$ RSM	To identify preferred turbulence models for vortex shedding formation
12-14	(1,2,3,4) (circular, square, square with rounded edge, rectangular with rounded edge cylinders)	0.15	Standard $k-\varepsilon$	To evaluate the velocity and pressure profiles.
15-19	(1,2,3,4,5) (circular cylinder)	0.0,0.1,0.2,0.4, 0.8	Standard $k-\varepsilon$	To evaluate the wall proximate effect on vortex, pressure over bed's surface, and wall shear stress over bed's surface

*****Simulation

3.8 Mesh independence and time step test

The domain is meshed using a structured and uniform square grid spacing for *x* and *y*-directions that are used for all the numerical simulation cases, see Fig.3.4. Mesh independence test is carried out using five different types of grids having cell number 30546, 80623, 156344, 236864, and 324895. Considering the characteristics of the flow within the solution domain, a Quad fine mesh is used near the pipe surface and the plane wall and near the bed. The domain with 156344 cells is selected throughout this study, because it shows reasonable accuracy for mean drag coefficient and mean lift coefficient when compared with Jensen laboratory data (B. Jensen et al., 1990) for flat-bed wall. Four different time step sizes (Δt = 0.0001, 0.001, 0.01, and 0.1) were tested and 0.01 is used throughout this current numerical study as there were no deviations observed below this value of time step. The numbers of iterations for this study are kept between 80.

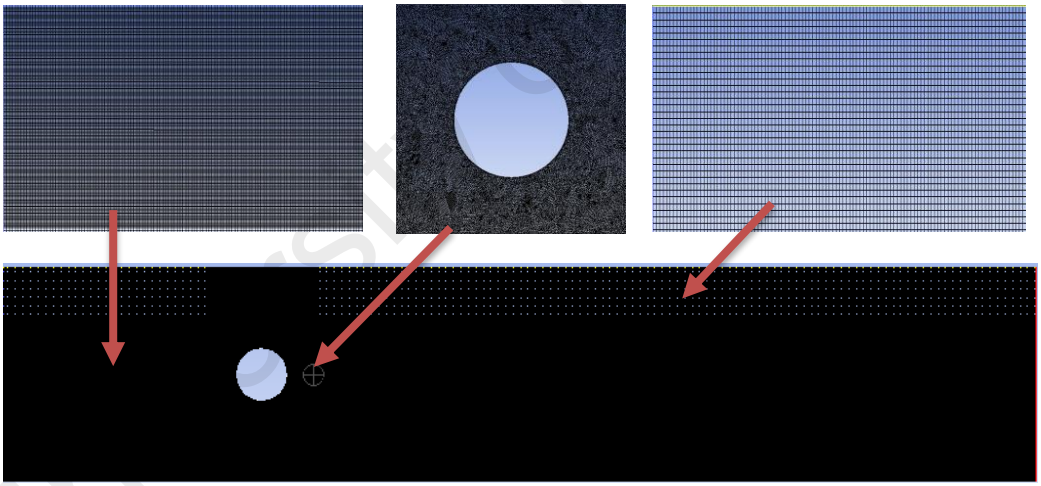

Figure 3.4: The grid for the model

3.9 Results and discussion

3.9.1 Validation

For validation of the present numerical methods, the drag (C_d) and lift (C_l) coefficients on the pipe surface was calculated using simulation Cases 1-5. The results are compared with the same experimental study and shown in Figure 3.5. This domain has been discussed in detail in Section 3.2, Chapter 4. The study of $\overline{C_d}$ and $\overline{C_l}$ of the flow have been obtained for assessing the flow field behavior. The obtained results show good agreement when compared with Jensen et al. (1990) experimental results. It is observed a reduction of 74.36 % in $\overline{C_l}$ and an increase of 12.11% in $\overline{C_d}$ between the gaps of G/D 0 and 0.8. This study aims to investigate the changes of flow parameters with flat bed and compare it when the bed is scoured.

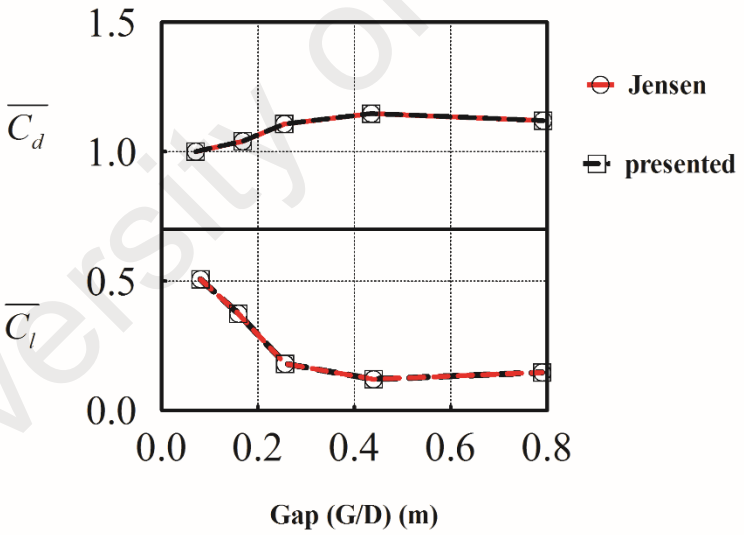

Figure 3.5: The effect of gaps on (a) mean Drag coefficient ($\overline{C_d}$), and (b) Lift coefficient ($\overline{C_l}$) for cylinder surface.

.

3.9.2 Turbulence models sensitivity in predicting vortex shedding

Simulation Cases 1-6 are used to analyze the effect of turbulence models viz. *k*- ε models, *k*-ω models, and RSM model on vortex shedding and the results are presented in Figure 3.6. An arbitrary domain of dimensions 2m × 0.4m and pipe diameter is 0.1m has been chosen for this sensitivity analysis. The vortices are generated at the downstream and get separated periodically from the top and the bottom side of the bluff bodies. Referring to Figure 3.6 (a), the Standard *k*- ε model is capable of producing the vortex around both sides of the circular cylinder. However, it shows the inability to predict the periodic behavior of the vortex shedding around the circular shape in the downstream. This is because; the late transition of the separation boundary layer from laminar to turbulent on both sides of the circular cylinder occurs and the wall function treatment for the circular cylinder wall was not applied. Figure 3.6 (b) and (c) show the prediction of vortex using Realizable and RNG *k*- ε models, both of the models are able to produce the vortex in both sides of the circular cylinder and show the ability to produce the periodic behavior of the vortex shedding. As shown in the Figures, the vortexes from both sides come together in the wake region and separate to be shed along the domain. However, the vortex shedding still is not continuously sheds till the end of the domain. Both models show good separation boundary layer on the circular cylinder.

Nearly the same can be said about *k*-ω models, for both *k*-ω models either Standard *k*-ω model or SST *k*-ω model as shown in Fig .3.6 (d) and (e), the transition to form a vortex occurs. However, they show the inability to predict the periodic behavior of the vortex shedding. This is because the transitional flow option is activated in the naturally low-Re models which are valid all the way to the wall. SST *k*-ω model shows a bit of the interaction and it can be more recommendable than Standard *k*-ω model because of its transport of turbulence shear stress principle. Fig.3.6 (f) shows the prediction of vortex using RSM model. It shows the ability of producing vortex and the periodic behavior of

vortex shedding with limited extend. RSM model has the ability to deal with high flow streamline curvature and strong pressure gradient. It is observed that RANS models is not appropriate for high Reynolds number (Re) simulation, thus they are not suitable to model periodic behavior of vortex shedding.

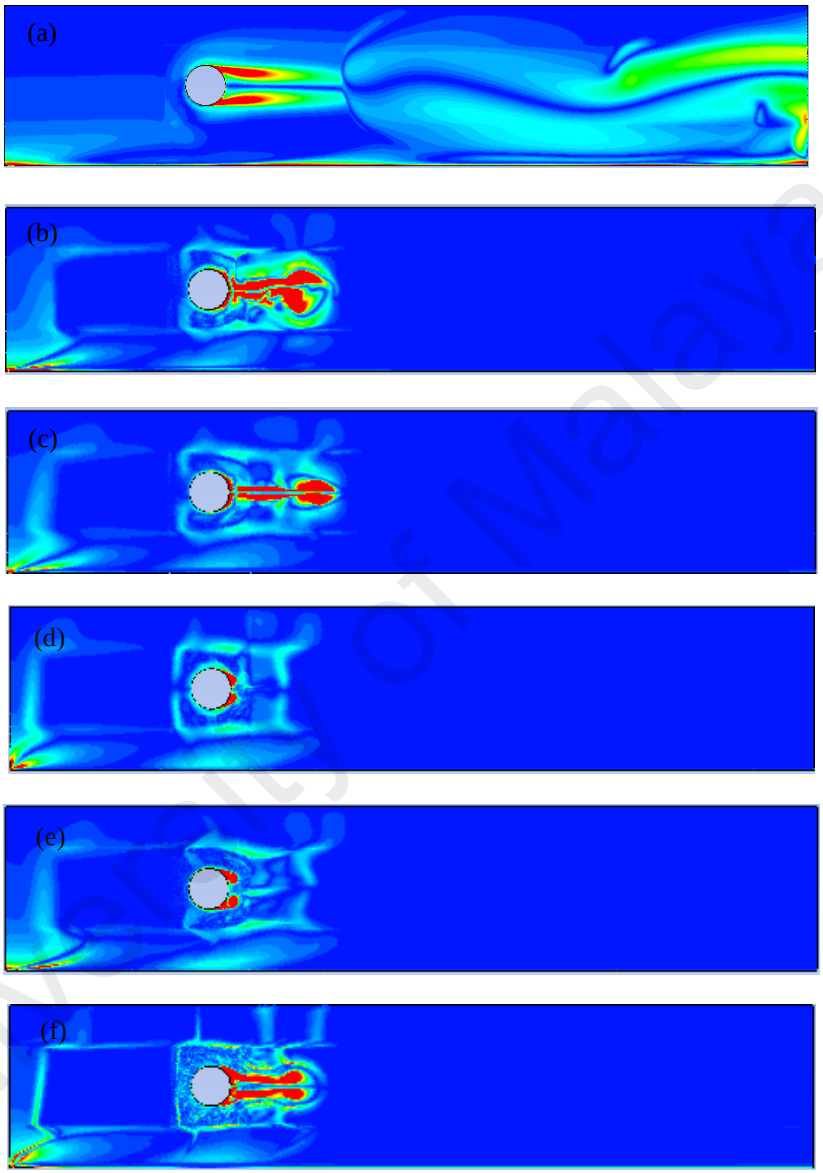

Figure 3.6: Vortex shedding at the downstream of the circular cylinder with different turbulent models, (a) Standard *k*- ε model, (b) Realizable *k*- ε model, (c) RNG *k*- ε model, (d) Standard *k*-ω model, (e) SST *k*-ω model, and (f) RMS model.

3.9.3 Effect of different types of bluff bodies

3.9.3.1 Velocity profiles around bluff bodies

Figure 3.7 shows velocity streamline profiles for different bluff bodies viz. circular cylinder, square cylinder, square rounded edge cylinder and rectangular rounded edge cylinder at downstream of the pipe. Despite the simplicity of bluff body geometry, the flow passes over it causes some very important phenomena such as complex vortex dynamics of the wake, unsteady boundary layer separation points, and shear layer instability. The flow smoothly passes the cylinder and then it separates and creates a highly turbulent region behind the cylinder, which is known as wake region. The pressure distribution in the wake region decreases compared to the pressure at the stagnation point in the front side of the cylinder. In the circular cylinder, the wake region is smaller and narrower with axial lengths x/d=1.7 and y/d=1.0 compared to others. This is because of the asymmetrical boundary layer separation on both sides of the cylinder; see Fig.3.7 (a).The flow at the wake region varies from one geometrical structure to another and vortex shedding changes as well. For example, as it is seen in Fig.3.7(b), the wake region behind the square cylinder with sharp edges shows wider and longer region with axial lengths x/d= 2.2 and y/d= 1.277 compared to others created by flow separation. Early boundary layer separation occurs at both edges and it results larger eddies circulation in the case of square cylinder, while it becomes less wider and longer behind the square with rounded edge cylinder with axial lengths x/d= 1.8069 and y/d= 1.97.This is because of the rounded edges delays a bit the boundary layer separation and as a result eddies circulation becomes smaller, see Fig.3.7(c).For the rectangular rounded edge cylinder the boundary layer separation points create eddies in two stages as shown in Fig 3.7 (b).

First, the eddies are generated on the pipe surface after passing the front round edges and then in the second stage they get generated in the downstream flow which eventually

creates the wake region with x/d= 2.0 and y/d= 1.37.The first stage after passing the in front rounded edge that cause eddies on along the cylinder's surface and then separates in the second stages causing a wake region that includes eddies as well with axial lengths x/d= 2.0 and y/d= 1.37 and as a results there are many circulations eddies on the cylinder sides and at its wake region. As a result, the circular cylinders or circular structures have less circulation eddies and lesser turbulence in the wake region which makes them less prone to failure due to forces the structure experiences during flow.

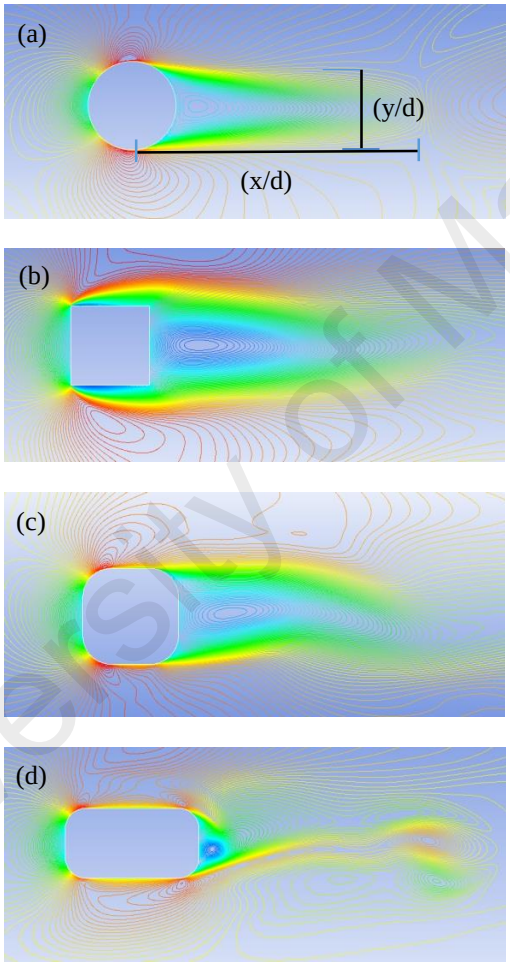

Figure 3.7: Velocity streamlines profiles fat different bluff bodies, (a) circular cylinder, (b) square cylinder, (c) square rounded edge cylinder, (d) rectangular with rounded edge cylinder.

3.9.3.2 Pressure distribution around geometrical structures

The pressure distribution has been plotted for predicting the drag and lift forces and shown in Fig. 3.8. The figure shows the pressure distribution around bluff bodies e.g. circular cylinder, square cylinder, square rounded edge cylinder and rectangular rounded edge cylinder. The pressure at the upstream in the front cross section varies from one geometry to another. Since the cross-section of the bluff bodies in the direction of the flow is larger than that of the circular pipe, so they experience comparatively higher force/pressure during the flow.

The square shape with straight edges (Fig.3.8 b) and rectangular shape with rounded corner (Fig.3.8 d) has the higher values of pressure that dominates the formation the drag and lift coefficients compared to circular shape (Fig.3.8a) and square with round corners (Fig.3.8c). The rounded edge square cylinder shows less pressure distribution on its front cross section (in the direction of flow) compared to the square cylinder with sharp edges. This is because, when fluid flows over bluff body, the boundary layer typically separates from the surface and the separation occurs near the maximum width of the body or at a sharp corner. Thus, most of the structures which are constructed to be exposed to fluid flow are preferred to be circular to avoid the effect of drag and lift forces compared to those constructed by having square shape with sharp edge. The body shape changes from a bluff body with fixed points of separation to a more aerodynamic shape, the effect of pressure and the drag coefficient will decrease. It is observed that the pressure distribution is relatively higher at bodies that have sharper edge and larger cross section while it reduces at the cylinders that have smaller cross section.

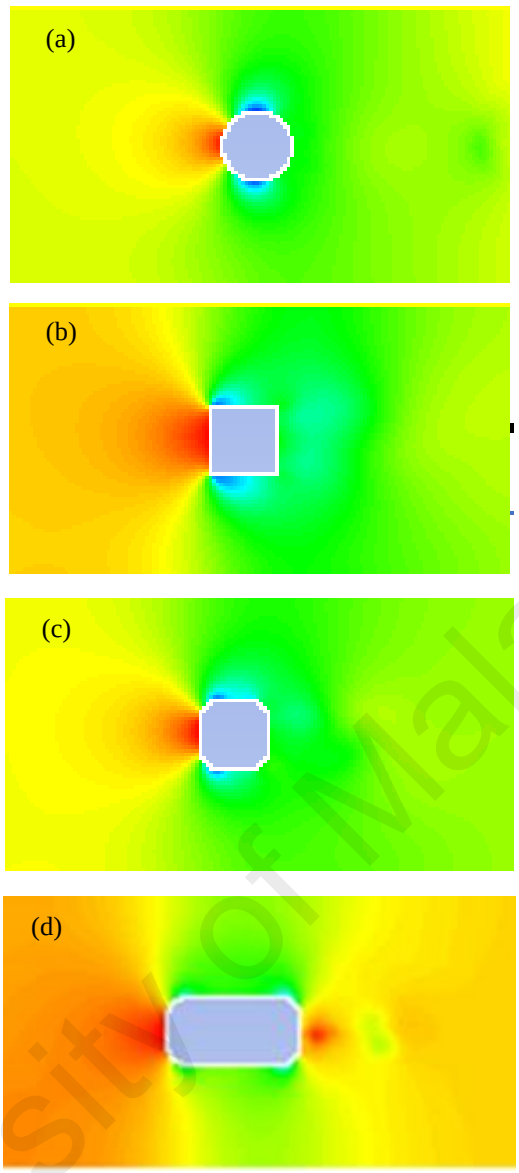

Figure 3.8: Pressure distribution around bluff bodies, (a) circular cylinder, (b) square cylinder, (c) square rounded edge cylinder, (d) rectangular with rounded edge cylinder.

3. 9.4 Effect of gap between circular body and wall of sand bed

In this section, the effect of the gap between the wall bed and the cylinder on the flow parameters has been investigated. To study the effect of the gap, five different gaps have been chosen to simulate their effect on the flow. Figure 3.9 shows five bed profiles at different gaps, G/D= 0.0, 0.1, 0.2, 0.4, and 0.8 to conduct a study on gap effect between circular cylinder and wall bed which were taken from Jensen experimental study with flat-bed profiles (B. Jensen et al., 1990). This section is divided into three sections, velocity profiles around bluff bodies, pressure distribution around bluff bodies, and turbulence models sensitivity in producing vortex shedding.

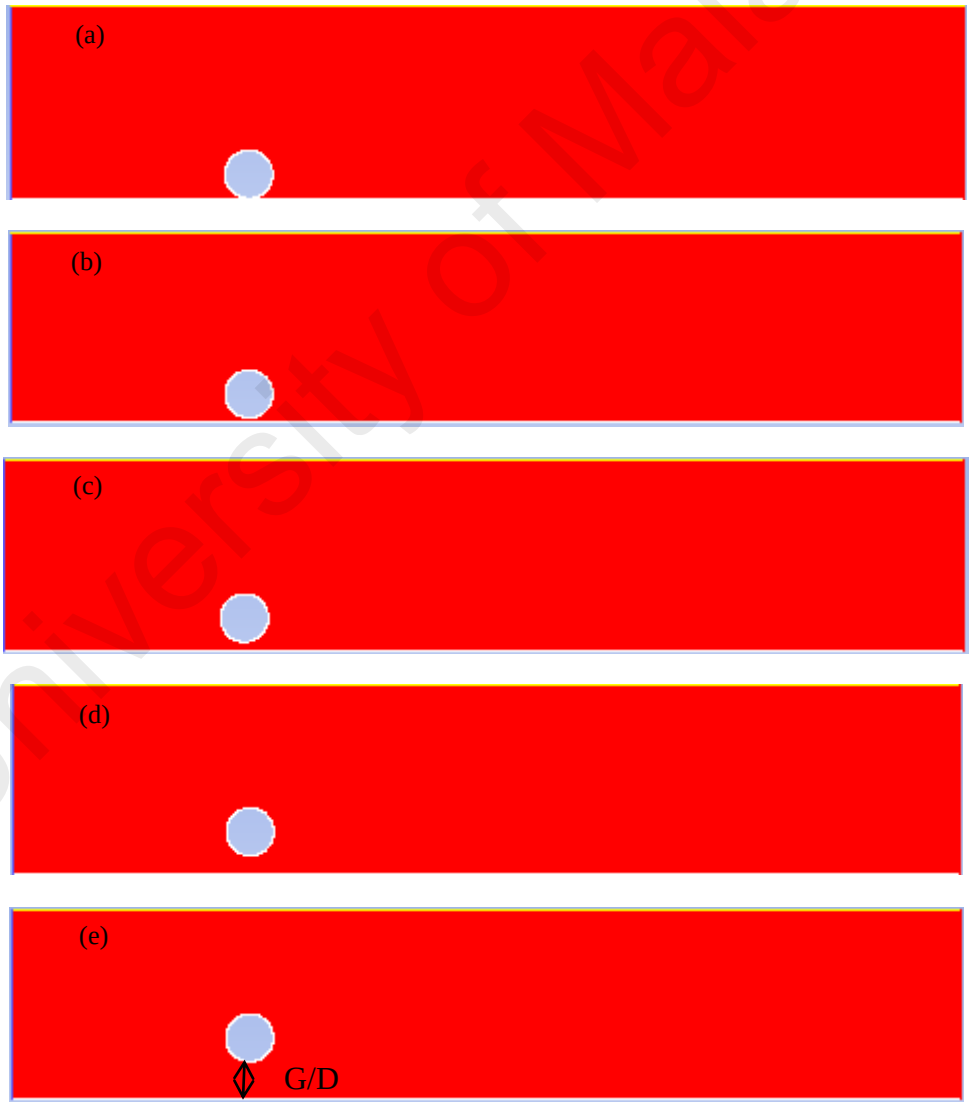

Figure 3.9: Circular cylinder profiles at different gaps (G/D), (a) G/D= 0.0, (b) G/D= 0.1, (c) G/D=0.2, (d) G/D= 0.4, and (e) G/D= 0.8.

3. 9.4.1 Vortex

Figure 3.10 shows the effect of wall approximate on vortex formation at different gap ratio (G/D=0.0, 0.01, 0.02, 0.04, and 0.08). The vortex shedding occurs only when the two shear layers interact with each other. If the interaction is inhibited in one way or another, for example in this case when the cylinder is placed close to the wall, the wall-side shear layer will not develop as strongly as the opposing shear layer; this will lead to a wake interaction between the shear layers or no interaction if the cylinder is placed very close to the wall. In such situation, the shedding would be prevented and therefore no vortex shedding would occur. It is observed that the flow around the circular cylinder indicates that vortex shedding behind the cylinder does not take place until a substantial amount of wall gap ratio to the cylinder has been developed below the cylinder. For example, at G/D=0, when there is no passage for the flow between the circular cylinder and the bed's surface, there is circulation in front and behind the cylinder that cause because of the inability of vortex interaction or boundary layer separation. However, when the gap increases from G/D=0.1 to 0.8, the vortex interaction at the rear surface of the circular cylinder occurs. The suppression of vortex shedding is linked with the asymmetry in the development of the vortices on the two sides of the cylinder. The free-stream side vortex grows larger and stronger than the wall-side vortex. Therefore the interaction of the two vortices is largely inhibited resulting in partial or complete suppression of the regular vortex shedding. It is observed that when the cylinder surface's edge is closer to the bed, the vortices behind the circular cylinder is unsymmetrical because of the interaction of the shear layers of the flow between the bed surface and the cylinder.

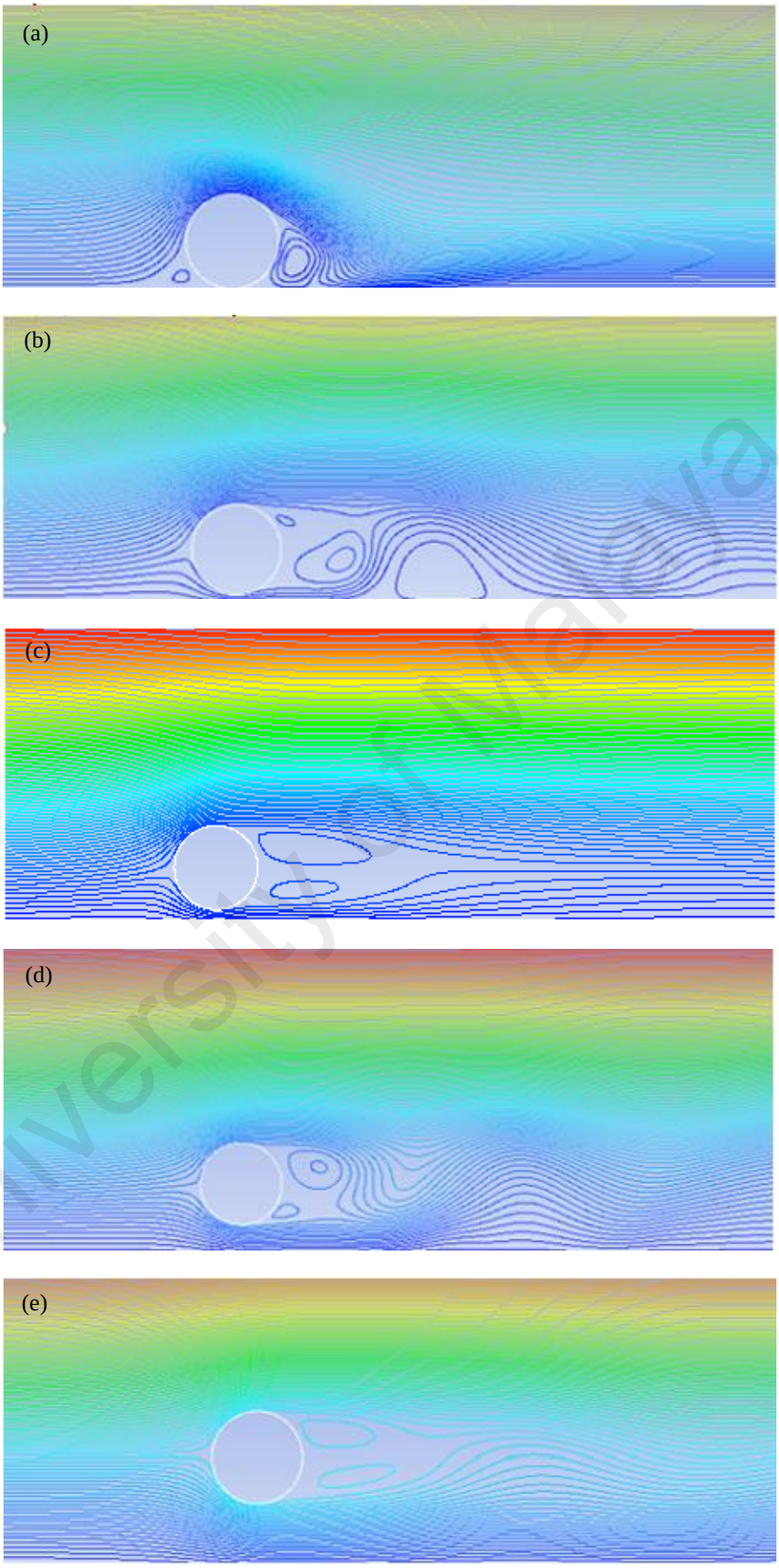

Figure 3.10 : Streamlines for circular cylinders at, (a) G/D= 0.0, (b) G/D=0.1, (c) G/D=0.2, (d) G/D=0.4, and (e) G/D=0.8.

3.9.4.2 Pressure over surface bed for different G/D

Figure3.11. Shows the pressure distribution along the bed surface at axial length (x-position) at different gap ratio (G/D=0.0, 0.01, 0.02, 0.04, and 0.08) between the cylinder's surface and bed. The pressure is relatively high at downstream and near the cylinder and becomes higher when the cylinder is placed close to the bed surface. For example, at position x=0 to 0.81m, the pressure distribution shows high changes due to the gap ratio variation, while having approximately the same value at upstream. For example, at position x=0.81 to 0.2, the pressure distribution is mostly linear. This change is due to the strength of the turbulent flow around the cylinder that gets strongly accelerated as the gap between bed surface and cylinder is narrow. As shown in Table 3.2, as the gap ration (G/D) increases, the pressure decreases. A reduction of around 80 % in the pressure distribution over the bed's surface is observed.

Table 3.2: Pressure distribution along the bed surface

G/D	0.0	0.01	0.02	0.04	0.08
Pressure (Pa)	-98.6471	-85.1309	-39.6471	-25.1986a	-24.3935

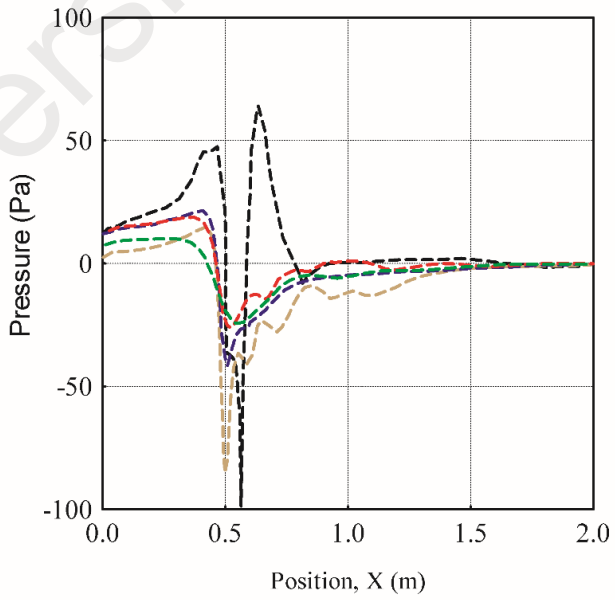

Figure 3.11 : Effect on pressure at bed 's surface of different gaps, ---- G/D=0.0, ----G/D=0.01 , ----G/D=0.02 , ----G/D=0.04, ---- G/D=0.08

3. 9.4.3 Wall shear stress over surface's bed for different G/D

Fig 3.12 shows the wall shear stress along the bed surface at axial length (x-position) at different gap ratio (G/D=0.0, 0.01, 0.02, 0.04, and 0.08) between the cylinder's surface and bed. The wall shear stress is relatively high at locations near the cylinder. It becomes higher when the cylinder is placed close to the bed surface. For example, at position x=0.41 to 0.6m where the cylinder is placed , the wall shear stress shows high changes due to the gap ratio variation, while having the same value at downstream, at position x=0.0 to 0.41, and upstream, at position x=0.6 to 2m. The changes are due to strong turbulence flow and narrow ratio gap. As shown in Table 3.3, as the gap ration (G/D) increases, the wall shear stress decreases. A reduction of around 82.3 % in the pressure distribution over the bed's surface is observed.

Table 3.3: Wall shear stress along the bed surface

G/D	0.0	0.01	0.02	0.04	0.08
shear stress (Pa)	2.61471	1.52271	0.983124	0.66305	0.463949

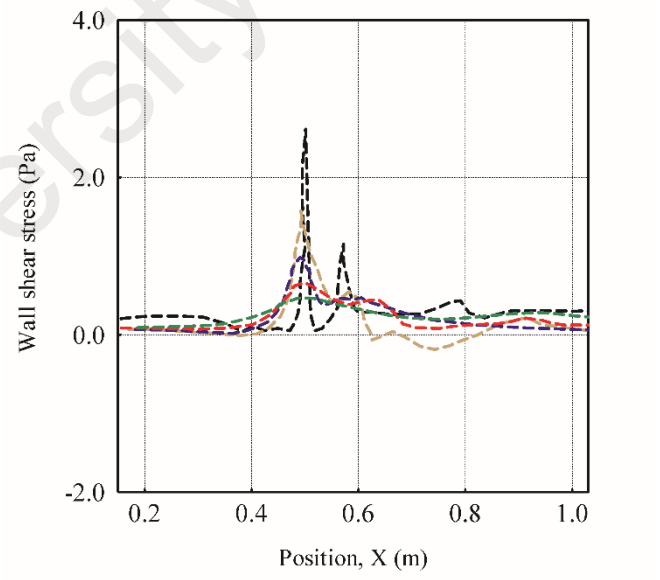

Figure 3.12 : Effect on wall shear stress at bed 's surface of different gaps, ---- G/D=0.0, ----G/D=0.01 , ----G/D=0.02 , ----G/D=0.04, ---- G/D=0.08.

3.10 Conclusions

Two dimensional (2D) CFD analyses were carried to investigate fluid flow over an obstruction under different G/D using a number of turbulence models. The numerical study has been carried out into two major sections. First part deals with the effect of geometrical structures while the second one deal with the effect of wall approximate on velocity profile, pressure distribution over surface bed, and wall shear stress distribution over bed surface. The conclusions are as follow:

- It is observed a reduction of 74.36 % in $\overline{C_l}$ and an increase of 12.11% in $\overline{C_d}$ between the gaps of G/D 0 and 0.8.
- It has been observed that the flow velocity at the wake region changes from bluff body to another causing large eddy circulation for cylinders having sharp edges.
- It is observed that the pressure distribution is relatively higher at bodies that have sharper edge and larger cross section while it reduces at the cylinders that have smooth edges and smaller cross sections.
- It is observed that RANS models is not appropriate for high Reynolds number (Re) simulation, thus they are not suitable to model periodic behavior of vortex shedding, because to their large late transition of the boundary layer from laminar to turbulent.
- It is found that when the pipe is closer to the bed, the vortices behind the circular cylinder is unsymmetrical because of the interaction of the shear layers of the flow between the bed surface and the cylinder.
- It is observed that there is a reduction of around 80% in the pressure distribution over the bed surface.
- It is observed that there is a reduction of around 82.3 % in the wall shear stress distribution over the bed surface.

Chapter 4.0

Turbulence models sensitivity study and effect of scour depth

4.1 Introduction

This chapter attempts to carry out the turbulence models sensitivity study and the effect of scour gap (the deformed sand bed profile) which have been investigated numerically. First part to test the performance of various turbulence models on the flow. The results of horizontal velocity profiles (U_x) and turbulent kinetic energy square (TKE) at various axial locations were compared with that of Jensen experimental data (B. Jensen et al., 1990) to identify a suitable turbulence model for a further study. Six turbulence models (namely variants *k*- ε models, variants *k*-ω models, and Reynolds Stress Model (RSM)) have been chosen to conduct the sensitivity study. Spatial distribution of velocity, the vortex formation, the pressure and wall shear stress distribution around the pipe were obtained.

Five scoured bed profiles at different period of time at 10, 30, 100, 200, and 300 min of experimental data from literature have been used.

4.2 Geometrical selection

Fig.4.1 shows the schematic of the two dimensional (2D) geometrical domain used in the present study along with the corresponding boundary conditions.

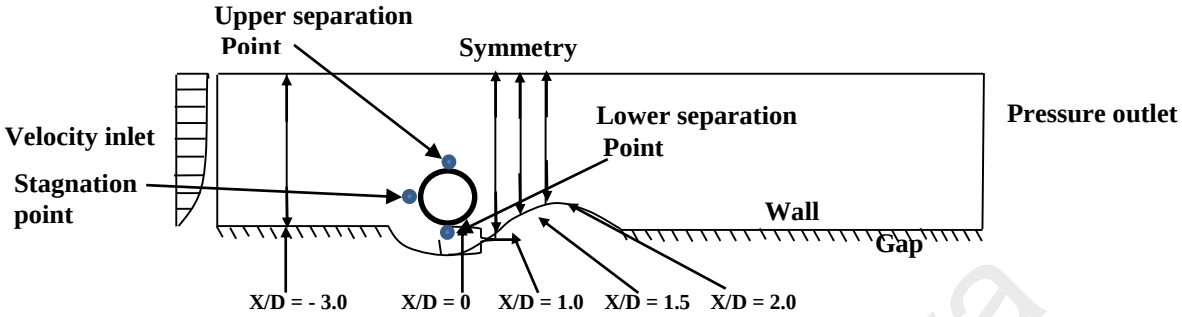

Figure 4.1: Geometrical model of computational domain and boundary conditions.

4.2.1 Mao (1986) experimental description

The experiments conducted by Mao (1986) were used as the benchmark for further investigations (Jensen et al., 1990) and modeling efforts (Brors, 1999; Li and Cheng, 2011). Mao (1986) observed the scour around horizontal cylinders in steady current and wave conditions, as well as with different Reynolds numbers (R*e*), shields parameters (θ), and pipeline gaps. These experiments investigated scour features such as the shape and size of the scour hole and time scale of scour void formation. Figure 4.2 shows a sketch of the experimental setup of Mao (1986).

The case considered in the study is a clear water case (θ=0.048, d_{50} =0.036cm) where scour and deposition are caused only by the local fluid forcing, with no net transport downstream. The cylinder has a diameter of 10 cm (R*e*=37,000) for these experiments. A sand bed follower was used to measure the bed profile at five along pipe locations.

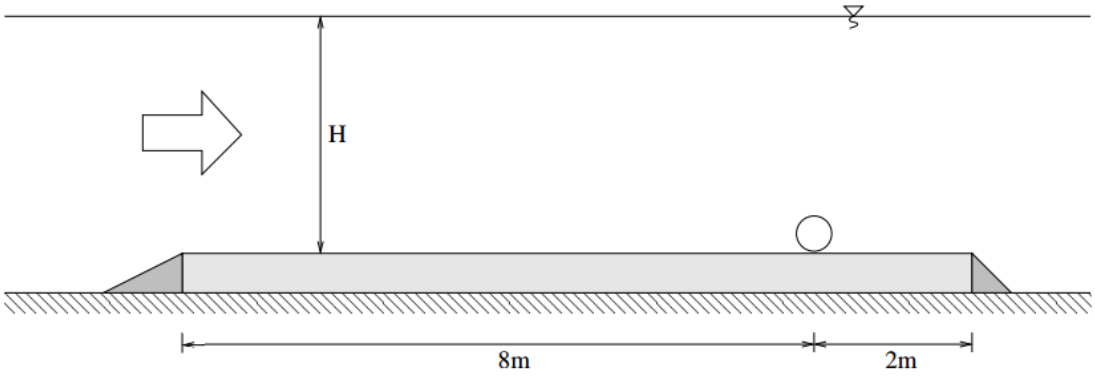

Figure 4.2: The laboratory setup for the laboratory investigations of Mao (1986).

4.4.2 Jensen et al. (1990) Experiment Description

Jensen at al. (1990) measured the flow around 3 cm (Re=6000) diameter fixed cylinder above five scoured bed profiles, representing the five phases of the scour process observed by Mao (1986). Jensen et al. (1990) (seen Fig.4.3) reported horizontal and vertical profiles at several upstream and downstream longitudinal locations with one-component tracker-based and frequency-shifted. The forces on the cylinder, vortex shedding frequencies and near bed velocities for each of the bed profiles were also evaluated with the velocity observations.

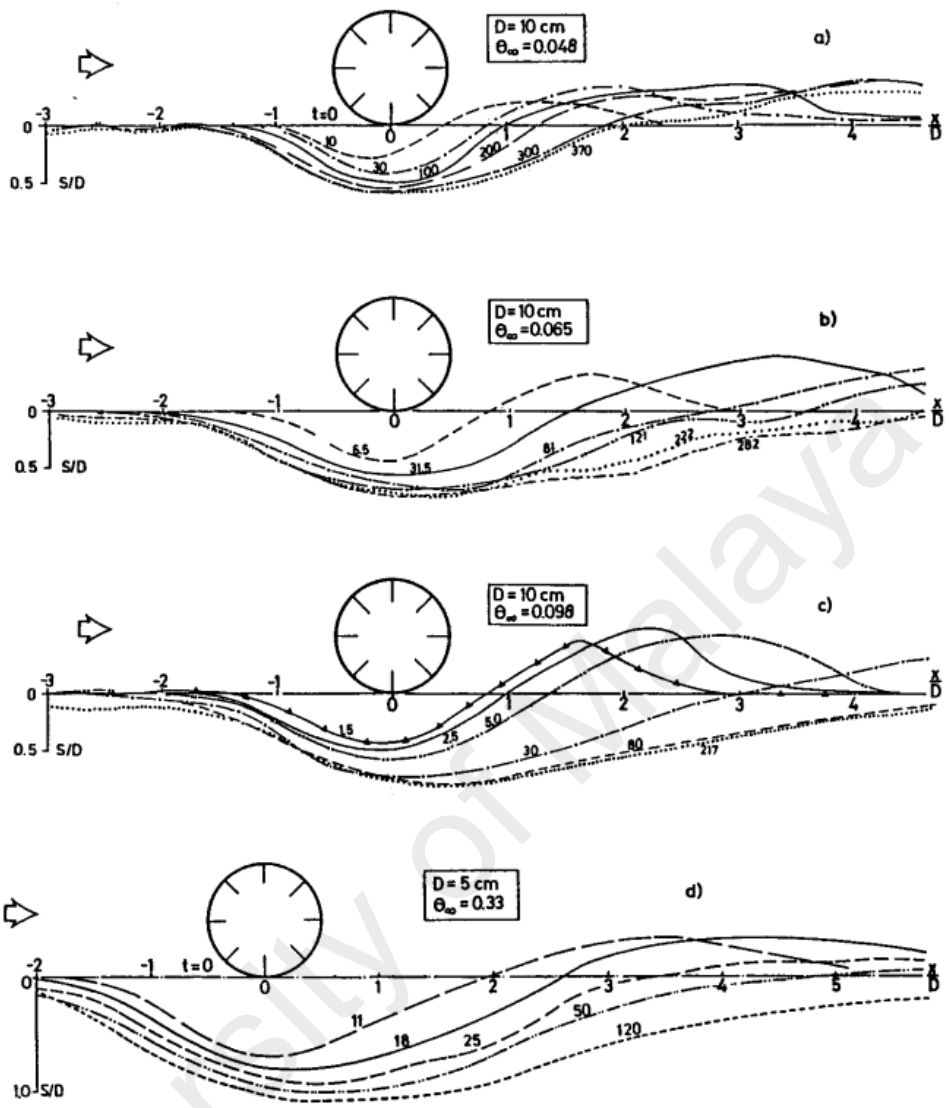

Figure 4.3: Development of bed profiles with time (in min) taken from Mao (1986). The shields parameters are 0.048, 0.056 and 0.096 correspond to free stream velocities of 37, 44 and 53 cm/s, respectively.

4.3 Governing equations

The governing equations for this section are the same as presented in Section 3.3.

4.4 Turbulence models

The governing equations for turbulence models in this section are the same as presented in Section 3.4.

4.5 Boundary conditions

A logarithmic velocity profile as shown in Fig.4.4 is generated using user-defined functions (UDF) in Fluent 14.0 (see Appendix (A)) based on the formulation in equation 20, given in Section 3.5.

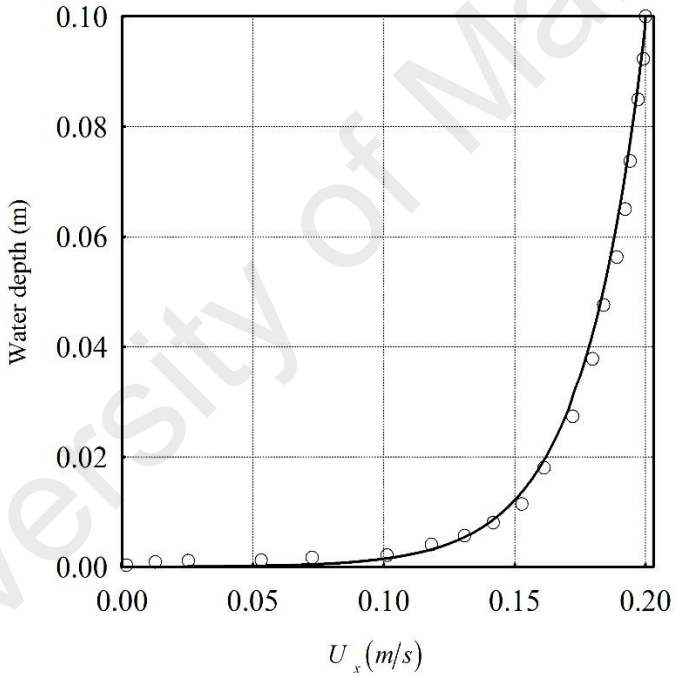

Figure 4.4 : Comparison of the horizontal logarithmic velocity-inlet (U_0) in the total water depth between, present numerical investigation and, experimental work of Dudley RD (Dudley, 2007).

The inlet and exist boundary conditions were placed, respectively, 4D and 9D from the center of the cylinder by which D is a diameter of the cylinder that equals 0.3 D and the velocity inlet and pressure outlet vertical distances equal 0.6D. In addition, a logarithmic velocity profile with U_∞ = 0.2 m/s and the turbulent kinetic energy and turbulent

dissipation rate were set for the velocity inlet and pressure outlet, respectively, in range from 0.001 m^2/s^2 to 0.0017 m^2/s^2 and from 0.000052 m^2/s^3to0.00052 m^2/s^3.

The velocity profile is applied at the flow inlet. The profile from the presented CFD model is compared with that from the experimental study of Dudley (2007) for consistency, see Fig.4.4. Zero pressure outlet boundary condition is applied at the flow exist. The water surface (top wall) is set as a symmetry boundary condition by which zero normal velocity and zero gradients of all variables are satisfied. No-slip boundary condition is applied on the pipe surface and the scour bed. Gravity acts in the negative y-direction.

4.6 Numerical method

The numerical method for this section is the same as presented in Section 3.6.

4.7 Simulation cases

A total of 35 cases as shown in Table 4.1 were simulated in the present study. The effect of different turbulence models such as *k*-ε models (standard, RNG, Realizable), *k*-*ω* models (SST, standard) and Reynolds stress model (RSM) on horizontal velocity and kinetic energy square root will be investigated. For studying this effect, the domain proposed by Jensen e al.(1990) is adopted to validate the results of Mao et al. (1987). This domain is of 0.5 m length and 0.1 m height with pipe diameter of 0.03 m. Turbulence models were tested for scour gap at time 0 min, 1 min, 6 min, 30 min, and 300 min and four positions (X/D = -3.0, 1.0, 1.5, and 2.0) in-front and behind the pipe. Qualitatively the results of a particular turbulence model were the same for all scour gaps, so, the results of Cases (1-6) for scour gap at time 30 min are presented. The turbulence model that produces a similar result as of experimental investigation of Jensen et al. is chosen for all further simulation cases in the current study.

In sections 4.9.2, 4.9.3, 4.9.4, 4.9.5, and 4.9.6 of this study, a parametric study has been carried out by using five bed profiles suggested by Mao (1987) at 10 min, 30 min, 100

min, 200 min, and 300 min. Five simulation cases (7-11) were run to obtain the horizontal velocity profile under the pipe, pressure coefficient C_p, wall shear stressτ_x, drag coefficient C_d and lift coefficient C_l around the pipe with different gaps at position X/D = 0 using Standard $k-\varepsilon$ turbulence model.

Table 4.1: Simulation cases

Sim.*	**Domain**	**Cases**	**Turbulence Models**	**Positions (X/D)**	**Remarks**
1	(1,2,3,4,5) (0,1,6,30,300 min)	1-30	Standard $k-\varepsilon$ RNG $k-\varepsilon$ Realizable $k-\varepsilon$ Standard $k-\omega$ SST $k-\omega$ RSM	3.0,1.0,1.5,2.0	To identify The preferred turbulence model
2	(1,2,3,4,5) (10,30,100,200, 300 min)	31-35	Standard $k-\varepsilon$	0	To evaluate velocity profile under the pipe, C_p , wall shear stress, C_d and C_l

*Simulation

4.8 Mesh independence and time step test

The domain is meshed using a structured and uniform square grid spacing for *x* and *y*-directions that are used for all the numerical simulation cases, see Fig.4.5, Mesh independence is carried out using five different types of grids having cell number of 40,000, 82,500, 130,225, 223404, and 315,623, see Fig.4.5 and 4.6. A Quad fine mesh is used near the pipe surface and the plane wall and near the bed. The domain with 223,404 cells is selected throughout this study, because it shows reasonable accuracy and the lowest deviations of the velocity profile and turbulent kinetic energy (TKE) for turbulence models compared to Jensen laboratory data (B. Jensen et al., 1990). Four different time step sizes (Δt = 0.0002, 0.002, 0.02, and 0.2) were tested and 0.002is used throughout this current numerical study as there were no deviations observed below this value of time step. The numbers of iterations for this study are kept between 3000-3500.

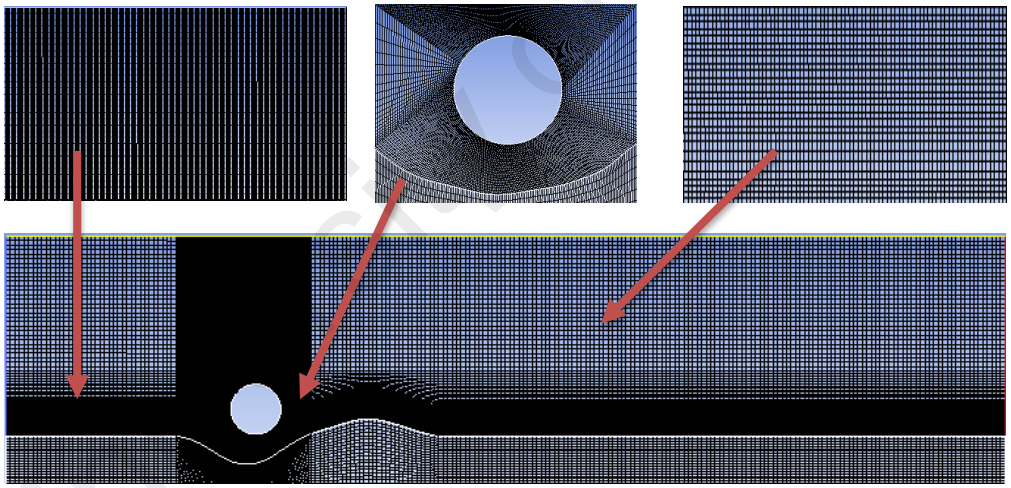

Figure 4.5: The grid for the model calculation

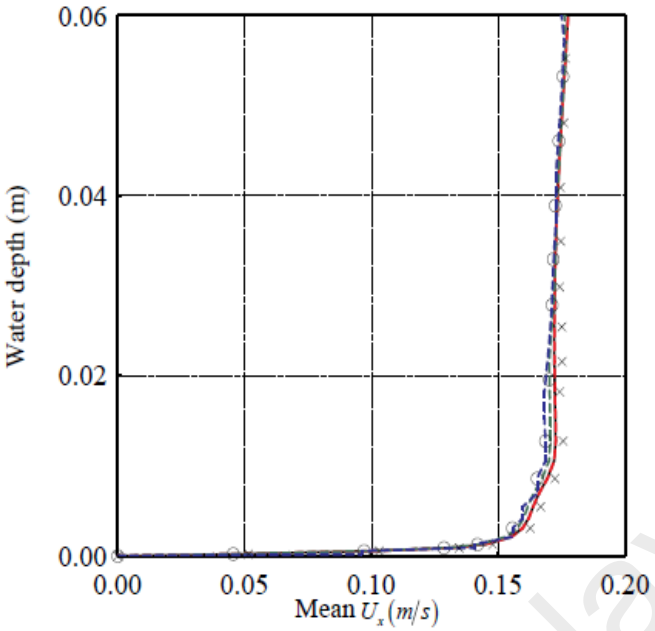

Figure 4.6: Mesh independence test for mean U_x(m/ s) at location X/D=-3.0, —Jensen, —400,000, o 82500, — 130,255, — 223,404 , **x** 315,623.

4.9 Results and discussion

The present numerical study has been carried out into two major sections. First part deals with the effect of different turbulence models on horizontal velocity profile and kinetic energy square root while the second deals with the effect of scour gap on velocity profile under the pipe, wall shear stress and others.

4.9.1 Effect of different turbulence models

4.9.1.1 Horizontal velocity profile

The prediction of the horizontal velocity profile (U_x) for five different types of scouring domains (Cases 1-30) at different axial length positions (i.e., X/D = -3.0, 1.0, 1.5, and 2.0) using different turbulence models are presented in Section 4.9.1. For comparisons, the experimental results reported in Jensen et al. (1990) are also presented in the figure. Note that, the location of the axial positions covers the front and rear part of the pipe (or obstruction). The prediction of the standard *k*-ε turbulence model is much closer to the experimental data at different water depths (see Figs 4.7, to 4.11); In fact, some of them are overlap each other. Nearly the same can be said for the realizable *k*-ε model and RSM model, but some deviations are seen at some of the water depths, e.g., see at water depths below 0.01m and those between 0.03 to 0.04m at X/D = 2.0 (Fig. 4.10(d)) for the both models. RNG *k*-ε model prediction is quite accurate for X/D = -3.0 and 1.0 (Fig. 4.10(a) and 4.10(b)), but this is not the case for X/D = 1.5, and 2.0 (Figs. 4.10(c) and 4.1(d)); over prediction of the velocity is seen at water depths between 0.01 to 0.03m. Relatively, standard *k*-*ω* and SST *k*-*ω* models are the most inaccurate among the turbulence models studied. A significant under-prediction of velocity is seen at water depths from 0 to 0.04m at X/D = 1.0, 1.5, and 2.0.

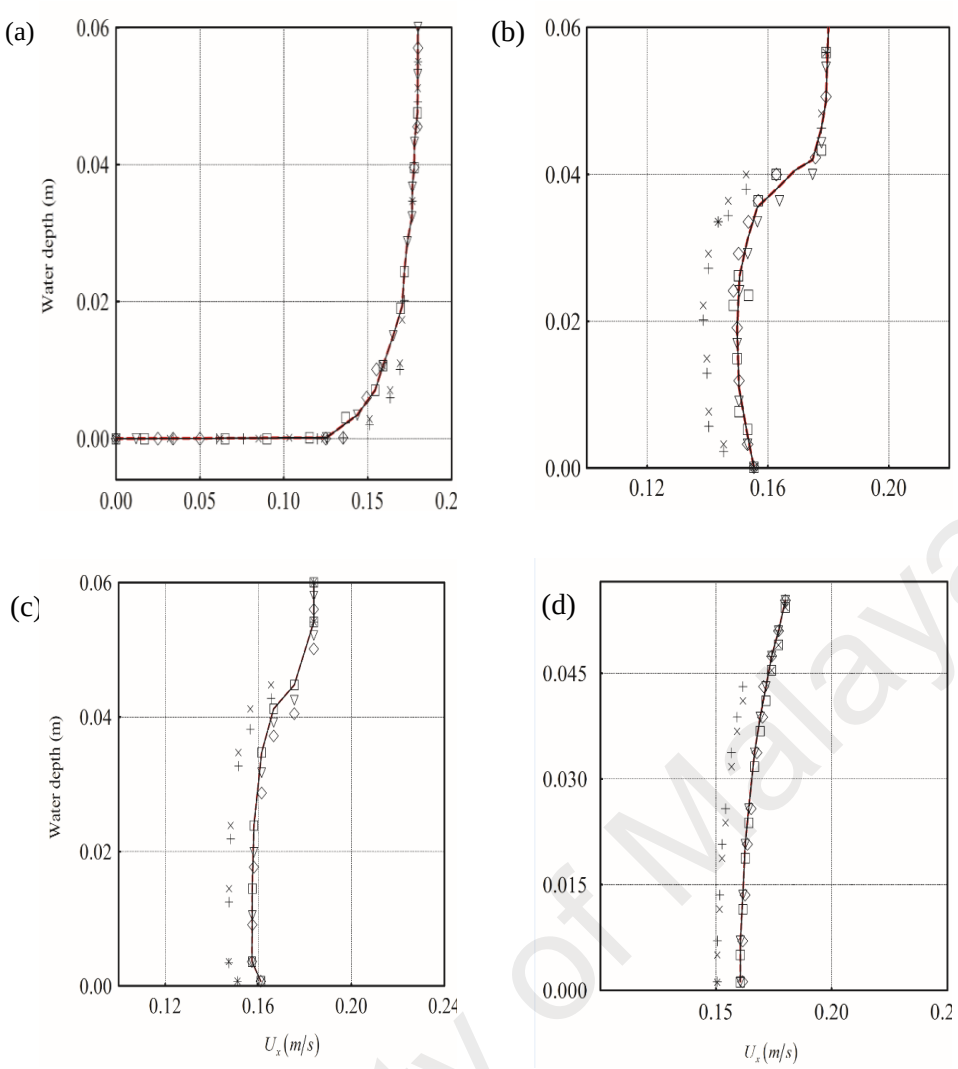

Figure 4.7: Unsteady horizontal velocity (U_x) at 0 min and at different positions, (a) X/D= -3.0, (b) X/D=1.0,(c) X/D=1.5, and (d) X/D=2.0 with different turbulent models, ▬ Standard $k-\varepsilon$, ◊ RNG $k-\varepsilon$, Δ Realizable $k-\varepsilon$, × Standard $k-\omega$, + SST $k-\omega$, □ Reynolds Stress Modles (RSM), - - - Jensen (B. L. Jensen et al., 1990).

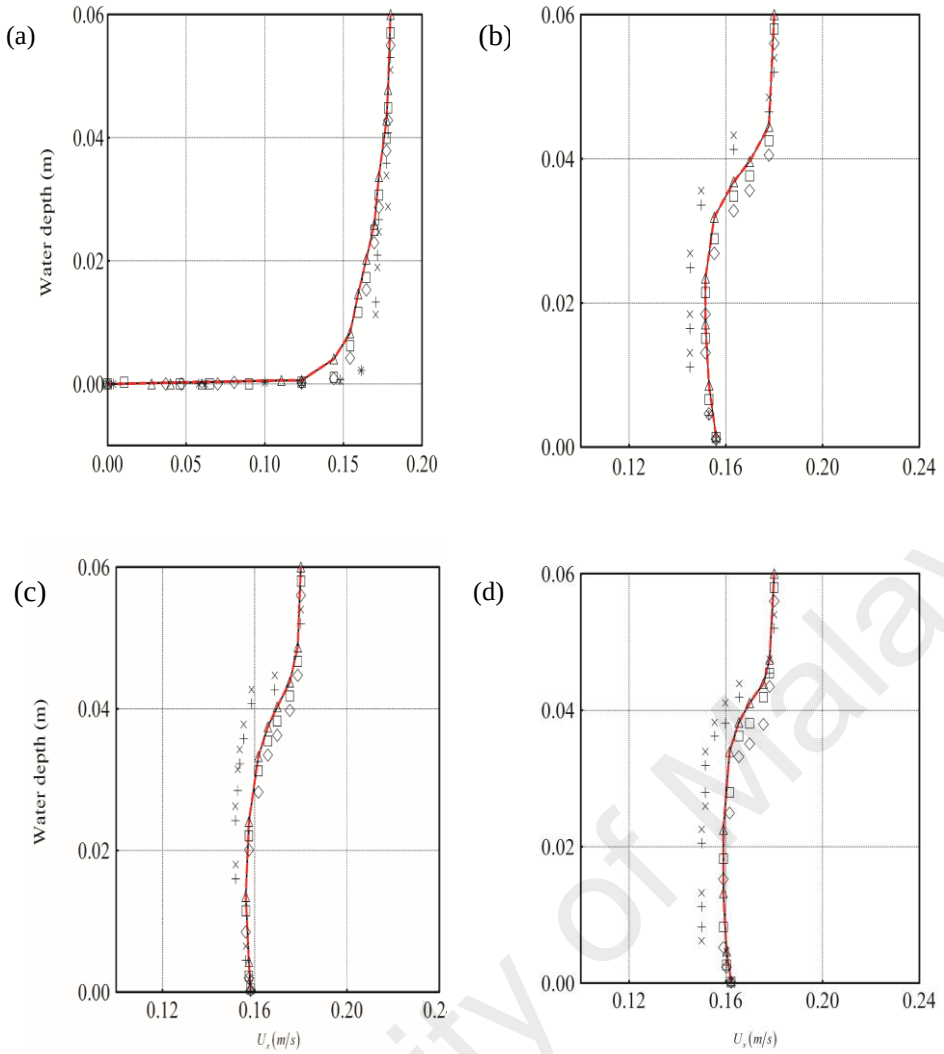

Figure 4.8: Unsteady horizontal velocity (U_x) at 1 min and at different positions, (a) X/D= -3.0, (b) X/D=1.0,(c) X/D=1.5, and (d) X/D=2.0 with different turbulent models, ▬ Standard $k-\varepsilon$, ◊ RNG $k-\varepsilon$, Δ Realizable $k-\varepsilon$, × Standard $k-\omega$, + SST $k-\omega$, □ Reynolds Stress Modles (RSM) , - - - Jensen (B. Jensen et al., 1990).

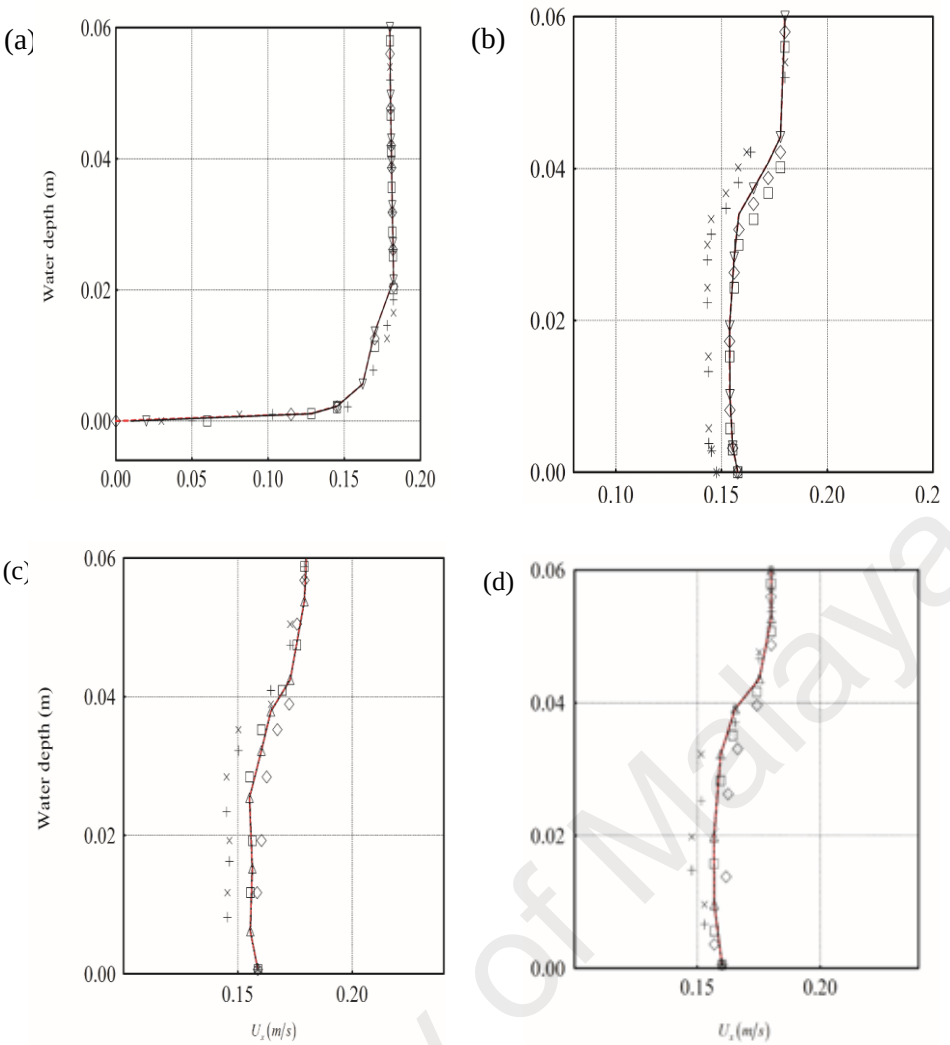

Figure 4.9: Unsteady horizontal velocity (U_x) at 6 min and at different positions, (a) X/D= -3.0, (b) X/D=1.0,(c) X/D=1.5, and (d) X/D=2.0 with different turbulent models, ▬ Standard $k-\varepsilon$, ◊ RNG $k-\varepsilon$, Δ Realizable $k-\varepsilon$, × Standard $k-\omega$, + SST $k-\omega$, □ Reynolds Stress Modles (RSM), - - - Jensen (B. Jensen et al., 1990).

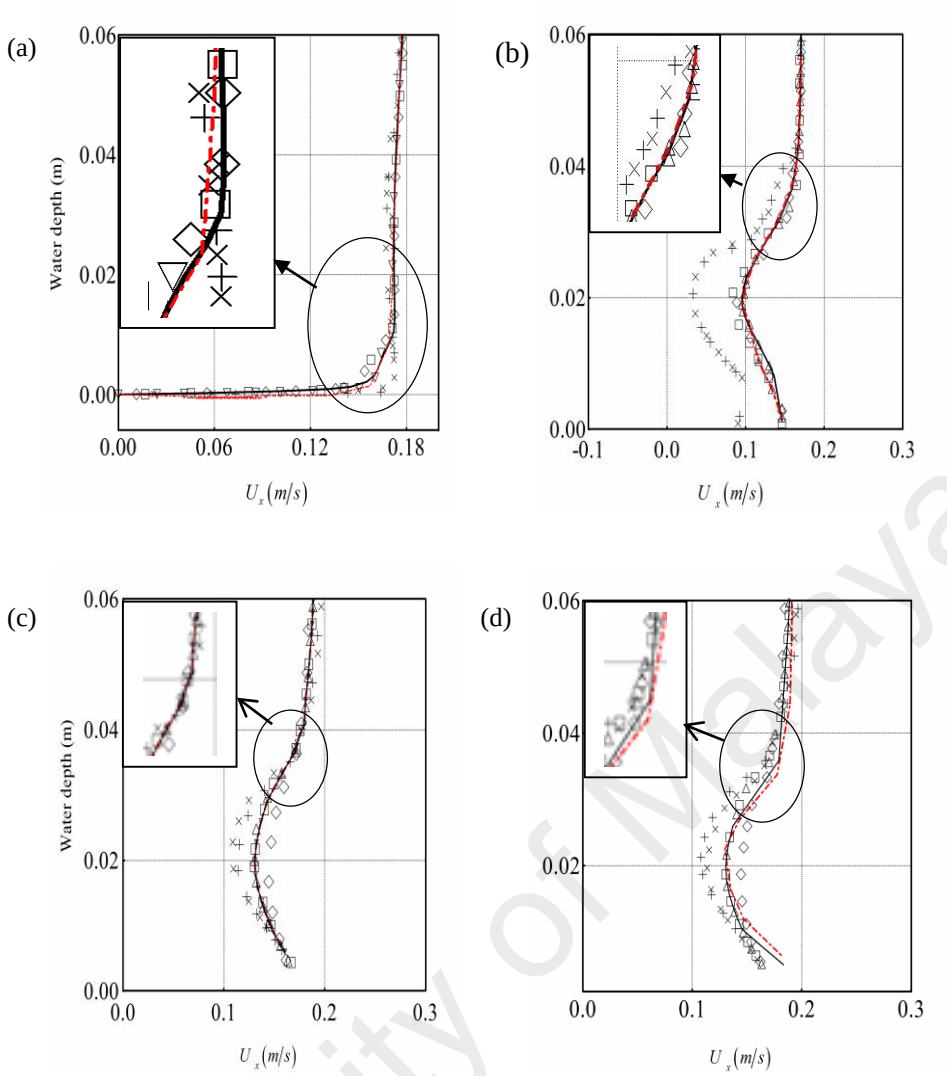

Figure 4.10: Unsteady horizontal velocity (U_x) at 30 min at different positions, (a) X/D= -3.0, (b) X/D=1.0,(c) X/D=1.5, and (d) X/D=2.0 using different turbulent models, ▬ Standard $k-\varepsilon$, ◊ RNG $k-\varepsilon$, Δ Realizable $k-\varepsilon$, × Standard $k-\omega$, + SST $k-\omega$, □ Reynolds Stress Model (RSM), - - - Jensen (B. Jensen et al., 1990).

.

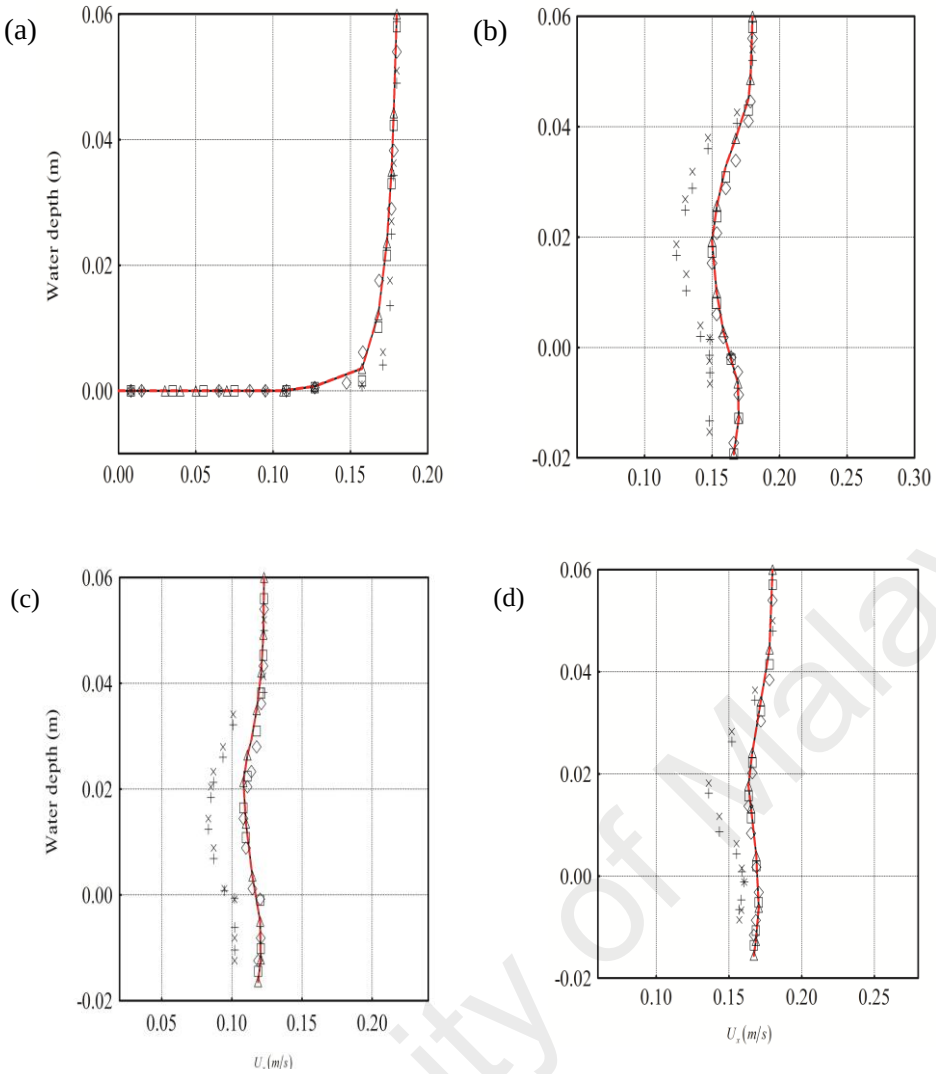

Figure 4.11: Unsteady horizontal velocity (U_x) at 300 min and at different positions, (a) X/D= -3.0, (b) X/D=1.0,(c) X/D=1.5, and (d) X/D=2.0 with different turbulent models, ▬ Standard $k-\varepsilon$, ◊ RNG $k-\varepsilon$, Δ Realizable $k-\varepsilon$, × Standard $k-\omega$, + SST $k-\omega$, □ Reynolds Stress Modles (RSM) ,- - - Jensen (B. Jensen et al., 1990).

4.9.1.2 Turbulent Kinetic Energy square root ($\sqrt{k}$)

Fig.4.2 shows the Turbulent Kinetic Energy (TKE) profiles at axial length (X/D) of -3.0, 1.0, 1.5, and 2.0 using different turbulence models for different types of scoured bed profiles. For comparisons, the experimental results reported in Jensen et al. (1990) are also presented in the figure (see Figs 4.12 to 4.16). TKE is well predicted using the Standard k -ε turbulence with some deviation at X/D of 2.0 (Fig. 4.15(d)) in comparison to other turbulence models. RNG k-ε model and RSM model also reasonably predicts TKE especially for X/D= 1.5 and 2.0 and Realizable k-ε model has a good prediction only at X/D = 1.0. On overall, Realizable k-ε model, Standard k-ω and SST k-ω models can be regarded as the least accurate among the turbulence models studied in predicting TKE.

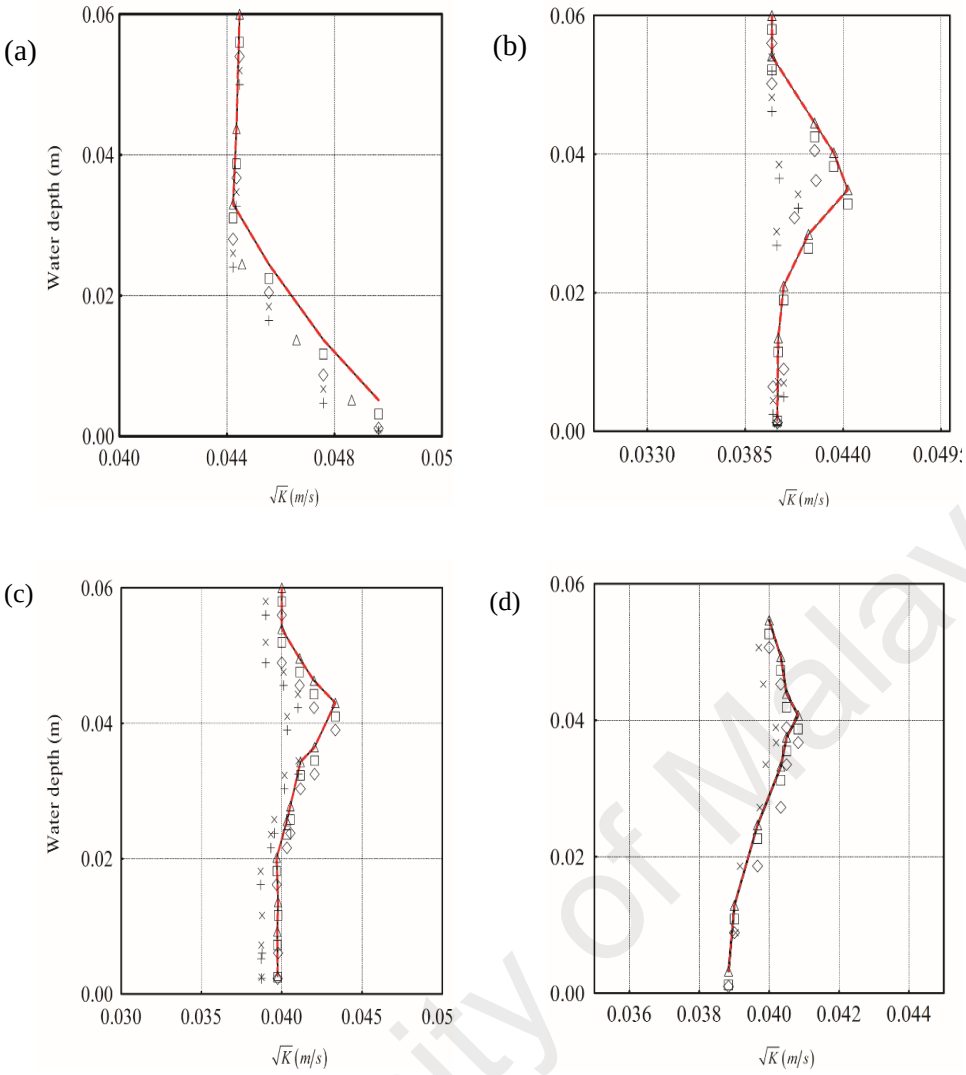

Figure 4.12: Turbulent Kinetic Energy Square Root ($\sqrt{k}$) at 0 min and at differnet locations,(a) X/D= -3.0, (b) X/D=1.0, (c) X/D=2.0, and (d) X/D=4.0, ▬ Standard $k-\varepsilon$,◊RNG $k-\varepsilon$,Δ Realizable $k-\varepsilon$,×Standard $k-\omega$,+SST $k-\omega$,□Reynolds Stress Modles (RSM), - - - Jensen (B. Jensen et al., 1990).

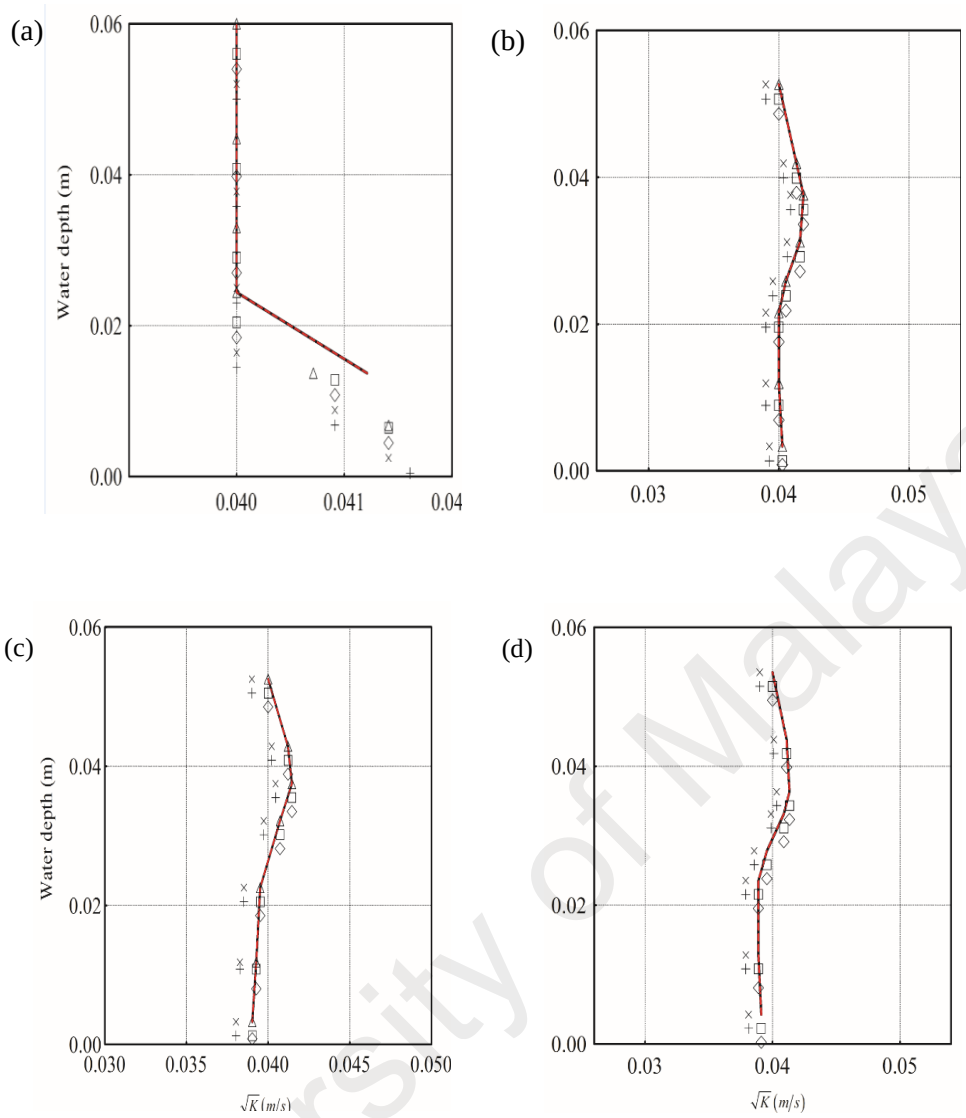

Figure 4.13: Turbulent Kinetic Energy Square Root ($\sqrt{k}$) at 1 min and at differnet locations,(a) X/D= -3.0, (b) X/D=1.0, (c) X/D=1.5, and (d) X/D=2.0, ▬ Standard $k-\varepsilon$,◊RNG $k-\varepsilon$,Δ Realizable $k-\varepsilon$,×Standard $k-\omega$,+SST $k-\omega$,□Reynolds Stress Modles (RSM),- - - Jensen (B. Jensen et al., 1990).

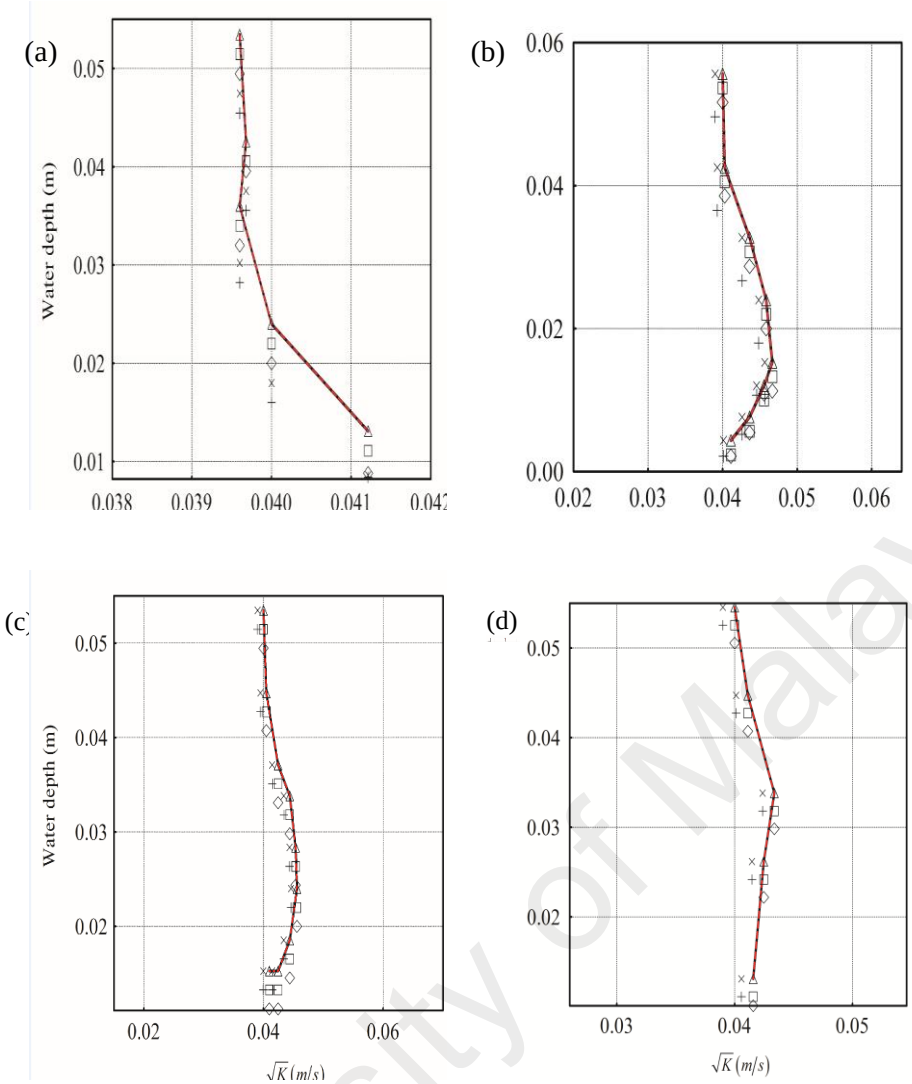

Figure 4.14: Unsteady horizontal velocity (U_x) at 6 min and at different positions, (a) X/D= -3.0, (b) X/D=1.0,(c) X/D=1.5, and (d) X/D=2.0 with different turbulent models, ▬ Standard $k-\varepsilon$, ◊ RNG $k-\varepsilon$, Δ Realizable $k-\varepsilon$, × Standard $k-\omega$, + SST $k-\omega$, □Reynolds Stress Modles (RSM), - - - Jensen (B. Jensen et al., 1990).

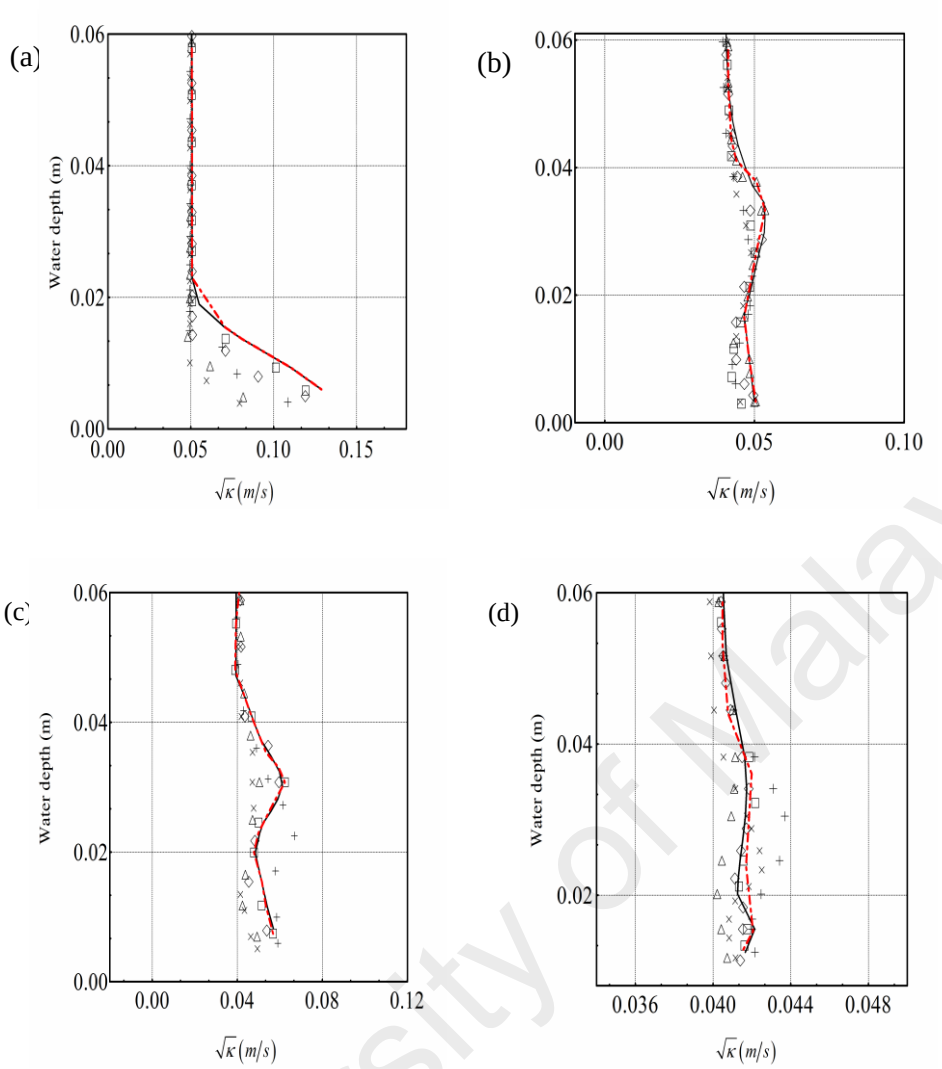

Figure 4.15: Unsteady horizontal velocity (U_x) at 30 min and at different positions, (a) X/D= -3.0, (b) X/D=1.0,(c) X/D=1.5, and (d) X/D=2.0 with different turbulent models, ▬ Standard $k-\varepsilon$, ◊ RNG $k-\varepsilon$, Δ Realizable $k-\varepsilon$, × Standard $k-\omega$, + SST $k-\omega$, □Reynolds Stress Modles (RSM), - - - Jensen (B. Jensen et al., 1990).

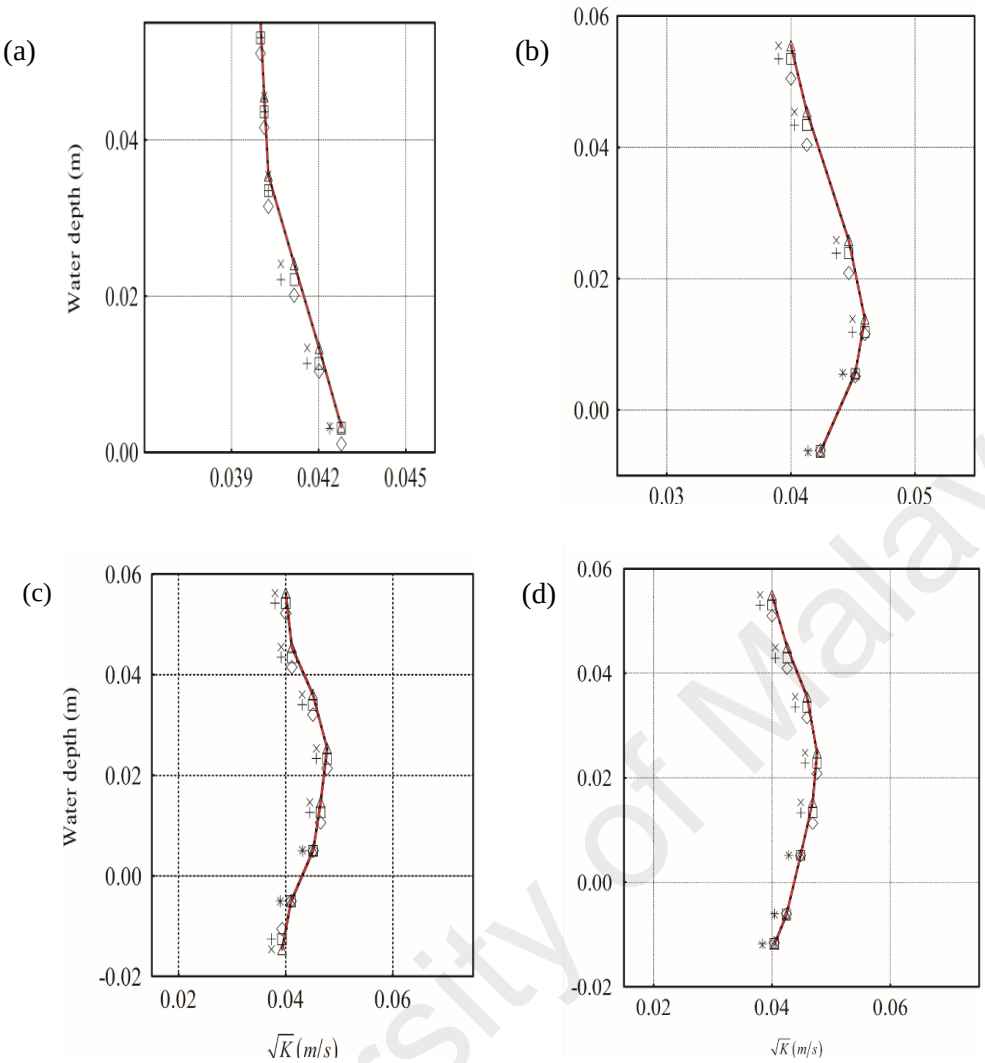

Figure 4.16: Unsteady horizontal velocity (U_x) at 300 min and at different positions, (a) X/D= -3.0, (b) X/D=1.0,(c) X/D=1.5, and (d) X/D=2.0 with different turbulent models, ▬ Standard $k-\varepsilon$, ◊ RNG $k-\varepsilon$, Δ Realizable $k-\varepsilon$, × Standard $k-\omega$, + SST $k-\omega$, □Reynolds Stress Modles (RSM), - - - Jensen (B. Jensen et al., 1990).

Among all turbulence models, standard k-ε model gives better predictions when compared with the experimental data of Jensen et al.(1990) standard k-ε model is widely acceptable for scour process modelling because of its better accuracy, reasonable computation time and does not require high computational facilities. However, the k-ω models show a discrepancy with the experimental data and the velocity profile deviates mostly near the wake region (highly turbulent region) and less in the farther area in the downstream profile. This deviation is more significant at the bottom (near the wall bed) and around the pipeline and reduces towards the water surface. This deviation may be because k-ω model produces slightly large turbulence in the weak area which is less encountered with the variants k-ε models and the Reynolds Stress Model (RSM). It may also be because of the absence of the wall treatment function in k-ω models, and they are also very sensitive to the inlet boundary conditions flow.

4.9.2 Spatial distribution of velocity profile

Fig.4.17 shows the horizontal velocity (U_x) contours based on Standard k- ε for domains of scoured bed profiles at times 10, 30, 100, 200, and 300 min. The velocity magnitude at the stagnation point (i.e., at the center & front side of the pipe) and separation point (i.e., at the center and back of the pipe) on the pipe wall is given in Tables 4.2 and 4.3, respectively. The velocity at stagnation points has a negative value to indicate that the U_x are in the opposite direction to the main stream flow. The velocity, initially, increases and then reduces with the increase in the scour depth.

Table 4.2: Velocity at stagnation point at front side of pipe

Domain	10 min	30 min	100 min	200 min	300 min
Velocity	-0.0394 m/s	-0.046 m/s	-0.075 m/s	-0.04 m/s	-0.045 m/s

The separation points at the upper and bottom side of the pipe surface vary with scour gap. Because of the interaction of the flow and bed surface, the bottom section gets more affected than upper one and this interaction causes the scour to occur which increases with time. As shown in the Table 4.3, as the scour gap increases, separation point velocity decreases, and beyond 300 min the velocity and the scour gap both remain unchanged and this stage is called equilibrium stage. A reduction of around 24.8% in the horizontal velocity between the time 10 min and 300 min is observed at the upper separation point.

Table 4.3: Velocity at upper separation point

Domain	10 min	30 min	100 min	200 min	300 min
Velocity	0.48 m/s	0.479 m/s	0.434 m/s	0.389 m/s	0.361m/s

At the bottom separation point, the flow velocity decreases as the scour gap increases. For example, at time 10 min the velocity at bottom separation point is 0.48 m/s while it becomes 0.337 m/s at 300 min, as shown in Table 4.4. A reduction of around 29.8 % of the horizontal velocity is seen from time 10 min to 300 min at bottom separation point.

Table 4.4: Velocity at bottom separation point

Domain	10 min	30 min	100 min	200 min	300 min
Velocity	0.48 m/s	0.453 m/s	0.391 m/s	0.369 m/s	0.337 m/s

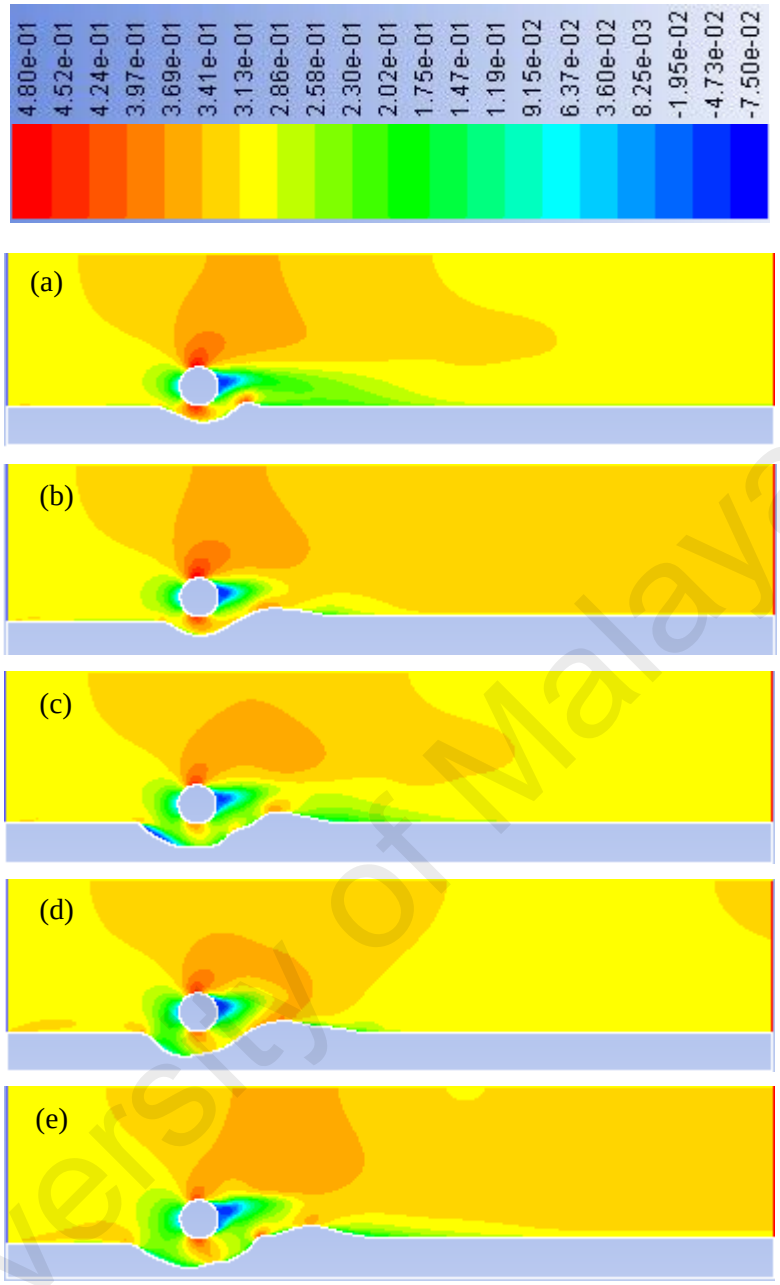

Figure 4.17: Horizontal velocity contour at different scour gaps, (a) 10 min, (b) 30 min, (c) 100 min, (d) 200 min, and (e) 300 min.

4.9.3 Effect of vortex shedding

The vortex shedding is shown for different types of scoured bed profiles in Fig.4.18. As expected, the vortex shedding varies with the scour gap size. The size of the vortex shedding increases with increase in the scour gap. Because the vortex on the free-stream side in the upper side of pipe grows larger and stronger than the vortex on the bottom side of pipe, the vortex shedding in the narrow gaps is prevented to be formed. However, it forms very well as the scour depth gets larger and the vortices in the bottom separation point sheds symmetrically with vortices in the upper side of pipe and the vortex shedding dominates the scour process till scour reaches its equilibrium stage. The standard k- ε turbulence model shows the inability to model the strong vortex shedding for a circular pipe over the scour bed and this may resulted from using the wall function or due to insufficient grid resolution.

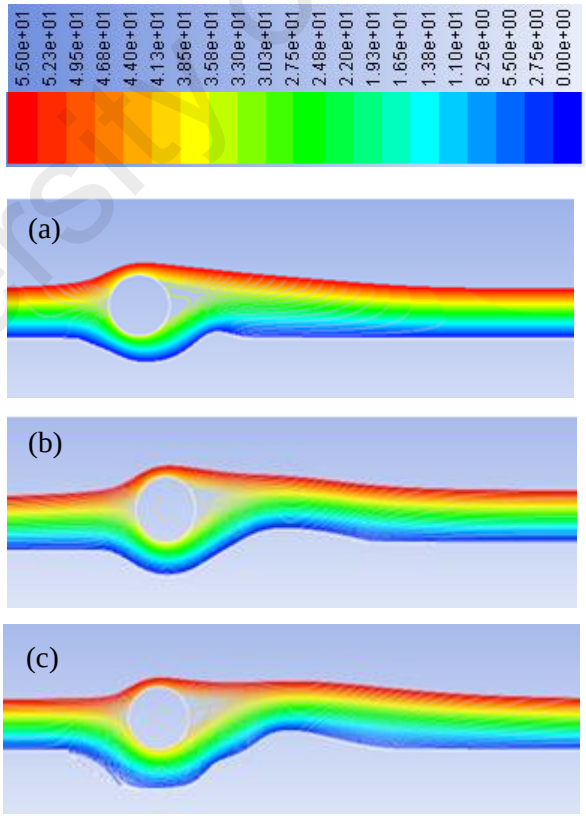

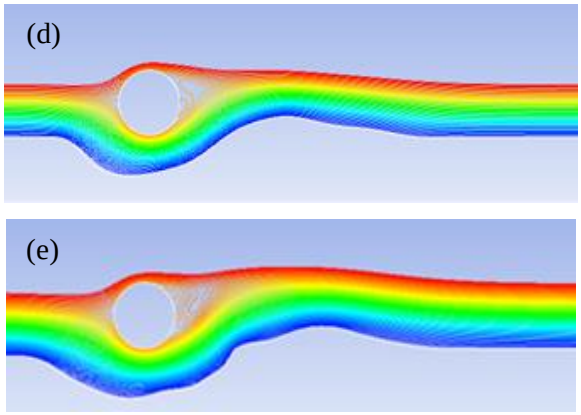

Figure 4.18: Streamlines at different scour gaps, (a) 10 min, (b) 30 min, (c) 100 min, (d) 200 min, and (e) 300 min.

4.9.4 Pressure distribution around pipe

Fig.4.19 shows the pressure distribution around pipe for different types of scoured bed profiles. The pressure is relatively higher at locations near the separation points (on the upper and bottom pipe surface) compared to other locations while the pressure reduces as the flow approaches the stagnation point in the front side of pipe and increases after passing the wake region. It is observed that at narrow gaps at times 10 and 30 min, the pressure distribution is higher compared to larger scour depth at times of 100, 200, and 300 min. For example, at time 10 min, the pressure on the upper separation point is118 Pa near the top surface of the pipe and reduces when it moves towards the free stream. The pressure distribution at the upper separation points decreases with increase in scour depth. For example, the pressure at time 30 min,is118 Pa which is same as that at 10 while it is 101 Pa at time of 100 min, 98 Pa at time of 200 min, and 92.8 Pa at time of 300 min. A reduction of around26.3% in pressure is observed at upper separation point from time 10 to 300 min.

Similarly, the pressure at bottom separation point decreases with increase in scour depth and it becomes almost negligible at the bed surface. For example, at time 10 min the pressure at bottom separation point is 118 Pa similar to the upper separation point at the same time. This is because the scour gap is very narrow and due to this, the stagnation point appears on the center of the front side of pipe. However, it is not so for the other cases, as shown in Fig. 4.19. For example, at time 30 min, the pressure is 100 Pa and at 100 min 85.3 Pa. At 300 min, the pressure is 70 Pa which is almost 40.7 % lesser than that at 10 min.

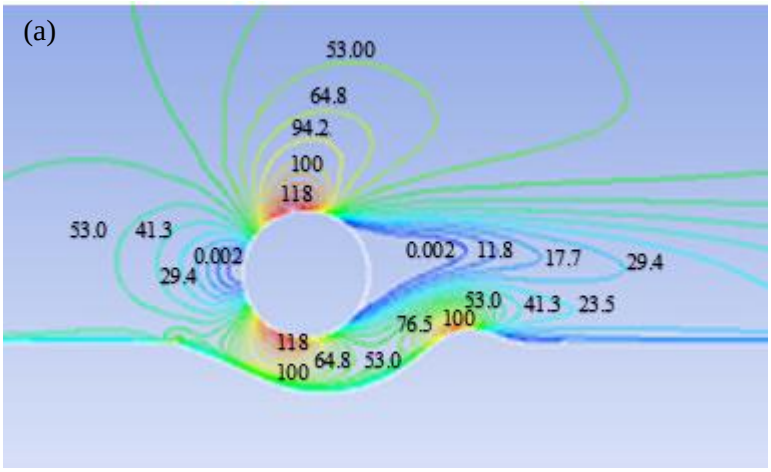

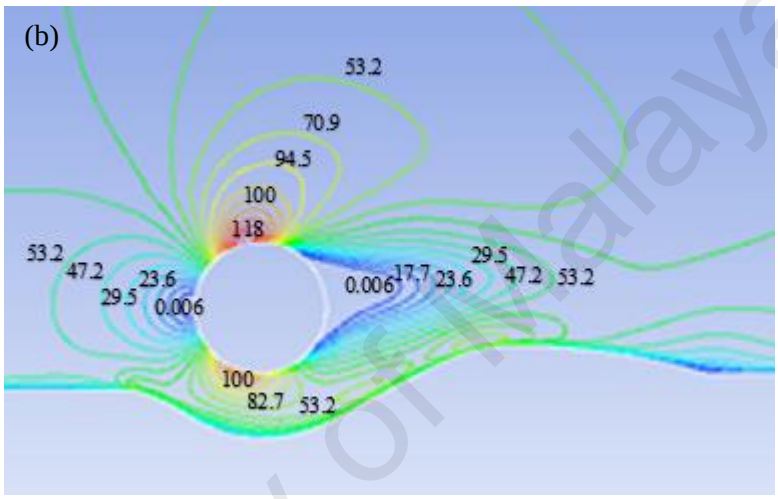

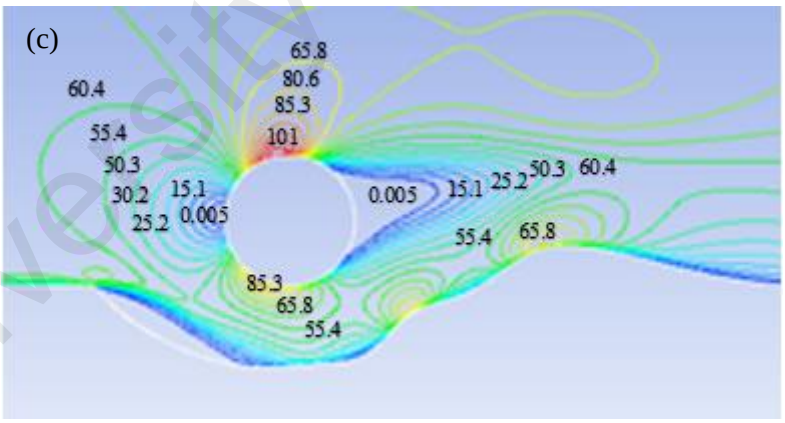

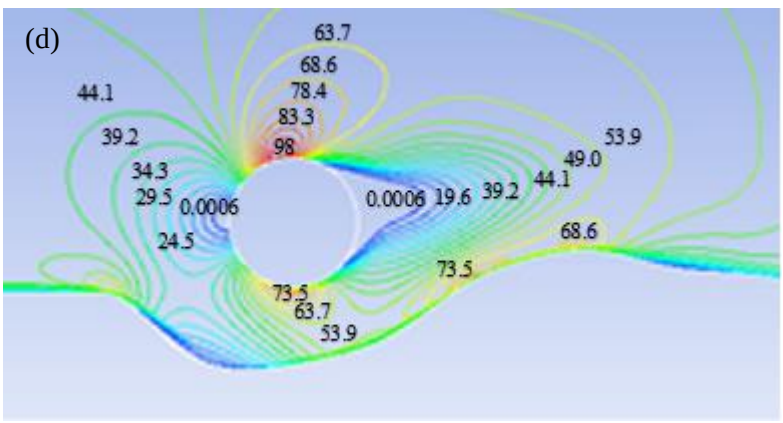

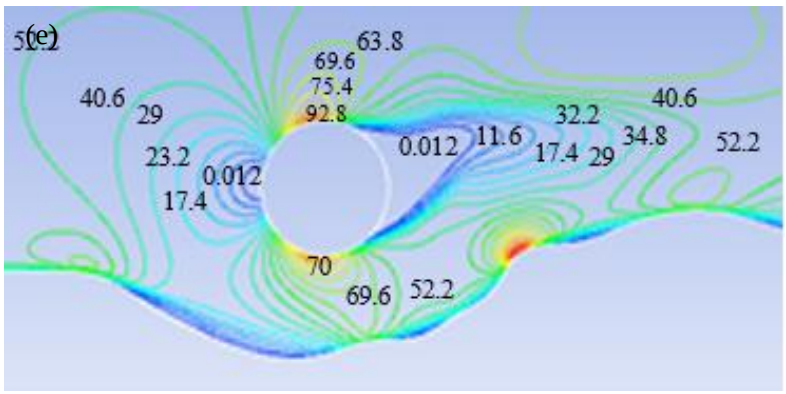

Figure 4.19: Pressure distribution around pipe at different scour gaps, (a) 10 min, (b) 30 min, (c) 100 min, (d) 200 min, and (e) 300 min.

4.9.5 Wall shear stress at bed surface

Fig.4.20 shows the wall shear stress along bed surface at different types of scoured bed profiles. The bed wall shear stress forms as a result of parallel flow along the bed surface. A wall shear stress can be expected to be highly changed at the scour depth from times of 10 min till 300 min while having the same value at other bed surface regions. For example, at Fig. 4.20 it can be clearly seen that the wall shear stress along the domain having a value of 0.5 Pa at the five different types of scoured bed while its value is changed below the pipe at the gap area. These changes due to the strength of the horizontal velocity flow into the gap after being reduced at the front side of the pipe at the stagnation point and then accelerated at the separation points. A higher bed wall shear stress can be expected to be high at narrow gaps (such as bed profiles at 10 min and 30 min) and lower for large gaps (such as 100,200 and 300 min) as shown in Fig.4.21. The results obtained found that a reduction of around 80 % of bed wall shear stress observes from time 10 min to 300 min.

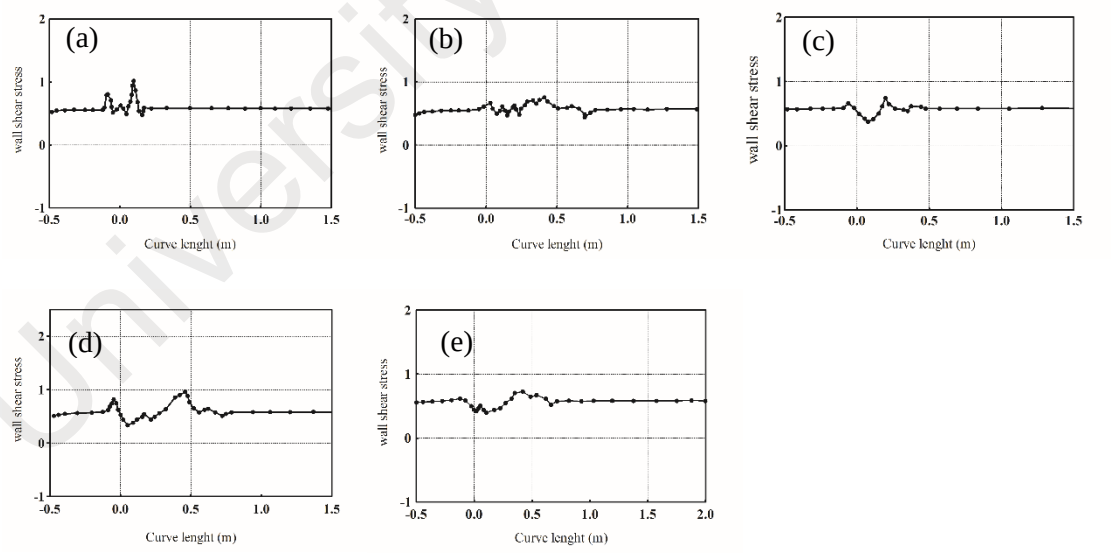

Figure 4.20: Effect on wall shear stress at bed surface of different scour gaps, (a) 10 min, (b) 30 min, (c) 100 min, (d) 200 min, and (e) 300 min.

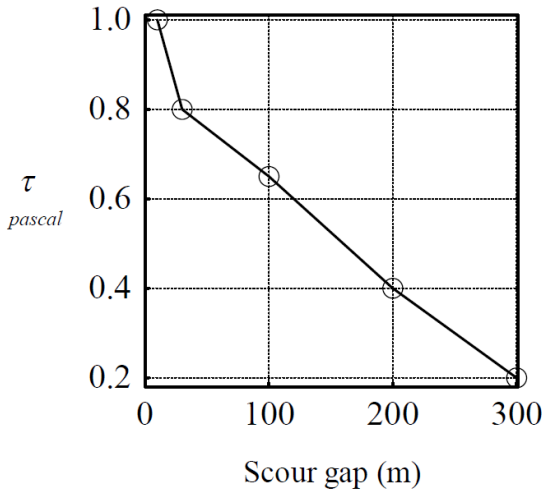

Figure 4.21: Wall shear stress (τ) at bed surface at location X/D= 0

4.9.6 Effect of scouring depth

In this section, the effect of the scour gap between the sand bed and the cylinder on the flow parameters has been investigated. To study the effect of the gap, five different gaps have been chosen to simulate their effect on the flow. Fig.4.8 shows five bed profiles suggested by Mao (1987) at 10 min, 30 min, 100 min, 200 min, and 300 min to conduct a parametric study on scouring depth effect.

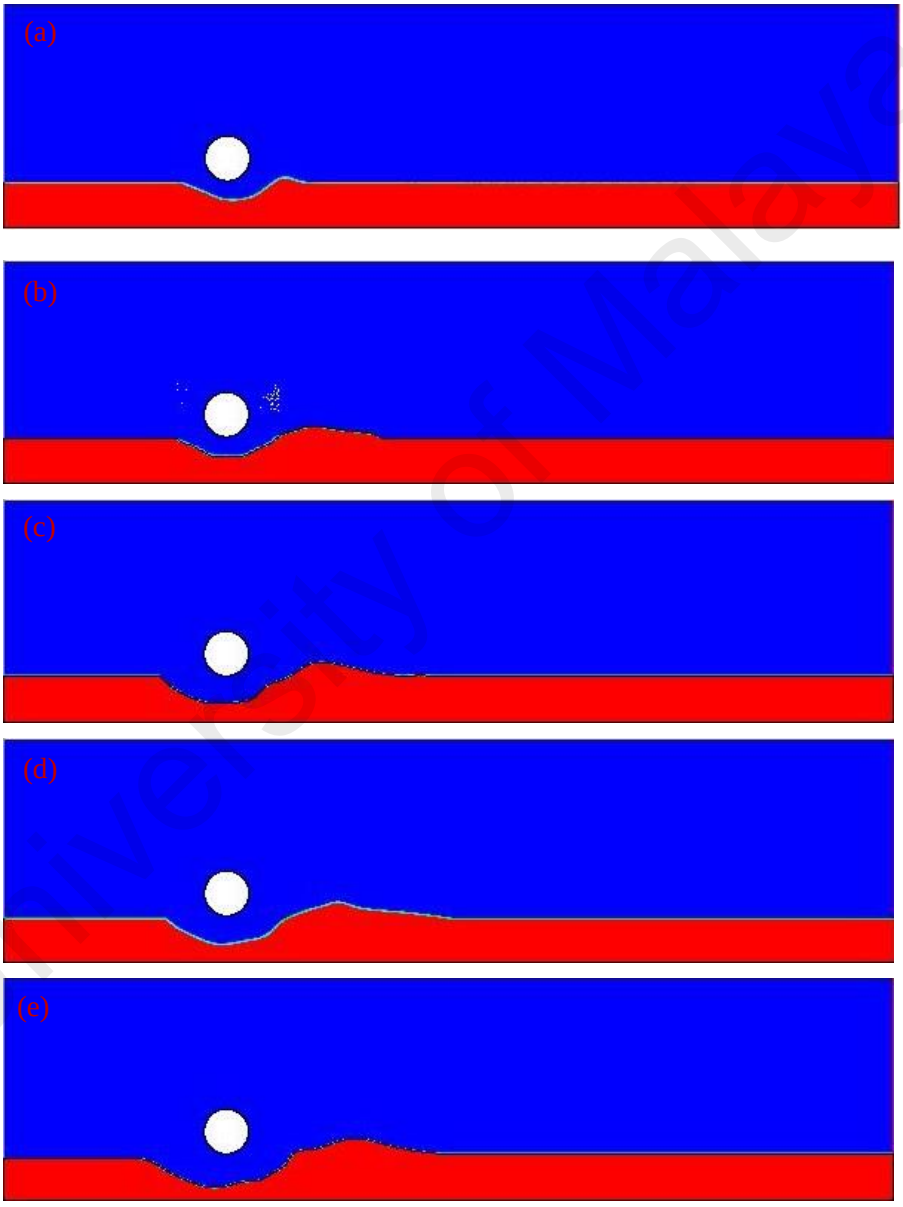

Figure 4.22: Bed profiles during the development of scouring, (a) 10 min, (b) 30 min, (c) 100 min, (d) 200 min, and (e) 300 min.

4.9.6.1 Horizontal velocity (U_x) in the gap at (X/D=0)

Fig.4.23 shows the horizontal velocity profile under the pipe (obstruction) at X/D=0 for different types of scoured bed profiles as presented in Fig.4.22.A higher horizontal velocity can be expected for the scoured bed profiles of 10 min and 30 min due to a narrow gap under the pipe to the surface of the bed. The opposite can be said for the scoured bed profiles of 100, 200 and 300 min. A reduction of around 18% of horizontal velocity is seen from time phase of 10 min to 300 min.

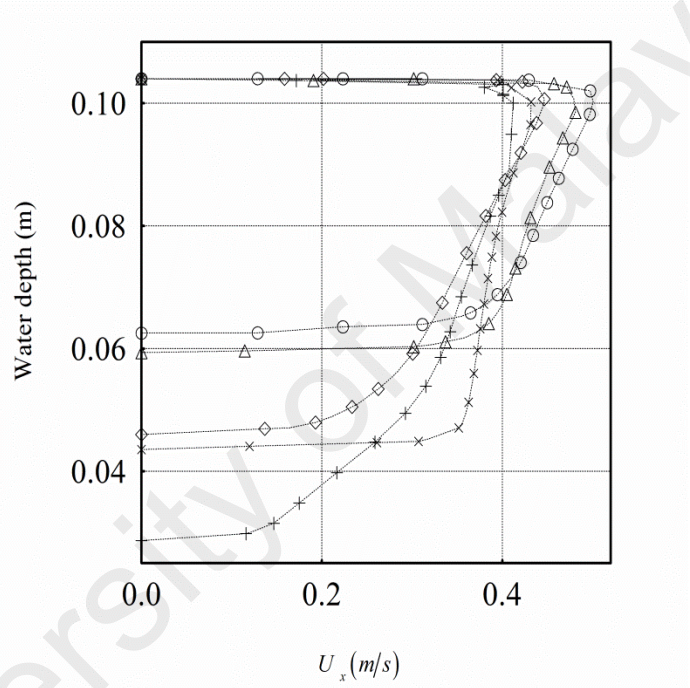

Figure 4.23: Horizontal velocity profile (U_x) in the gap at (X/D=0) and at different scour gaps, ○10 min , Δ 30 min, ◊ 100 min , × 200 min , + 300 min

4.9.6.2 Pressure coefficient (Cp) around pipe

Fig.4.24 shows the variation of the pressure coefficient with gap depth at different circumferential positions (θ) around the pipe. The angle θ indicates the location of the pressure coefficient around the pipe surface from 0º the point nearest to the wall to 360º in a clockwise direction. The stagnation and separation points which can be referred as maximum and minimum peak are clearly delineated in the figure. The positive value of the pressure coefficient indicates that the pressure rises and the water level increases at that location, whereas, a negative value indicates that the pressure drops and the water level decreases.

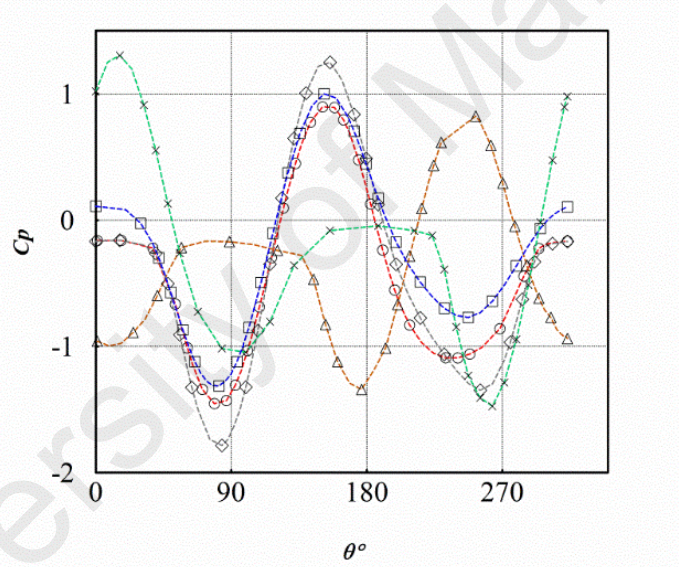

Figure 4.24: Effect on pressure coeffcient(Cp) at cylinder surface of different scour gaps, ○ 10 min, Δ 30 min, ◊100 min, □ 200 min, × 300 min

4.9.6.3 Wall shear stress around pipe

Fig.4.25 shows the variation of the wall shear stress with gap depth. The wall shear stress forms as a sequence of approaching the flow on the pipe parallel to bed surface and it experiences the maximum value τ_{max}at the flow separation point which makes scouring to begin. At an early stage, τ_{max} occurs near the bottom in each side of the pipe forming shedding vortex that creates a space on both sides of the pipe which is quickly occupied with water and leads to scour formation. Further, the maximum shear stress moves downward approaching the bed and move the sand particles in the flow direction. It is observed that, the higher the shear stress, the deeper the scour hole below the pipe.

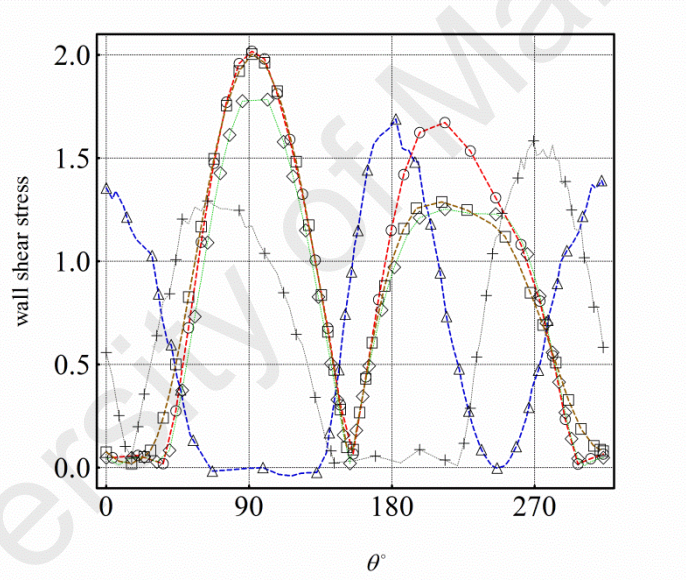

Figure 4.25: Effect on wall shear stress at cylinder surface of different scour gaps, ○ 10 min, Δ 30 min, ◊100 min, □ 200 min, × 300 min

4.9.6.4 Drag and lift coefficients

When the flow approaches the pipe, it imparts drag and lift forces on the pipe. In the current numerical study, variation in these forces is seen in terms of drag and lifts coefficients for five different time phases and presented in Fig.4.26. Shear stress causes the bed erosion and as soon as it comes into action, the pipe experiences to negative lift coefficient (C_l) and it decreases with time and consequently increases the scour gap. The negative lift can be attributed to the suction below and behind the pipe caused by the scour gap. For the velocity, negative lift can be explained by the position of the stagnation point pipe and the angle of attack of the approaching flow. As a result of lift coefficient elimination, the drag coefficient is reduced with time as well. A reduction of 23.7% in C_d and 51.3% in C_l was observed between the time phases of 10 min and 300 min.

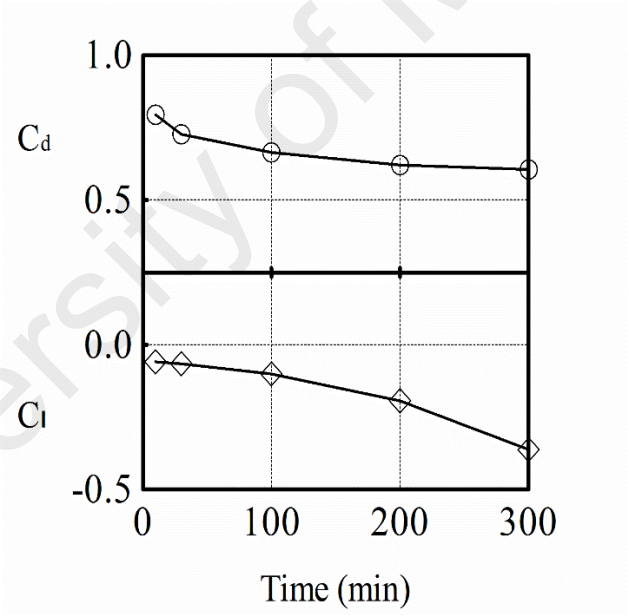

Figure 4.26: Effecton (a) Drag coefficient (C_d), and Lift coefficient (C_l) at cylinder surface of different time phases

4.10 Conclusions

Two dimensional (2D) CFD analyses were carried to investigate fluid flow over an obstruction under different bed profiles using a number of turbulence models. Unsteady horizontal velocity profile and the kinetic energy square root at few axial directions are examined. The effect of scour depth on the velocity distribution under the pipe, the wall shear on the bed, the pressure coefficient, the drag coefficient, and the lift coefficient of the obstruction body were numerically investigated. The conclusions of the current study are as follows:

- The standard *k*-ε model can predict accurate results in comparison to other turbulence models when compared to experimental data for unsteady horizontal velocity and turbulent kinetic energy square root.
- From the spatial distribution velocity, results shows that the velocity magnitude at stagnation and separation points on the pipe wall changes as the time progress and a reduction of around 24.8% and 29.8 %of the horizontal velocity at the separation and bottom points observed respectively.
- It is found that the size of the vortex shedding increases with increase in the scour gap and the *k*-ε model is not appropriate to predict vortex shedding due to the use of wall function or insufficient grid resolution.
- It is observed that there is a reduction of around 26.3 % in pressure at upper point of the separation point from times 10 min to 300 min and a reduction of around 40.7% in pressure at bottom point of the separation point from times 10 min to 300 min.
- From the bed shear stress, results obtained found that at narrow gaps (such as bed profiles at 10 min and 30 min) a bed shear stress is high compared to large gaps (such as 100,200 and 300 min). A reduction of around 80 % of bed wall shear stress observes from time 10 min to 300 min.

- From the velocity behavior under the pipe, results show that the maximum velocity at each phase decreases with increasing time till the scour reaches its equilibrium depth and a decrease of around 18% of horizontal velocity is seen from time period of 10 min to 300 min.
- The drag and lift coefficients decrease as the gap under the pipe increases. A reduction of 23.7% in C_d and 51.3% in C_l was observed between the time phases of 10 min and 300 min.

Among existing turbulence models, the standard *k- ε*turbulence model is preferred over others for more accurate prediction of local scour surrounding circular cylinder over sandy bed. To enhance the accuracy of prediction of local scour, symmetric drag and Eulerian model are recommended as drag models and multiphase models, respectively. The lift model and added mass forces are often used in the investigation of local scour, and they are given a value of 0.5. A proper measurement technique for sand sediment removal, shape and diameter can enhance the accuracy of the simulation.

Chapter: 5.0

Conclusions and Future work

5.1 Conclusions

Two dimensional (2D) CFD analyses were carried out to conduct this study .A total of fifty four (54) Cases were simulated to present this study. 19 Cases were simulated to investigate the effect of bluff body shapes and gap between circular body and wall of sand bed and the other 35 Cases were simulated to investigate turbulence models sensitivity study and effect of scour depth. The conclusions of the current study can be summarized as followed:

- The standard *k*-ε model can predict accurate results for scour bed simulation.
- It is observed that RANS models is not appropriate for high Reynolds number (Re) simulation, thus they are not suitable to model periodic behavior of vortex shedding, because to their large late transition of the boundary layer from laminar to turbulent.
- It is found that in both cases with flat and scoured bed, the size of the vortex shedding increases with the increase in the gap and when the pipe closer to the bed the vortices behind the circular cylinder is unsymmetrical.
- It is observed that in both cases with flat and scoured bed, the drag coefficient reduces as the gap increases and lift coefficient as well. However, for the scoured bed the lift coefficient has a negative value which indicates the void under the pipe.
- It is observed that that in both cases with flat and scoured bed, the pressure distribution around the pipe reduces with the increase of the gap.
- It is found that in both cases with flat and scoured bed shear stress reduces as the gap increases. A reduction of around 82.3 % in the pressure distribution over the bed's surface is observed with falt-bed, and a reduction of around 80 % of bed wall shear stress observes from time 10 min to 300 min at scoured bed.

- It is observed that that in both cases with flat and scoured bed there is a reduction in the wall shear stress distribution over the bed surface.

- From the velocity behavior under the pipe, results show that the maximum velocity at each phase decreases with increasing time till the scour reaches its equilibrium depth and a decrease of around 18% of horizontal velocity is seen from time period of 10 min to 300 min.

5.2 Future work

One way to improve understanding the basic local mechanisms and sand sediment removal is to use the digital image processing that properly measures and captures the movement of sand sediment due to the strong flow subject to the obstruction and increasing the bed shear stress. This method can be used to measure the flow filed parameters, sand bed deformation, diameter size and velocity flow behaviour in scour pit. Using digital image processing to evaluate the sand bed deformation and velocity behavior in scour void in the numerical method can be a useful way to assess various numerical techniques. The digital image processing method is more significant where the numerical methods are usually not able to predict appropriately e.g. the flow filed in downstream (turbulence region). The flow around obstruction is important because of it affects the accuracy of the results of the shedding vortex formation. However, using fine mesh at the upstream and downstream around the obstruction and especially the wake region with wall function boundary may improve the numerical results.

Other way for local scour mechanisms understanding, fluid flow and sand sediment movement is by using Particle Image Velocimetry (PIV). PIV is an optical method of flow visualization used in education and research. PIV can be employed to measure the velocity filed in a granular flows. It is particularly well-suited for nontransparent media such as sand, gravel and quartz or other granular materials. This method also can be used to measure the flow filed parameters, sand bed deformation, diameter size and velocity flow behavior in scour pit.

The hydraulic structures such as bridge piers subjected to strong flow filed, external wind forces and heavy trucks are mostly encountered failures. Thus, regular maintenance and deep understanding of the main reasons contributing to their failures may avoid a lot of losses in terms of cost losses or human losses. To enhance the accuracy of hydraulic structures failures due to local scour and undesirable vibration, Fluid Structure Interaction

(FSI) is recommended to be employed and study this phenomenon. FSI is the interaction of oscillatory structure with fluid flow. It is a critical prediction in the design of many engineering applications, e.g. aircraft and bridges. FSI problems are too complex to be solved analytically. Thus, they have to be analysed either by experiments or numerical simulation, numerically by using two way Fluid Structure Interaction (FSI) in Ansys Workbench and experimentally by Experimental Modal Analysis (EMA) (EMA is the studying of the dynamic structure properties behaviour under vibrational excitation). Both can be used to demonstrate the effect of scouring on structure motion or vibration on hydraulic structures and examine the dynamic structure characteristics such as structural field natural frequency, damping and mode shapes. Through the dynamic structures characteristics, it can be observed the changes occur to dynamic structure characteristics due to enlarge of local scour and vibration that may lead to resonance.

References

Adhikary, BD, Majumdar, P, & Kostic, M. (2009). CFD simulation of open channel flooding flows and scouring around bridge structures. *Proceedings of the 6th WSEAS International Conference on Fluid Mechanics (FLUIDS'09)*.

Aghaee, Y, & Hakimzadeh, H. (2010). Three Dimensional Numerical Modeling of Flow around Bridge Piers Using LES and RANS. *Bundesanstalt für Wasserbau 7*.

Akib, Shatirah, Fayyadh, MM, Shirazi, SM, Primasari, Budhi, & Idris, MF. (2011). Innovative countermeasure for integral bridge scour. *Int. J. Phy. Sci*, *6*(21), 4883-4887.

Akib, Shatirah, Fayyadh, Moatasem M, & Othman, Ismail. (2011). Structural behaviour of skewed integral bridge affected by different parameters *Baltic Journal of Road & Bridge Engineering*, *6*(2).

Akib, Shatirah, Jahangirzadeh, Afshin, & Basser, Hossein. (2014). Local scour around complex pier groups and combined piles at semi-integral bridge. *J. Hydrol. Hydromech*, *62*(2), 108-116.

Akib, Shatirah, Mohammadhassani, Mohammad, & Jahangirzadeh, Afshin. (2014). Application of ANFIS and LR in prediction of scour depth in bridges. *Computers & Fluids*, *91*, 77-86.

Akib, Shatirah, Othman, Ismail, Othman, Faridah, Fayyadh, MM, Tunji, Lawal Abdul Qayoom, & Shirazi, SM. (2011). Epipremnum aureum: An environmental approach to reduce the impact of integral bridge scour. *International Journal of Physical Sciences*, *6*(27), 6342-6357.

Akoz, M Sami. (2009). Flow structures downstream of the horizontal cylinder laid on a plane surface. *Proceedings of the Institution of Mechanical Engineers, Part C: Journal of Mechanical Engineering Science*, *223*(2), 397-413.

Akoz, M Sami, & Kirkgoz, M Salih. (2009). Numerical and experimental analyses of the flow around a horizontal wall-mounted circular cylinder. *Transactions of the Canadian Society for Mechanical Engineering, 33*(2), 189-215.

Alabi, Patrick Dare. (2006). Time development of local scour at a bridge pier fitted with a collar.

Ali, Kamil HM, & Karim, Othman. (2002). Simulation of flow around piers. *Journal of hydraulic research, 40*(2), 161-174.

Ali, Kaniil HM, Karim, Othman A, & O'Connor, Brian A. (1997). Flow patterns around bridge piers and offshore structures.

Asyikin, Muhammad Tedy. (2012). CFD Simulation of Vortex Induced Vibration of a Cylindrical Structure.

Ataie-Ashtiani, B, & Beheshti, AA. (2006). Experimental investigation of clear-water local scour at pile groups. *Journal of Hydraulic Engineering, 132*(10), 1100-1104.

Bateman, A, Fernández, M, & Parker, G. (2005). Morphodynamic model to predict temporal evolution of local scour in bridge piers. *River, Coastal and Estuarine Morphodynamics: RCEM*, 911-920.

Beg, Mubeen, & Beg, Salman. (2013). Scour reduction around bridge piers: A review. *International Journal of Engineering Inventions, 2*(7), 7-15.

Beheshti, AA, & Ataie-Ashtiani, B. (2009). Experimental study of three-dimensional flow field around a complex bridge pier. *Journal of engineering mechanics, 136*(2), 143-154.

Bihs, Hans, & Olsen, Nils Reidar B. (2010). Numerical investigations of local scour around a trapezoidal abutment using the finite volume method. *1st Conference of the European section of the IAHR, Edinburgh, Scotland*.

Blackburn, Hugh, & Henderson, Ron. (1996). Lock-in behavior in simulated vortex-induced vibration. *Experimental Thermal and Fluid Science, 12*(2), 184-189.

Breusers, HNC, Nicollet, G, & Shen, HW. (1977). Local scour around cylindrical piers. *Journal of hydraulic research, 15*(3), 211-252.

Briaud, Jean-Louis, Ting, Francis CK, Chen, HC, Gudavalli, Rao, Perugu, Suresh, & Wei, Gengsheng. (1999). SRICOS: Prediction of scour rate in cohesive soils at bridge piers. *Journal of Geotechnical and Geoenvironmental Engineering, 125*(4), 237-246.

Brørs, B. (1999). Numerical modeling of flow and scour at pipelines. *Journal of Hydraulic Engineering, 125*(5), 511-523.

Bruschi, R., Cimbali, W., Leopardi, G., & Vincenzi, M. (1986, April). Scour induced free span analysis. In *Proceedings of the 5th International Offshore Mechanics and Arctic Engineering Symposium* (pp. 656-669).

Carmo, Bruno Souza. (2009). On wake interference in the flow around two circular cylinders: direct stability analysis and flow-induced vibrations.

Carmo, BS, Sherwin, SJ, Bearman, PW, & Willden, RHJ. (2011). Flow-induced vibration of a circular cylinder subjected to wake interference at low Reynolds number. *Journal of Fluids and Structures, 27*(4), 503-522.

Celik, Ismail, & Rodi, Wolfgang. (1988). Modeling suspended sediment transport in nonequilibrium situations. *Journal of Hydraulic Engineering, 114*(10), 1157-1191.

Chang, Howard H. (1992). *Fluvial processes in river engineering*.

Cheong, Hin Fatt, & Xue, Hong. (1997). Turbulence model for water flow over two-dimensional bed forms. *Journal of Hydraulic Engineering, 123*(5), 402-409.

Chiew, Y, & Lim, S. (2003). Protection of bridge piers using a sacrificial sill. *Proceedings of the ICE-Water and Maritime Engineering, 156*(1), 53-62.

Chiew, Yee-Meng. (1991). Prediction of maximum scour depth at submarine pipelines. *Journal of Hydraulic Engineering, 117*(4), 452-466.

Chrisohoides, Antonis, Sotiropoulos, Fotis, & Sturm, Terry W. (2003). Coherent structures in flat-bed abutment flow: Computational fluid dynamics simulations and experiments. *Journal of Hydraulic Engineering, 129*(3), 177-186.

Chunning, JI. (2010). A numerical investigation on vortex-induced vibration of an elastically mounted circular cylinder at low Reynolds number using the fictitious domain method.

Coleman, Stephen E. (2005). Clearwater local scour at complex piers. *Journal of Hydraulic Engineering, 131*(4), 330-334.

Coleman, Stephen E, Lauchlan, Christine S, & Melville, Bruce W. (2003). Clear-water scour development at bridge abutments. *Journal of hydraulic research, 41*(5), 521-531.

Dargahi, Bijan. (1990). Controlling mechanism of local scouring. *Journal of Hydraulic Engineering, 116*(10), 1197-1214.

Das, Subhasish, Das, Rajib, & Mazumdar, Asis. (2013). Comparison of Characteristics of Horseshoe Vortex at Circular and Square Piers.

Das, Subhasish, Das, Rajib, & Mazumdar, Asis. (2013). Comparison of Characteristics of Horseshoe Vortex at Circular and Square Piers. *Research Journal of Applied Sciences, Engineering and Technology, 5*(17), 4373-4387.

Debnath, Koustuv, & Chaudhuri, Susanta. (2010). Bridge pier scour in clay-sand mixed sediments at near-threshold velocity for sand. *Journal of Hydraulic Engineering, 136*(9), 597-609.

Defanti, Emanuele, Di Pasquale, Giancarlo, & Poggi, Davide. (2010). *An experimental studies of scour at bridge piers: Collars as a countermeasure.* Paper presented at the Proc., 1st IAHR European Congress.

Dey, Subhasish, & Barbhuiya, Abdul Karim. (2005). Time variation of scour at abutments. *Journal of Hydraulic Engineering, 131*(1), 11-23.

Dey, Subhasish, & Raikar, Rajkumar V. (2007). Characteristics of horseshoe vortex in developing scour holes at piers. *Journal of Hydraulic Engineering, 133*(4), 399-413.

Dey, Subhasish, & Singh, Navneet P. (2007). Clear-water scour depth below underwater pipelines. *Journal of Hydro-environment Research, 1*(2), 157-162.

Dudley, Russell David. (2007). A boroscopic quantitative imaging technique for sheet flow measurements.

Eghbali, Parvin, Dehghani, AmirAhmad, Arvanaghi, Hadi, & Menazadeh, Maryam. (2011). The Effect of Geometric Parameters and Foundation Depth on Scour Pattern around Bridge Pier.

Elghobashi, SE, & Abou-Arab, TW. (1983). A two-equation turbulence model for two-phase flows. *Physics of Fluids (1958-1988), 26*(4), 931-938.

Esmaeili, T, Dehghani, AA, Zahiri, AR, & Suzuki, K. (2009). 3D Numerical simulation of scouring around bridge piers (Case Study: Bridge 524 crosses the Tanana River). *World Academy of Science, Engineering and Technology, 58*, 1028-1032.

Ettema, Robert, Melville, Bruce W, & Barkdoll, Brian. (1998). Scale effect in pier-scour experiments. *Journal of Hydraulic Engineering, 124*(6), 639-642.

Fard, Mani Golparvar, Yeganeh-Bakhtiary, Abbas, & Cheng, Liang. Two-Phase Flow modeling of clear-water onset and jet scour under offshore pipelines.

Fayyadh, MM, Akib, S, Othman, I, & Razak, H Abdul. (2011). Experimental investigation and finite element modelling of the effects of flow velocities on a skewed integral bridge. *Simulation Modelling Practice and Theory, 19*(9), 1795-1810.

Fisher, Murray, Atamturktur, Sez, & Khan, Abdul A. (2013). A novel vibration-based monitoring technique for bridge pier and abutment scour. *Structural health monitoring, 12*(2), 114-125.

FLUENT, ANSYS. (2014). 6.3, 2006, FLUENT 6.3 User's Guide, Fluent. *Inc., Lebanon, NH*.

Fluent, Ansys. (2014). Users Guide (nd).

Gao, Fu-Ping, Yang, Bing, Wu, Ying-Xiang, & Yan, Shu-Ming. (2006). Steady current induced seabed scour around a vibrating pipeline. *Applied Ocean Research, 28*(5), 291-298.

Ge, Liang, Lee, Seung Oh, Sotiropoulos, Fotis, & Sturm, Terry. (2005). 3D unsteady RANS modeling of complex hydraulic engineering flows. II: Model validation and flow physics. *Journal of Hydraulic Engineering, 131*(9), 809-820.

Ge, Liang, & Sotiropoulos, Fotis. (2005). 3D unsteady RANS modeling of complex hydraulic engineering flows. I: Numerical model. *Journal of Hydraulic Engineering, 131*(9), 800-808.

Ghosal, Sandip, & Moin, Parviz. (1995). The basic equations for the large eddy simulation of turbulent flows in complex geometry. *Journal of Computational Physics, 118*(1), 24-37.

Gislason, Kjartan, Fredsøe, Jørgen, & Sumer, B Mutlu. (2009). Flow under standing waves: Part 2. Scour and deposition in front of breakwaters. *Coastal Engineering, 56*(3), 363-370.

Grimaldi, C, & Cardoso, AH. (2010). Methods for local scour depth estimation at complex bridge piers. *Proc., 1st IAHR European Division Congress, Heriot-Watt Univ., Edinburgh*.

Guney, MS, Aksoy, AO, & Bombar, G. (2011). *Experimental Study of Local Scour Versus Time Around Circular Bridge Pier*. Paper presented at the 6th International Advanced Technologies Symposium (IATS'11), 16-18 May 2011, Elazığ, Turkey.

Hajivalie, Fatemeh, Yeganeh-Bakhtiary, Abbas, Houshanghi, Hamid, & Gotoh, Hitoshi. (2012). Euler–Lagrange model for scour in front of vertical breakwater. *Applied Ocean Research, 34*, 96-106.

Haltigin, Timothy W, Biron, Pascale M, & Lapointe, Michel F. (2007). Predicting equilibrium scour-hole geometry near angled stream deflectors using a three-dimensional numerical flow model. *Journal of Hydraulic Engineering, 133*(8), 983-988.

Hossein Kazeminezhad, Mohammad, Yeganeh-Bakhtiary, Abbas, Etemad-Shahidi, Amir, & Baas, Jaco H. (2011). Two-Phase Simulation of Wave-Induced Tunnel Scour beneath Marine Pipelines. *Journal of Hydraulic Engineering, 138*(6), 517-529.

Huang, Wenrui, Yang, Qiping, & Xiao, Hong. (2009). CFD modeling of scale effects on turbulence flow and scour around bridge piers. *Computers & Fluids, 38*(5), 1050-1058.

Jain, Anil B. (2012). Vortex-Induced Vibrations of an Inclined Cylinder in Flow. *Masters Theses*.

Jensen, B. L., Sumer, B. M., Jensen, H. R., & Fredsoe, J. (1990). Flow around and forces on a pipeline near a scoured bed in steady current. *Journal of Offshore Mechanics and Arctic Engineering, 112*(3), 206-213.

Jensen, BL, Sumer, BM, Jensen, HR, & Fredsoe, J. (1990). Flow around and forces on a pipeline near a scoured bed in steady current. *Journal of Offshore Mechanics and Arctic Engineering, 112*(3), 206-213.

Jensen, BL, Sumer, BM, Jensen, HR, & Fredsoe, J. (1990). Flow around and forces on a pipeline near a scoured bed in steady current. *Journal of Offshore Mechanics and Artic Engineering, 112*.

Jia, Yafei, Kitamura, Tadanori, & Wang, Sam SY. (2001). Simulation of scour process in plunging pool of loose bed-material. *Journal of Hydraulic Engineering, 127*(3), 219-229.

Jin-Ping, O, Xu, Feng, & Yi-Qing, X. (2009). *Numerical simulation of vortex induced vibration of three cylinders in regular triangle arrangement.* Paper presented at the Proceeding of the The 7th Asia-Pacific Conference on Wind Engineering, Taipei, Taiwan.

Jones, J Sterling, Kilgore, Roger T, & Mistichelli, Mark P. (1992). Effects of footing location on bridge pier scour. *Journal of Hydraulic Engineering, 118*(2), 280-290.

Kang, Joongu, & Yeo, Hongkoo. (2012). Shear Stress Variation at Scour Hole of Circular Pier.

Kattell, John, & Eriksson, M. (1998). Bridge Scour Evaluation: Screening, Analysis, & Countermeasures.

Kazeminezhad, M. H., Yeganeh-Bakhtiary, A., & Etemad-Shahidi, A. (2010). Numerical investigation of boundary layer effects on vortex shedding frequency and forces acting upon marine pipeline. *Applied Ocean Research, 32*(4), 460-470.

Kazeminezhad, MH, & Yeganeh-Bakhtiary, A. (2011). Two-Phase Simulation of Coastal Current-Induced Scour around Submarine Pipelines. *Journal of coastal research*, 542-546.

Khosronejad, Ali, Kang, Seokkoo, & Sotiropoulos, Fotis. (2012). Experimental and computational investigation of local scour around bridge piers. *Advances in Water Resources, 37*, 73-85.

Khwairakpam, Padmini, & Mazumdar, Asis. (2009). Local scour around hydraulic structures. *International Journal of Recent Trends in Engineering, 1*(6), 59-61.

Khwairakpam, Padmini, Ray, Soumendu Sinha, Das, Subhasish, Das, Rajib, & Mazumdar, Asis. (2012). Scour hole characteristics around a vertical pier under clearwater scour conditions. *Journal of Engineering & Applied Sciences, 7*(6).

Kirkil, G, Constantinescu, G, & Ettema, R. (2009). Detached eddy simulation investigation of turbulence at a circular pier with scour hole. *Journal of Hydraulic Engineering, 135*(11), 888-901.

Kirkil, Gokhan, Constantinescu, George, & Ettema, Robert. (2005). *The horseshoe vortex system around a circular bridge pier on equilibrium scoured bed.* Paper presented at the World Water and Environmental Resources Congress, EWRI, Alaska.

Kocaman, Selahattin, Seckin, Galip, & Erduran, Kutsi S. (2010). 3D model for prediction of flow profiles around bridges. *Journal of hydraulic research, 48*(4), 521-525.

Kozakiewicz, Andrzej, Sumer, B Mutlu, Fredsøe, Jørgen, & Hansen, EA. (1997). Vortex regimes around a freely vibrating cylinder in oscillatory flow. *International Journal of Offshore and Polar Engineering, 7*(2).

Lagasse, Peter F, & Richardson, Everett V. (2001). ASCE compendium of stream stability and bridge scour papers. *Journal of Hydraulic Engineering, 127*(7), 531-533.

Launder, BE, Reece, G Jr, & Rodi, W. (1975). Progress in the development of a Reynolds-stress turbulence closure. *Journal of fluid mechanics, 68*(03), 537-566.

Lee, Seung Oh, & Sturm, Terry W. (2009). Effect of sediment size scaling on physical modeling of bridge pier scour. *Journal of Hydraulic Engineering, 135*(10), 793-802.

Li, Fangjun, & Cheng, Liang. (1999). Numerical model for local scour under offshore pipelines. *Journal of Hydraulic Engineering, 125*(4), 400-406.

Li, T, Zhang, JY, Zhang, WH, & Zhu, MH. (2009). Vortex-induced vibration characteristics of an elastic circular cylinder. *World Acad Sci Eng Technol, 60*, 56-65.

Liang, Dongfang, & Cheng, Liang. (2005). Numerical modeling of flow and scour below a pipeline in currents: Part I. Flow simulation. *Coastal Engineering, 52*(1), 25-42.

Liang, Dongfang, Cheng, Liang, & Li, Fangjun. (2005). Numerical modeling of flow and scour below a pipeline in currents: Part II. Scour simulation. *Coastal Engineering, 52*(1), 43-62.

Liu, Qiang Li Chunhua, & Dong, Haiming. (2010). *Experimental Study on Scour Protective Equipment around Pile of Bridge under Wave and Current.* Paper presented at the The Twentieth International Offshore and Polar Engineering Conference.

Liu, Xiaofeng, & Garciá, Marcelo H. (2006). *Numerical simulation of local scour with free surface and automatic mesh deformation.* Paper presented at the Proceedings of World Environmental and Water Resource Congress. Omaha, NE.

Liu, Xiaofeng, & Garciá, Marcelo H. (2006). *Numerical simulation of local scour with free surface and automatic mesh deformation.* Paper presented at the Proc., EWRI World Water and Environmental Congress.

Liu, Xiaofeng, & García, Marcelo H. (2008). Three-dimensional numerical model with free water surface and mesh deformation for local sediment scour. *Journal of waterway, port, coastal, and ocean engineering, 134*(4), 203-217.

Lu, Lin, Li, Yucheng, & Qin, Jianmin. (2005). Numerical simulation of the equilibrium profile of local scour around submarine pipelines based on renormalized group turbulence model. *Ocean engineering, 32*(17), 2007-2019.

Mao, Ye. (1987). The interaction between a pipeline and an erodible bed. *SERIES PAPER TECHNICAL UNIVERSITY OF DENMARK*(39).

Mashahir, MB, Zarrati, AR, Rezaei, MJ, & Zokaei, M. (2009). Effect of collars and bars in reducing the local scour around cylindrical bridge piers. *International Journal of Engineering, Transaction B: Applications, 22*(4), 333-342.

Melling, Greg, Dix, JK, Turnock, SR, & Whitehouse, Richard. (2011). CFD-based methods for numerical modelling of scour.

Melville, B. (2008). *The physics of local scour at bridge piers.* Paper presented at the Fourth International Conference on Scour and Erosion.

Melville, Bruce W. (1997). Pier and abutment scour: integrated approach. *Journal of Hydraulic Engineering, 123*(2), 125-136.

Melville, Bruce W, & Raudkivi, Arved J. (1977). Flow characteristics in local scour at bridge piers. *Journal of hydraulic research, 15*(4), 373-380.

Melville, Bruce W, & Raudkivi, Arved J. (1996). Effects of foundation geometry on bridge pier scour. *Journal of Hydraulic Engineering, 122*(4), 203-209.

Millard, SG, Bungey, JH, Thomas, C, Soutsos, MN, Shaw, MR, & Patterson, A. (1998). Assessing bridge pier scour by radar. *NDT & E International, 31*(4), 251-258.

Mittal*, S, & Kumar, V. (2004). Vortex induced vibrations of a pair of cylinders at Reynolds number 1000. *International Journal of computational fluid dynamics, 18*(7), 601-614.

Moeng, Chin-Hoh. (1984). A large-eddy-simulation model for the study of planetary boundary-layer turbulence. *Journal of the Atmospheric Sciences, 41*(13), 2052-2062.

Molinas, Albert, Kheireldin, Khaled, & Wu, Baosheng. (1998). Shear stress around vertical wall abutments. *Journal of Hydraulic Engineering, 124*(8), 822-830.

Murrillo, Juan A. (1987). The scourge of scour. *Civil Engineering—ASCE, 57*(7), 66-69.

Mutlu Sumer, B. (2007). Mathematical modelling of scour: A review. *Journal of hydraulic research, 45*(6), 723-735.

Muzzammil, M, Gangadharaiah, T, & Gupta, AK. (2004). An experimental investigation of a horseshoe vortex induced by a bridge pier. *Proceedings of the ICE-Water Management, 157*(2), 109-119.

Nagata, Nobuhisa, Hosoda, Takashi, Nakato, Tatsuaki, & Muramoto, Yoshio. (2005). Three-dimensional numerical model for flow and bed deformation around river hydraulic structures. *Journal of Hydraulic Engineering, 131*(12), 1074-1087.

Negm, Abdelazim M, Abdelaal, GM, Mohamed, YA, & Fathy, Amira A. Optimal Shape of Collar to Minimize the Local Scour around Bridge Pier. *Proc. of IWTC13*, 12-15.

Nielsen, Anders Wedel, Liu, Xiaofeng, Sumer, B Mutlu, & Fredsøe, Jørgen. (2013). Flow and bed shear stresses in scour protections around a pile in a current. *Coastal Engineering, 72*, 20-38.

Oliveto, Giuseppe, & Hager, Willi H. (2002). Temporal evolution of clear-water pier and abutment scour. *Journal of Hydraulic Engineering, 128*(9), 811-820.

Olsen, Nils RB, & Melaaen, Morten C. (1993). Three-dimensional calculation of scour around cylinders. *Journal of Hydraulic Engineering, 119*(9), 1048-1054.

Pal, Mahesh, Singh, NK, & Tiwari, NK. (2011). Support vector regression based modeling of pier scour using field data. *Engineering Applications of Artificial Intelligence, 24*(5), 911-916.

Parker, Gary, Toro-Escobar, Carlos, & Voigt Jr, Richard L. (1998). Countermeasures to protect bridge piers from scour. *Final Rep. prepared for National Highway Research Program, Transportation Research Board, National Research Council*.

Rahmanian, Mehran, Zhao, Ming, Cheng, Liang, & Zhou, Tongming. (2012). Two-degree-of-freedom vortex-induced vibration of two mechanically coupled cylinders of different diameters in steady current. *Journal of Fluids and Structures, 35*, 133-159.

Salaheldin, Tarek M, Imran, Jasim, & Chaudhry, M Hanif. (2004). Numerical modeling of three-dimensional flow field around circular piers. *Journal of Hydraulic Engineering, 130*(2), 91-100.

Saneie, Mojtaba, Omidi, Faranak, & Fazlola, Ramin. Local scour around rectangular abutment and their countermeasures by using sacrificial piles.

Sheppard, D Max, Odeh, Mufeed, & Glasser, Tom. (2004). Large scale clear-water local pier scour experiments. *Journal of Hydraulic Engineering, 130*(10), 957-963.

Smith, DW. (1976). *Bridge failures.* Paper presented at the ICE Proceedings.

Smith, DW. (1976). *Bridge failures.* Paper presented at the ICE Proceedings.

Smith, Heather D, & Foster, Diane L. (2005). Modeling of flow around a cylinder over a scoured bed. *Journal of waterway, port, coastal, and ocean engineering, 131*(1), 14-24.

Smith, Heather D, & Foster, Diane L. (2007). Three-dimensional flow around a bottom-mounted short cylinder. *Journal of Hydraulic Engineering, 133*(5), 534-544.

Sturm, Terry W. (2006). Scour around bankline and setback abutments in compound channels. *Journal of Hydraulic Engineering, 132*(1), 21-32.

Sumer, BM, & Fredsøe, J. (1988). Transverse vibrations of an elastically mounted cylinder exposed to an oscillating flow. *Journal of Offshore Mechanics and Arctic Engineering, 110*, 387.

Teruzzi, A, Ballio, F, Salon, S, Armenio, V, & Cardoso, Leal. (2006). *Numerical investigation of the turbulent flow around a bridge abutment.* Paper presented at the River Flow 2006, III Int. Conf. on Fluvial Hydraulics, Lisbon, Portugal.

Thanh, Nguyen Viet, Chung, Dang Huu, & Nghien, Tran Dinh. (2014). prediction of the local scour at the bridge square pier using a 3D numerical model *Scientific Research 4*(34-42).

Ting, Francis CK, Briaud, Jean-Louis, Chen, HC, Gudavalli, Rao, Perugu, Suresh, & Wei, Gengsheng. (2001). Flume tests for scour in clay at circular piers. *Journal of Hydraulic Engineering, 127*(11), 969-978.

Tulimilli, Bhaskar Rao, Lottes, Steven A, Majumdar, Pradip, & Kostic, Milivoje. (2011). *Three-Dimensional Scouring Analysis for Open Channel Pressure Flow Scour Under Flooded Bridge Decks.* Paper presented at the ASME 2011 International Mechanical Engineering Congress and Exposition.

Unger, Jens, & Hager, Willi H. (2007). Down-flow and horseshoe vortex characteristics of sediment embedded bridge piers. *Experiments in fluids, 42*(1), 1-19.

Van Beek, FA, & Wind, HG. (1990). Numerical modelling of erosion and sedimentation around offshore pipelines. *Coastal Engineering, 14*(2), 107-128.

Van den Abeele, F, Voorde, J Vande, & Goes, P. (2008). *Numerical Modelling of Vortex Induced Vibrations in Submarine Pipelines.* Paper presented at the Excerpt from the Proceedings of the COMSOL Conference.

Vass, P, Benocci, C, Rambaud, P, & Lohász, MM. (2005). Large Eddy Simulation of a Ribbed Duct Flow with FLUENT: Effect of Rib Inclination.

Wardhana, Kumalasari, & Hadipriono, Fabian C. (2003). Analysis of recent bridge failures in the United States. *Journal of Performance of Constructed Facilities, 17*(3), 144-150.

Wei, ZHAO, & Aode, Huhe. (2006). Large-eddy simulation of three-dimensional turbulent flow around a circular pier. *Journal of Hydrodynamics, Ser. B, 18*(6).

Wilcox, David C. (1998). *Turbulence modeling for CFD* (Vol. 2): DCW industries La Canada.

Yakhot, Victor, & Orszag, Steven A. (1986). Renormalization group analysis of turbulence. I. Basic theory. *Journal of scientific computing, 1*(1), 3-51.

Yang, Bing, Gao, Fu-Ping, Jeng, Dong-Sheng, & Wu, Ying-Xiang. (2008). Experimental study of vortex-induced vibrations of a pipeline near an erodible sandy seabed. *Ocean engineering*, *35*(3), 301-309.

Yanmaz, A Melih, & Ustun, I. (2001). Generalized reliability model for local scour around bridge piers of various shapes. *TURK. J. ENG. ENVIRON. SCI.*, *25*(6), 687-698.

Yeganeh-Bakhtiary, Abbas, Kazeminezhad, Mohammad Hossein, Etemad-Shahidi, Amir, Baas, Jaco H, & Cheng, Liang. (2011). Euler–Euler two-phase flow simulation of tunnel erosion beneath marine pipelines. *Applied Ocean Research*, *33*(2), 137-146.

Zang, Zhipeng, Cheng, Liang, Zhao, Ming, Liang, Dongfang, & Teng, Bin. (2009). A numerical model for onset of scour below offshore pipelines. *Coastal Engineering*, *56*(4), 458-466.

Zhai, Yuan. (2010). Time-dependent Scour Depth Under Bridge-submerged Flow. *Civil Engineering Theses, Dissertations, and Student Research*, 4.

Zhao, Ming. (2013). Numerical investigation of two-degree-of-freedom vortex-induced vibration of a circular cylinder in oscillatory flow. *Journal of Fluids and Structures*.

Zhao, Ming, & Cheng, Liang. (2008). Numerical modeling of local scour below a piggyback pipeline in currents. *Journal of Hydraulic Engineering*, *134*(10), 1452-1463.

Zhao, Ming, & Cheng, Liang. (2010). Numerical investigation of local scour below a vibrating pipeline under steady currents. *Coastal Engineering*, *57*(4), 397-406.

Zhao, Ming, Kaja, Kalyani, Xiang, Yang, & Yan, Guirong. (2013). Vortex-induced vibration (VIV) of a circular cylinder in combined steady and oscillatory flow. *Ocean engineering*, *73*, 83-95.

Zhao, Zhihe, & Fernando, HJS. (2007). Numerical simulation of scour around pipelines using an Euler–Euler coupled two-phase model. *Environmental Fluid Mechanics, 7*(2), 121-142.

Zhao, Zhihe, & Fernando, HJS. (2008). Numerical modeling of a sagging pipeline using an Eulerian two-phase model. *Journal of Turbulence*(9).

Zhou, CY, So, RMC, & Lam, K. (1999). Vortex-induced vibrations of an elastic circular cylinder. *Journal of Fluids and Structures, 13*(2), 165-189.

Zhu, Zhi-wen, & Liu, Zhen-qing. (2012). CFD prediction of local scour hole around bridge piers. *Journal of Central South University, 19*, 273-281.

List of publications

1. Turbulence model sensitivity and scour gap effect of unsteady flow around pipe: A CFD study, *Scientific World Journal, year, issue, page number.* *http://www.hindawi.com/journals/tswj/2014/412136/*.

2. Computational Fluid Dynamic (CFD) Study of Scour Gap Effect around a Pipe. *1st International Conference of Recent Trends in Information and Communication Technologies. http://www.ysrgst.org/irict/wp-content/uploads/2014/10/54.pdf.*

3. Basic mechanisms, interfacial forces and turbulence models for predicating local scour (Under review).

4. The effect of bluff body shapes and gap between circular body and wall of sand bed (Under review).